การสังเคราะห์โซลคีทาลด้วยตัวเร่งปฏิกิริยาซัลโฟนิกอะลูมิโนซิลิเกต

นางสาวรชตวัน ใยสำลี

วิทยานิพนธ์นี้เป็นส่วนหนึ่งของการศึกษาตามหลักสูตรปริญญาวิทยาศาสตรมหาบัณฑิต
สาขาวิชาปิโตรเคมีและวิทยาศาสตร์พอลิเมอร์
คณะวิทยาศาสตร์ จุฬาลงกรณ์มหาวิทยาลัย
ปีการศึกษา 2559

SYNTHESIS OF SOLKETAL USING SULFONIC ALUMINOSILICATE CATALYST

Miss Rachatawan Yaisamlee

A Thesis Submitted in Partial Fulfillment of the Requirements

for the Degree of Master of Science Program in Petrochemistry and Polymer Science

Faculty of Science

Chulalongkorn University

Academic Year 2016

Thesis Title	SYNTHESIS OF SOLKETAL USING SULFONIC ALUMINOSILICATE CATALYST
By	Miss Rachatawan Yaisamlee
Field of Study	Petrochemistry and Polymer Science
Thesis Advisor	Duangamol Tungasmita, Ph.D.

Accepted by the Faculty of Science, Chulalongkorn University in Partial Fulfillment of the Requirements for the Master's Degree

....Dean of the Faculty of Science

(Associate Professor Polkit Sangvanich, Ph.D.)

THESIS COMMITTEE

....Chairman

(Associate Professor Kejvalee Pruksathorn, Ph.D.)

....Thesis Advisor

(Duangamol Tungasmita, Ph.D.)

....Examiner

(Assistant Professor Puttaruksa Varanusupakul, Ph.D.)

....External Examiner

(Papapida Pornsuriyasak, Ph.D.)

รชตวัน ใยสำลี : การสังเคราะห์โซลคีทาลด้วยตัวเร่งปฏิกิริยาซัลโฟนิกอะลูมิโนซิลิเกต (SYNTHESIS OF SOLKETAL USING SULFONIC ALUMINOSILICATE CATALYST) อ.ที่ปรึกษาวิทยานิพนธ์หลัก: ดร. ดวงกมล ตุงคะสมิต, 131 หน้า.

ทำการสังเคราะห์โพรพิลซัลโฟนิกซีโอไลต์บีตาโดยการเติมหมู่โพรพิลซัลโฟนิกด้วยวิธีเชื่อมต่อ โดยใช้ 3-เมอร์แคปโตโพรพิลไตรเมทอกซีไซเลนเป็นสารให้หมู่โพรพิล-ไทออล จากนั้นออกซิไดซ์หมู่ไทออลเป็นหมู่ซัลโฟนิกด้วยไฮโดรเจนเปอร์ออกไซด์ร้อยละ 30 โดยมวล ทำการตรวจลักษณะเฉพาะของตัวเร่งปฏิกิริยาที่สังเคราะห์ได้ด้วยเทคนิคการเลี้ยวเบนของรังสีเอกซ์ (XRD) การดูดซับแก๊สไนโตรเจน กล้องจุลทรรศน์แบบส่องกราด (SEM) เทคนิคฟูเรียร์ทรานฟอร์มอินฟราเรดสเปคโตรสโคปี (FTIR) เทคนิคคาร์บอน-นิวเคลียร์แมกเนติกเรโซแนนซ์สเปคโตรสโคปี (^{13}C NMR) และการไทเทรต เพื่อนำตัวเร่งปฏิกิริยาที่สังเคราะห์ได้ไปใช้ในปฏิกิริยาอะซีทาลไลเซชันระหว่างกลีเซอรอลและอะซีโตนให้ได้โซลคีทาลในเครื่องปฏิกรณ์แบบกะ (batch reactor) โดยปราศจากตัวทำละลาย ตรวจสอบผลิตภัณฑ์ด้วยเทคนิคแก๊สโครมาโทกราฟี-แมสสเปคโทรเมสตรี พร้อมทั้งศึกษาผลของชนิดของตัวเร่งปฏิกิริยา เวลาในการทำปฏิกิริยา อุณหภูมิ อัตราส่วนโดยโมลของสารตั้งต้นและปริมาณตัวเร่งปฏิกิริยา ผลการทดลองพบว่าตัวเร่งปฏิกิริยาซีโอไลต์บีตาที่มีหมู่โพรพิลซัลโฟนิกแสดงร้อยละการเปลี่ยนกลีเซอรอลสูงสุดถึง 90.8 และได้ร้อยละผลิตภัณฑ์โซลคีทาลถึง 89.9 พร้อมทั้งได้ร้อยละความเลือกจำเพาะต่อผลิตภัณฑ์สูงถึง 99 ที่อุณหภูมิ 32 องศาเซลเซียส เมื่อใช้อัตราส่วนกลีเซอรอลต่ออะซีโตน 1:10 โดยโมล โดยใช้ปริมาณตัวเร่งปฏิกิริยาร้อยละ 2.5 โดยน้ำหนักเมื่อเทียบกับน้ำหนักกลีเซอรอล เป็นเวลา 1 ชั่วโมง พร้อมทั้งศึกษาการนำตัวเร่งปฏิกิริยากลับมาใช้ซ้ำ นอกจากนี้ยังศึกษาปฏิกิริยาอะซีทาลไลเซชันกลีเซอรอลด้วยคีโตนและแอลดีไฮด์ชนิดอื่น เช่น ไซโคลเฮกซาโนน ไซโคลออกทาโนน ไซโคลโดเดกคาโนน และเบนซาลดีไฮด์ โดยใช้ตัวเร่งปฏิกิริยาที่มีหมู่ซัลโฟนิก ได้แก่ H-beta-Pr-SO$_3$H, MCM-41-Pr-SO$_3$H และตัวเร่งปฏิกิริยาทางการค้า ได้แก่ ซีโอไลต์บีตา และแอมเบอร์ลิสต์-15

สาขาวิชา   ปิโตรเคมีและวิทยาศาสตร์พอลิเมอร์   ลายมือชื่อนิสิต ....

ปีการศึกษา 2559   ลายมือชื่อ อ.ที่ปรึกษาหลัก ....

5772111923 : MAJOR PETROCHEMISTRY AND POLYMER SCIENCE

KEYWORDS: SOLKETAL / SULFONIC ALUMINOSILICATE / ACETALIZATION OF GLYCEROL

RACHATAWAN YAISAMLEE: SYNTHESIS OF SOLKETAL USING SULFONIC ALUMINOSILICATE CATALYST. ADVISOR: DUANGAMOL TUNGASMITA, Ph.D., 131 pp.

The propyl sulfonic functionalized on H-beta was synthesized by grafting with 3-mercaptopropyltrimethoxysilanegroup. Then, thiol moiety (-SH) was oxidized to sulfonic acid group ($-SO_3H$) using 30% (w/w) hydrogen peroxide (H_2O_2). The synthesized catalyst was characterized by powder X-ray diffraction (XRD), N_2 adsorption/desorption, scanning electron microscopy (SEM), Fourier transform infrared spectroscopy (FTIR), carbon-13 nuclear magnetic resonance Spectroscopy (^{13}C NMR) and acid-base titration. The catalytic activity of this catalyst was investigated for acetalization of glycerol with acetone to produce solketal. This reaction was carried out in batch reactor under solvent free condition. A gas chromatography-mass spectrometry (GC-MS) method was used for products characterization. The effect of various type of catalysts, reaction time, reaction temperature, reactants mole ratio and catalyst amount have been studied. The result showed that the highest glycerol conversion (90.8%) and solketal yield (89.9%) with excellent solketal selectivity (99%) were obtained by using H-beta-Pr-SO_3H as catalyst at $32^{\circ}C$, glycerol: acetone mole ratio of 1:10 with catalyst 2.5 wt% based on glycerol and reaction time for 1 h. The reused H-beta-Pr-SO_3H was also investigated. Moreover, the acetalization of glycerol with other ketones or aldehyde such as cyclohexanone, cyclooctanone, cyclododecanone and benzaldehyde were also studied over sulfonated catalysts (H-beta-Pr-SO_3H and MCM-41-Pr-SO_3H) and commercial catalysts (H-beta and Amberlyst-15).

Field of Study: Petrochemistry and   Student's Signature ....
                 Polymer Science   Advisor's Signature ....
Academic Year: 2016

ACKNOWLEDGEMENTS

I would like to express my sincere thanks to my thesis advisor, Dr. Duangamol Tungasmita for her invaluable help and constant encouragement. I would not have achieved this far and this thesis would not have been completed without all the support that I have always received from her.

I would like to give my gratitude to Assoc. Prof. Dr. Kejvalee Pruksathorn as chairman, Assist. Prof. Dr. Puttaruksa Varanusupakul and Dr. Papapida Pornsuriyasak, who have been members of thesis committee, for their very valuable comments on this thesis.

In addition, I am grateful thank Dr. Duangkamon jiraroj and Miss Isara Mongkolpichayarak for advising and teaching the research methodologies. I would also like to thank all of members of Materials Chemistry and Catalysis Research Laboratory for their assistances and friendships.

I would like to thank the financial support from Science Achievement Scholarship of Thailand (SAST). Moreover, I am grateful to the 90th anniversary of Chulalongkorn University (Ratchadaphiseksomphot Endowment Fund) for research grants. In addition, I am also indebted to program of Petrochemistry and Polymer Science, Faculty of Science, Chulalongkron University for experience and knowledge.

Finally, I most gratefully acknowledge my parents and my friends for providing me with unfailing support and continuous encouragement throughout my years of study and through the process of researching and writing this thesis.

CONTENTS

LIST OF TABLE

LIST OF FIGURE

LIST OF SCHEME

LIST OF ABBREVIATIONS

a.u.	Arbitrary unit
Å	Angstrom unit
BJH	Barret, Joyner, and Halenda
BET	Brunauer-Emmett-Teller
$^{\circ}$C	Degree Celsius
CTAB	Cetyltrimethylammonium bromide
DMF	Dimethylformamide
FTIR	Fourier transform infrared spectroscopy
GC	Gas chromatography
GC-MS	Gas chromatography – mass spectrometry
h	Hour
mL	Milliliter
M	Molar
MPTMS	(3-mercaptopropyl) trimethoxysilane
NMR	Nuclear magnetic resonance spectrometer
nm	Nanometer
SEM	Scanning electron microscope
TEOS	Tetraethyl orthosilicate
wt%	Percent by weight
XRD	X-ray diffraction

CHAPTER 1

INTRODUCTION

1.1 Background

Recently, the requirement of biofuel is continuously increasing because of exhausting of non-renewable fossil fuel reserves. The new report, biofuels markets and technologies, estimates steady growth through 2016 but rapid production increases between 2017 and 2021 as a result of higher oil prices, emerging mandates, new feedstock availability, and advanced technologies, as shown in figure 1.1. Total global biofuel production is projected to reach 65.7 billion gallons per year by 2021. Moreover, biodiesel is an excellent alternative to fossil fuels which presents the advantage of enhanced biodegradation, reduced toxicity and a lower emission profile [1].
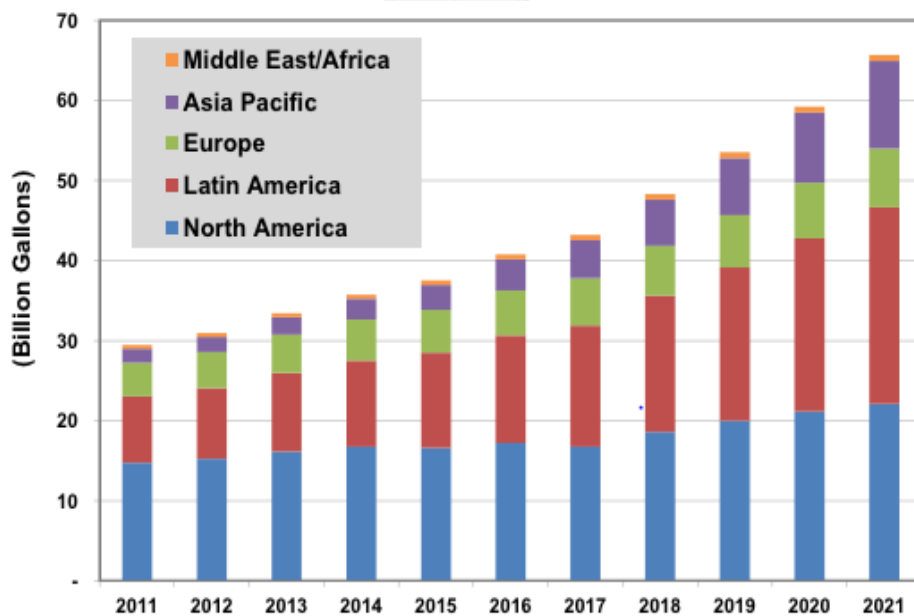
Figure 1.1 Biodiesel production by region, world market: 2011-2021

Biodiesel can be synthesized by transesterification of triglyceride with primary alcohol in presence of base catalyst (Scheme 1.1). However, biodiesel production is glowing up resulting to an increase of crude glycerol which is the main by-product during biodiesel production with 10 wt% [2], [3]. An increment of biodiesel production led to a massive oversupply of low cost crude glycerol.
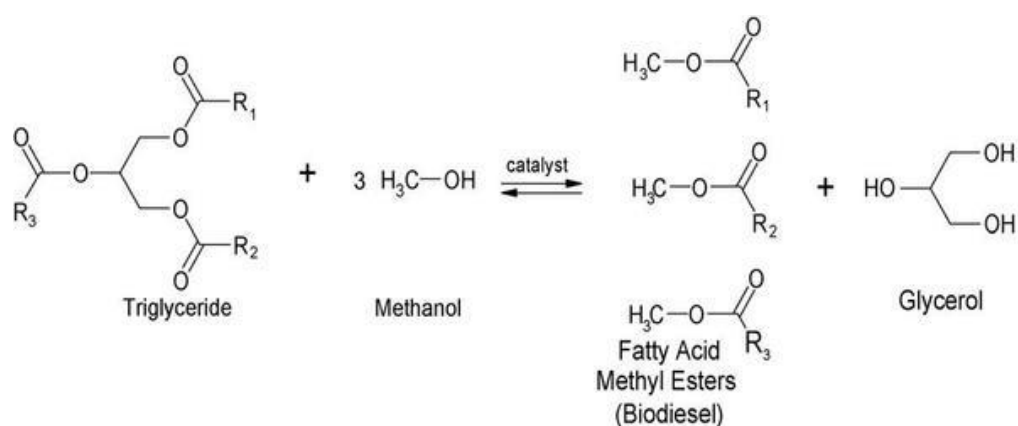
Scheme 1.1 Biodiesel production via tranesterification of triglycerides

Glycerol (1,2,3-propanetriol) is a polyalcohol with numerous applications in the chemical, pharmaceutical, cosmetic, pulp, tobacco, and food industries. Moreover, glycerol is a versatile bio feedstock that is non-toxic and multifunctional structure [4]. The global consumption of glycerol was about 750,000 t/a. in 2008. Although glycerol is being extensively used, markets are incapable to absorb its overwhelming surpluses. Consequence, the value added glycerol is interesting to transform to higher value and more useful products by various catalytic processes involving oxidation, hydrogenolysis, etherification, dehydration, esterification and acetalization [3].

In the middle of various catalytic processes of glycerol conversion, glycerol is a good reactant for oxygenated compounds such as acetal and ketal which produce from acetalization of glycerol and aldehyde or ketone using acid catalyst. The acetalization of glycerol with acetone gives two isomer products as fuel additive,

namely (2,2-dimethyl-[1,3]dioxane-4-yl)-methanol (also known as solketal) and 2,2-dimethyl-[1,3]dioxane-5-ol (Scheme 1.2).

Solketal is utilized for the additive in fuel and anti-knocking which increase the octane and cetane numbers, reduce coke and decrease in harmful emissions when blended with diesel [4], [5]. In addition, this compound can be used as plasticizer in polytrimethylene terephthalate and polyurethane process [6]. Furthermore, solketal can be used in perfume and cosmetic industries [7].
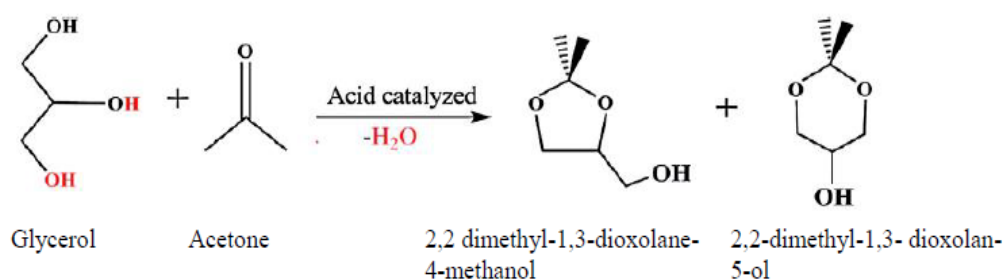
Scheme 1.2 Acetalization of glycerol with acetone

Traditionally, acetalization of glycerol with acetone was carried out in batch reactor using homogeneous catalysts such as *p*-toluenesulphonic acid [8] , H_2SO_4 [9] and $SnCl_2$ [10]. However, there is several disadvantages such as corrosion, catalyst separation from the product stream and environmental toxicity. Therefore, heterogeneous catalysts are preferred for this reaction. From previous researches, acetalization with acetone was studied with various heterogeneous catalysts for example silica-induced heteropolyacids [11], promoted zirconia [12], sulfonated carbon-silica composite [13], supported on metaloxides [14] , Amberlyst-15 [15] and zeolite beta [16].

Among of various catalysts, Amberlyst-15 was found to be more active than all the other solid acid catalysts because of the presence of sulfonic functionality with high amount of Brønsted acid site. Meanwhile, zeolite beta was also gave high glycerol conversion that may be its appropriate pore size and pore distribution. Thus, the sulfonated functionalized on zeolite beta is interesting to use as catalysts in acetalization of glycerol with acetone. However, zeolite beta have small pore size that limit their potential for acetalization with larger molecule due to diffusion problems.

In addition, the ordered MCM-41 has grated attention materials because of its uniform hexagonal mesoporous structure and high specific surface area [17]. Moreover, the pore size distribution of MCM-41 (ranges from 2-10 nm) is also facilitate the diffusion of the large molecule such as cyclohexanone, cyclooctanone, and cyclododecanone. However, MCM-41 has very low acidity. Therefore, MCM-41 were improved by the incorporation of sulfonic groups to increase the Brønsted acid sites, which is important role for acetalization reaction [18].

The aim of this work is to study the acetalization of glycerol with acetone using sulfonic functionalized beta zeolite and mesoporous MCM-41 as catalysts. These catalyst were synthesized by grafting method and characterized by X-ray diffraction, scanning electron microscopy, N_2 adsorption-desorption and acid-base titration. Moreover, the acetalization of glycerol with other ketone/aldehydes were investigated over sulfonated H-beta and MCM-41 catalysts, which compared to commercial catalyst like H-beta and Amberlyst-15.

1.2 Literature review

1.2.1 Sulfonic acid functionalized on catalyst

In 2000, Melero et al. developed for the syntheses of functionalized mesoporous materials SBA-15 with sulfonic groups involving the co-condensation of tetraethoxysilane and mercapto-propyltrimethoxysilane (MPTMS) in the presence of block copolymers (Pluronic P123) and hydrogen peroxide under acidic conditions. The XRD, N_2 adsorption-desorption, TGA, and ^{13}C NMR techniques were used for confirmation that the propyl-thiol groups and propyl- sulfonic groups were grafted on surface area [19].

In 2013, Valeria et al. studied the functionalization of three commercial faujasite zeolites (FAU) with difference chemical composition (Si/Al mole ratio of 3.4, 16.3 and 48.7) and textural properties. The propyl sulfonic functionalized FAU was synthesized by post grafting of mercapto-propyl groups followed by conversion into propyl sulfonic group. From the N_2 adsorption-desorption measurement, the BET surface area of FAU with Si/Al mole ratio of 3.4, 16.3 and 48.7 were 530, 813, 823 cm^2/g, respectively. They reported that the extent of surface functionalization of the zeolite is higher for Al-rich faujasite because of the number of hydroxyl groups on surface. However, the functionalization of the surface with the propyl sulfonic groups hinders the access of water molecules [20].

In 2015, Sirima et al. studied the performance of Pr-SO_3H functionalized mesoporous silica SBA-15 (rope, rod and fiber) MCM-41on esterification on fatty acids. The sulfonated MCM-41 and SBA-15 catalysts were successfully prepared by post grafting with 3-mercaptopropyltrimrethoxysilane as propyl-thiol precursor. The XRD, nitrogen adsorption-desorption, FTIR and acid-base titration were used for confirmed the incorporation of propyl sulfonic groups into the mesoporous silica. The MCM-41-Pr-SO_3H catalyst exhibited the BET surface area, pore diameter and total pore volume lower than MCM-41, with low activity because its smaller pore size than reactant [21].

1.2.2 Synthesis of solketal

1.2.2.1 Homogeneous catalysts

In 2011, Suriyaprapadilok and Kitiyanan reported the synthesis of solketal using 1 wt% *p*-toluenesulfonic acid as catalyst. The reaction was carried out in the batch reactor with total reflux. This research studied the effect of mole ratio and reaction time. The experimental results showed at 1:6 mole ratios of glycerol to acetone provided the highest conversion (82.7%) at 12 h. In conclusion, the increasing of mole ratio can increase the conversion of glycerol. However, it could not achieve 100% conversion due to the equilibrium limitation [8].

In 2012, Monbaliu et al. developed and optimized solketal production from glycerol using a Corning Advanced-Flow™ glass reactor to prevent corrosion of sulfuric acid. The impact of the temperature and the excess of acetone were investigated. It was found that 69% conversion of glycerol was achieved by using 10 mol % of sulfuric acid with 4 equivalence of acetone and 10 g min^{-1} flow of glycerol at 75°C. From the results, high temperature and concentration led to significant degradation reaction of glycerol [9].

In 2013, Fernanda et al. studied conversion of glycerol to solketal by SnCl$_2$ catalyst at room temperature and in solvent free condition. The effect of several parameters, such as catalyst loading, acetone/glycerol mole ratio, and temperature were investigated. The reaction condition was 1.5 mol% SnCl$_2$ with 4 equivalence of acetone at 25°C after 1 h. From the result, exhibited the highest value of 81% glycerol conversion, 98% solketal selectivity and 79% solketal yield. Moreover, they claimed that SnCl$_2$ was an efficient catalyst due to its solubility in the reaction medium and high water resistance. However, SnCl$_2$ has been classified as toxicity that possibly induce DNA damage and hazard embryo [10].

2.1.2.2 Heterogeneous catalyst

In 2011, Ferreira et al. reported the acetalization of glycerol with acetone using heteropolyacids immobilized in silica over batch reactor. In addition, the effect of and temperature on the glycerol acetalization were investigated. The highest 98% glycerol conversion with 97% solketal selectivity and 95% solketal yield was obtained by using 5wt% of PW_silica with 6 equivalence of acetone at 70°C after 3 h. However, the activity of immobilized catalysts lost 10–13% of its initial activity after the fourth used because of catalyst degradation [11].

In 2011, Reddy et al. studied the acetalization of glycerol with acetone over zirconia and promoted zirconia catalysts under mild reaction condition. They observed that the promoted zirconia catalysts exhibited promising catalytic activity. The highest catalytic activity provided the glycerol conversion of 98% with solketal yield of 95% and solketal selectivity of 97% using 5 wt% SO_4^{-2}/ZrO_2 with 6 equivalence of acetone at room temperature after 90 min [12].

In 2015, Gadamsetti et al. studied molybdenum phosphate catalysts supported on SBA-15 for the acetalization of glycerol with acetone. They reported that MoPO/SBA-15 catalyst was found to be highly catalytic activity. The effect of catalytic amount on the glycerol acetalization over various MoPO/SBA-15 catalysts was studied. At optimal condition, 40 wt% MoPO/SBA-15 to glycerol/acetone mole ratio of 1:3 at room temperature after 2 h gave high 90% glycerol conversion, 88.2 % solketal yield and 98% solketal selectivity. In catalyst reusability and stability studies, however, the catalytic activity of the spent 40 wt% MoPO/SBA-15 sample decreased due to the leaching of the MoPO species [14].

In 2011, Silva and Mota studied the influence of impurities on the catalytic performance of Amberlyst-15 and zeolite-beta toward acetalization of glycerol with acetone. Three main impurities which are water, methanol, and sodium chloride were added at various amount in the reaction. All among impurities, they found that glycerol conversion was dramatically decreased when water and NaCl were added. In addition, Amberlyst-15 is significantly less resistant to the presence of water than zeolite beta. Without impurities, however, Amberlyst-15 showed the glycerol conversion of 95% higher than zeolite beta, using 5 wt% of catalyst loading with glycerol/acetone mole ratio of 1:2 at room temperature after 1 h [16].

In 2015, Manjunathan et al. studied effect of crystallite size and the role of acidity of beta zeolite on acetalization of glycerol to produce solketal at room temperature. In batch reactor, 5 wt% of H-beta with acetone to glycerol mole ratio of 2 at room temperature, the result showed the best performance in 1 h with 86% of glycerol conversion and 98.5% of selectivity to solketal. Additional, they reported that the H-Beta zeolite with lower crystallite size (average: 135 nm) provided higher catalytic activity than H-Beta with high average crystallite size of 450 nm due to lower diffusion path length [22].

In 2013, Nanda et al. synthesized a carbon-mesoporous silica composite using glucose as both carbon source and structure directing agent for solketal production. From the results, the best performance was 82% glycerol conversion and 99% solketal yield using 5 wt% of catalyst with glycerol to acetone mole ratio of 1:6 at 70°C for 30 min. This material was functionalized with sulfonic acid in order to produce an acid catalyst. The results exhibited a high glycerol conversion and also remained an efficient catalyst after the fourth use. However, the disadvantage is that several synthesis step were need to obtain these composite materials [13].

In 2015, Swetha et al. reported organic–inorganic hybrid catalyst which prepared from organic ammonium salt and heteropolyacids. This material showed highly active and selective heterogeneous catalyst for the condensation reaction of glycerol with acetone at room temperature. From the results, the optimal condition (30°C, acetone to glycerol mole ratio of 6, reaction time of 1 h) provided 94% glycerol conversion and 98% solketal selectivity by using 3wt% $(C_3H_7)_4N^+$/PWA as catalyst. Moreover, this catalyst was truly heterogeneous and showed good reusability for 3 recycles of catalyst [23].

1.2.3 Acetalization of glycerol with other carbonyl compound.

In 2010, the organoiridium derivatives $[Cp^*IrCl_2]_2$(Cp^* = pentamethylcyclopentadienyl) and $[Cp^*Ir(Bu_2$-NHC)Cl$_2]$, (Bu_2-NHC = 1,3-di-*n*-butylimidazolylidene) catalyzed was found to be effective catalysts for glycerol acetalization with various aldehydes and ketone, including acetone, acetophenone, cyclohexanone 2,4-dimethylpentanone, benzaldehyde and octanal, as reported by CorradoCrotti et al. From the results, all the catalytic reactions produced the five-membered cyclic ketals, as main products, with selectivity of 94–100% for ketals, and up to 83% for acetals [24].

In 2015, Pawar et al. reported that solvent-free, conventional thermal activation, and non-conventional microwave/ultrasonic activation in the liquid phase are able to selectively transform glycerol into cyclic acetals and ketals. Moreover, they used an optimized acid activated clay catalyst bentonite clay for this reaction. The acetalization of glycerol with carbonyl compound such as cyclohexanone, benzaldehyde, phenyl acetaldehyde, and Furan aldehyde were studied. To summarized, the 6N H_2SO_4 treated clay was found to superior quantitative Brønsted acid and Lewis acidic sites with exhibiting a high conversion of glycerol and excellent selectivity within much less activation time [25].

1.3 Objective

1. To synthesize H-beta-Pr-SO$_3$H and MCM-41-Pr-SO$_3$H catalyst by grafting method and characterize all synthesized catalyst.
2. To study the effect of reaction time, reaction temperature, mole ration of glycerol to acetone and catalyst loading.
3. To study activity of reused catalyst.
4. To study acetalization of glycerol with other ketones or aldehyde.

1.4 Scopes of work

1. To synthesize H-beta-Pr-SO$_3$H and MCM-41-Pr-SO$_3$H by grafting method.
2. To characterize all synthesized catalysts.
3. To compare catalytic activity of synthesized catalysts with other commercial catalysts.
4. To study the effects of reaction time, reaction temperature, mole ratio of glycerol to acetone and catalyst loading on acetalization of glycerol with acetone.
5. To study activity of the reused catalyst.
6. To study acetalization of glycerol with other ketones/aldehyde.

CHAPTER 2

THEORY

2.1 Catalysts

A catalyst is a substance that increases in the rate of a chemical reaction without itself appearing in the products by lowering its activated energy. Moreover, catalysts can continue to act repeatedly because they are not consumed in the catalyzed reaction. Only a very small amount of catalyst is used in reaction. In addition, the catalyst may capacitate the reaction at lower temperatures, or expand reaction rate or selectivity. An energy profile diagram of reaction with and without catalyst is illustrated in Figure 2.1.
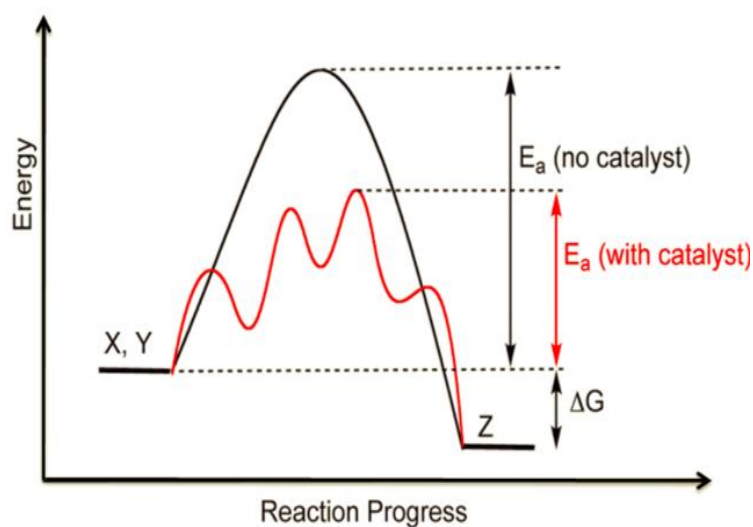
Figure 2.1 An energy profile diagram of reaction with and without catalyst [26].

2.2 Properties of industrial catalysts

Normally, efficiency of a catalyst for industrial process depends on three properties [27].

a) **Activity** of catalysts measure by rate of reaction compare with amount of catalyst. A high activity catalyst will be given high productivity which the less amount of the catalyst is utilized or the reaction is performed in mild condition, particularly temperature, which enhances selectivity and stability if the thermodynamic is more favorable. It is appropriate to measure reaction rate in the temperature that will be occurred in the reactor.

b) **Selectivity** is the ability of catalysts to direct reaction to yield particular products. The selectivity can be calculate by the fraction of starting material that is converted to expected product, whereas undesirable competitive and consecutive reactions are suppressed.

c) **Stability** of catalyst is a vary importance for economic process. It used for determining of its lifetime in industrial process. Catalyst stability is influenced by various factors such as decomposition, coking and poisoning. Deactivated catalysts can often be regenerated before they ultimately have to be replaced.

For various reasons, the target quantities should be given the following order of priority;

<div align="center">

Selectivity > Stability > Activity

</div>

In all process that uses zeolites as catalysts, their activity, selectivity and stability depends not only on the type of active sites, but also on their location inside the zeolite structure.

2.3 Type of catalysts

Catalysts can be categorized into two main type by boundary of catalyst and reactant: heterogeneous and homogeneous. In **homogeneous** catalyst, the catalyst is in the same phase as the reactants, whereas **heterogeneous** catalyst is in a different phase to the reactants and products [27]. The comparison of homogeneous and heterogeneous catalysts is shown in table 2.1.

Table 2.1 Comparison of homogeneous and heterogeneous catalysts

Consideration	Homogeneous catalyst	Heterogeneous catalyst
1. Active center	All metal atom	Only surface atom
2. Concentration	Low	High
3. Selectivity	High	Low
4. diffusion problems	Practically absent	Present
5. reaction condition	Mild	Severe
6. Application	Limited	Wide
7. Activity loss	Inversion reaction with product	Sintering of the metal crystallites, poisoning
8. Structure/stoichiometry	Defined	Undefined
9. Modification possibility	High	Low
10. Thermal stability	Low	High
11. Catalytic separation	Sometime laborious	Fixed-bed ; unnecessary Suspension : filtration
12. Catalytic recycle	Possible	Unnecessary
13. Cost of	high	Low

The major disadvantage of homogeneous catalyst is the difficulties in separation from product and catalyst regeneration. Consequence, heterogeneous catalyst is wider use in industry.

2.4 Porous molecular sieves

A molecular sieve is a material with pores of uniform size that exhibited adsorption properties which can be classified on the IUPAC deifications into three main types depending on their pore sizes [28]. Properties and examples of these materials are shown in Table 2.2.

Table 2.2 IUPAC classification of porous materials

Type of porous molecular sieve	Pore size (Å)	Example
Microporous material	<20	Zeolites, activated carbon
Mesoporous material	20-50	MCM-41, SBA-15, Pillared clay
Macroporous material	>50	glasses

2.5 Zeolite

2.5.1 Zeolite structures

Zeolites, a types of molecular sieve, are microporous crystalline aluminosilicate that contain uniform pores and captivity with molecular dimensions. Commonly, zeolites used as commercial adsorbents and catalyst. A zeolite has a three dimensional network structure of tetrahedral primary building unit (PBU) which consists of four oxygen anion with either silicon $[SiO_4]^{4-}$ or aluminum cation $[AlO_4]^{5-}$ in center, as illuminated in Figure 2.2. [29]
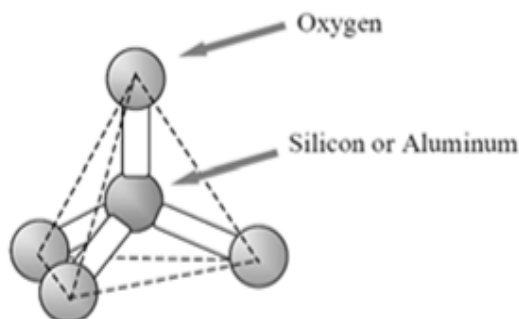
Figure 2.2 Primary building unit of zeolite structure

The primary building unit (PBU) of a molecular sieve is the individual tetrahedral unit. The topology of all known molecular sieve framework types can be described in terms of a finite number of specific combinations of tetrahedral called "secondary building units" (SBU's). A molecular sieve framework is made up of one type of SBU only. These secondary building units consist of 4, 5, 6, and 8 member single rings, 4-4, 6-6, and 8-8-member double rings, and 4-1, 5-1, and 4-4-1 branched rings as shown in Figure 2.3 [30].
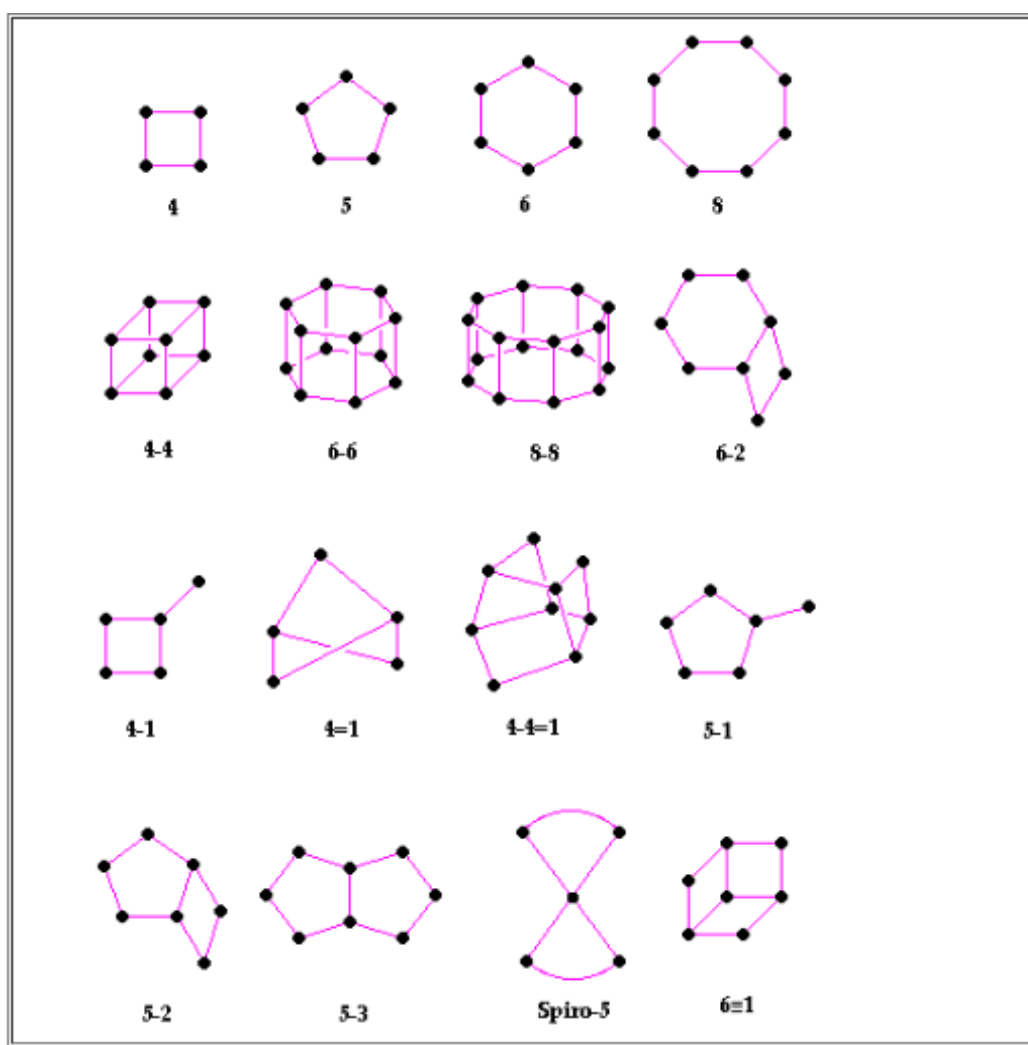
Figure 2.3 Secondary building units found in zeolite structures [31]

The aluminosilicate zeolites constructed from SiO_4 tetrahedral and AlO_4 tetrahedral possess an anionic framework, the negative charge of which is compensated by extra framework cations. The structure of zeolites is shown in Figure 2.4. The empirical formula of an aluminosilicate zeolite can be expressed as

$$M_{x/n}[(AlO_2)_x(SiO_2)_y \cdot wH_2O$$
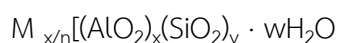
Where M atom is extra framework cation with valence of n, generally group I or II ions, but be other metals, nonmetals or even organic cations. Total number of alumina and silica per unit cell are represented by x and y, respectively. Thus, summation of x and y is the total amount of tetra unit in unit cell. The portion [ ] is the framework composition and z is the number of water molecule located in the channels and cavities inside the zeolite structure.
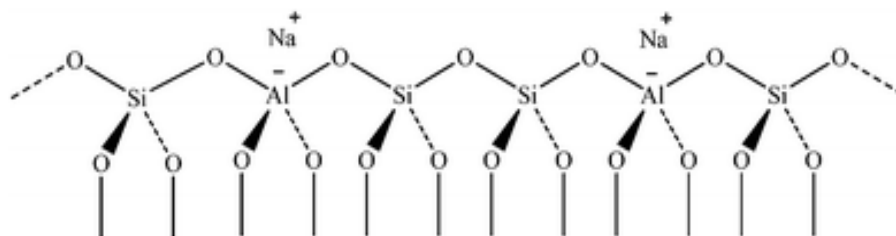
Figure 2.4 The structure of zeolites.

According to different pore sizes, zeolite can be classified into three group based on different number of tetrahedral atoms, as shown in Figure 2.5, which are small pore, medium pore and large pore. Small pore is consist of 8 membered of oxygen ring systems which pore size between 3.5-4.5 Å, for example, zeolite A and chabazite. In medium pore, zeolite is consist of 10 membered oxygen ring systems ring which pore size between 4.5-6.0 Å such as ZSM-5, ZSM-11 and TS-1. The large pore means 12–membered ring oxygen bring opening bigger than 6.0 Å such as zeolite beta, mordenite, zeolite x and zeolite Y [29].
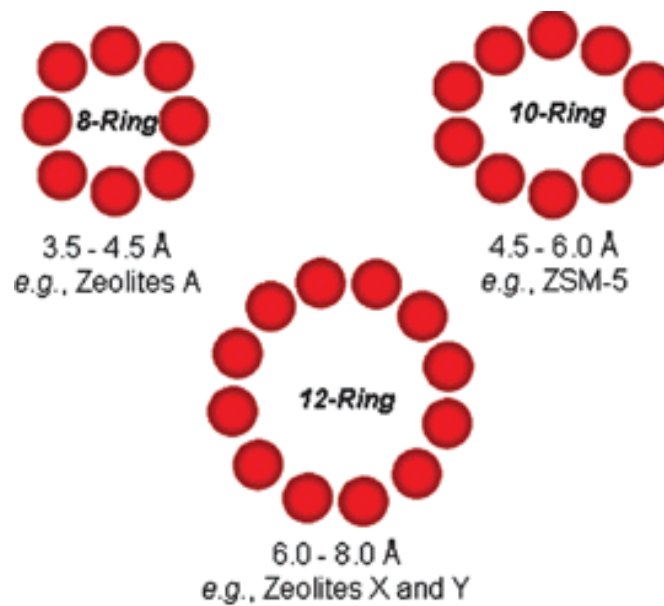
Figure 2.5 Three types of pore opening in the zeolite framework [29].

2.5.2 Acid sites of zeolites

Acidity is one of the most important characteristics of zeolites. There are two type of acid sites of zeolites which are Brønsted acid sites (BAS) and Lewis acid sites (LAS), as exhibited in Figure 2.6 [32]. Brønsted acid sites is proton donator, while Lewis acid sites is proton acceptor.
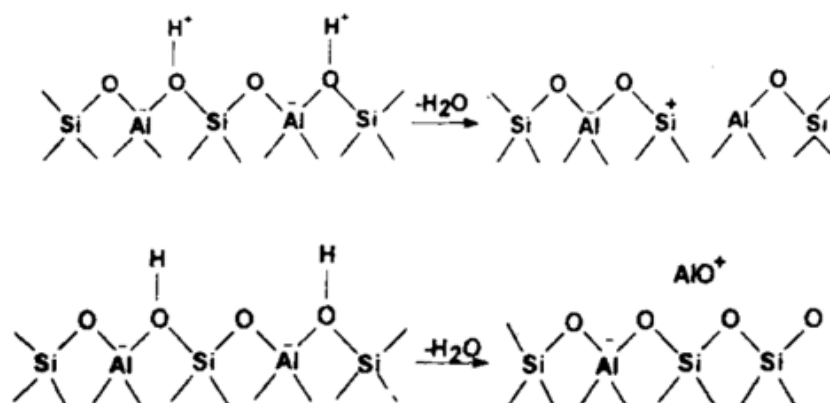
Figure 2.6 (a) Brønsted acid site and (b) Lewis acid sites in zeolites [33].

2.5.3 Selectivity of zeolite [34]

Selectivity of zeolite is important role for using specific reaction. There are three of selectivity in porous material as shown in Figure 2.7.

Product selectivity is the result of the differences between the diffusivities of the reaction products in the pores of the zeolite.

Transition state shape selectivity occurs when the configuration of a potential transition state is spatially constraint compared to other transition states and therefore only certain reaction pathways are possible.

Shape and size selectivity clearly highlight the important role of the size and shape of pore, cage and channels that constitute the zeolite framework.
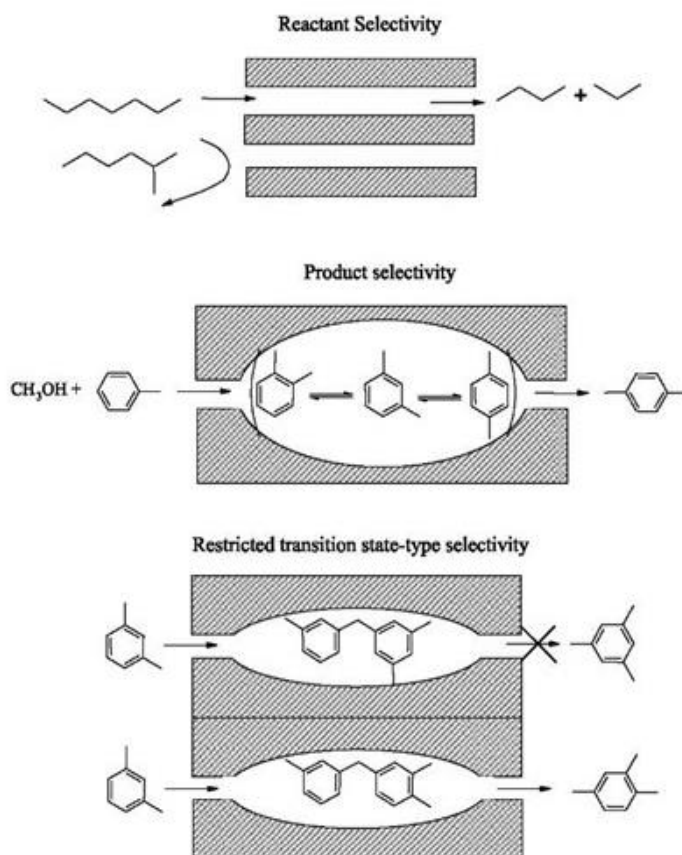
Figure 2.7 Three types of selectivity in porous material.

2.6 Mesoporous material

A mesoporous material, types of molecular sieve, is a material containing pores with diameters between 2 and 50 nm for example silica or transitional alumina or modified layered material [35].

2.6.1 Classification of mesoporous materials

Mesoporous materials can be classified by different synthetic method. By varying different types of templates used and pH or gel, synthesizing hexagonal mesoporous materials can be obtained. The interaction of various types of template with inorganic species for assembling these material and the condition typically employed for a synthesis are different, as summarized in Table 2.3 [35], [36], [37].

Table 2.3 Various synthesis condition of hexagonal mesoporous material and the types of interaction between templates and inorganic species

Material	template	Assembly	Solution
MCM-41	Quaternary ammonium salt	Electrostatic	Base or acid
FSM-16	Quaternary ammonium salt	Electrostatic	Base
SBA-15	Amphilic triblock copolymer	H- bonding	Acid
HMS	Primary amine	H- bonding	neutral

MCM-41 and FSM-16 can be prepared using quaternary ammonium salt as a template. Meanwhile, SBA-15 can be synthesized using amphilic triblock copolymer as modified template in presence of acidic condition. In cases of HMS, primary amine can be used as template and must be prepared in neutral and environmentally benign condition. Although these materials have the same hexagonal structure, some properties are different, as shown in Table 2.4.

Table 2.4 Properties of some hexagonal mesoporous material

materials	Pore size (Å)	Wall thickness (nm)	BET surface area (m^2/g)	Framework structure
MCM-41	20-100	1	>1000	Honey comb
FSM-16	15-32	-	680-1000	Fold sheet
SBA-15	46-300	3-6	630-1000	Rope-like
HMS	29-40	1-2	640-1000	wormhole

2.6.2 Synthesis schemes of mesoporous materials

Crystalline molecular sieves are generally obtained by hydrothermal crystallization. The reaction gel, usually, contains cations to form the framework; anions species organic template and solvent. Typically, the nature of template can be considered into two parts that are hydrophobic tail on the alkyl chain side and hydrophilic on to the other side. The primary, secondary tertiary and quaternary amines, alcohols, crown or linear ethers, and as well as polymers are used as template.

2.6.3 Interactions between inorganic species and surfactant micelles.

In general, the models of the formation of mesoporous material are predicted upon the presence of surfactants in a solution to direct the formation of inorganic microstructure from stabilized inorganic precursors [38]. The type of interaction between the surfactant and the inorganic species was significantly different depending on the various synthesis routes as shown in Table 2.5.

Table 2.5 Example routes for interactions between the surfactants and the inorganic soluble species

Surfactant type	Inorganic type	Interaction type	Example material
Cationic	I^-	S^+I^-	MCM-41, MCM-48
	I^+X^-	$S^+X^-I^+$	SBA-1, SBA-2, zinc phosphate
	I^oF^-	$S^+F^-I^o$	Silica
Anionic	I^+	S^-I^+	Al, Mg, Mn, Ga
	I^-M^+	$S^-M^+I^-$	Alumina, zinc oxide
Neutral S^o or N^o	I^o	S^oI^o or N^oI^o	HMS, MSU-X, aluminum oxide
	I^+X^-	$S^oX^-I^+$	SBA-15

Where S^x or N^x surfactant with charge of X

I^x : inorganic species with charge of X

X^- : halogenide anions

F^- : fluoride anion

M^{n+} : with charge of X

Using inorganic surfactant, the hydrophilic head binds with organic species though electrostatic interaction. There are two possible formation route. Firstly, direct pathway: surfactant and inorganic species of which charges are opposite interact together direct. Another is the indirect pathway, occurring when the charges of surfactant and organic species are the same, so the counter ion in solution get involved as charge compensating species for example the $S^+X^-I^+$ path takes place under acidic conditions, in the present of halogenide anion and the $S^-M^+I^-$ route is the characteristic of basic media, in the existence of alkaline cation. Figure 2.8 shows the possible hybrid inorganic- organic interfaces.
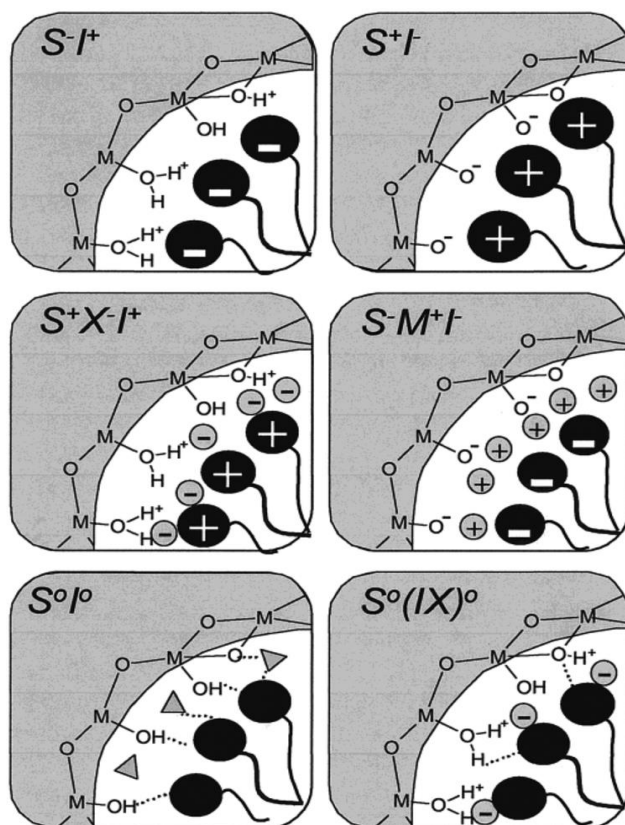
Figure 2.8 Schematic illustration of the different types of silica–surfactant interfaces [39].

In case of non-ionic surfactant, the main interaction between template and inorganic species is hydrogen bonding or dipolar. Nowadays, non-ionic surfactants give important commercial advantages in comparison to ionic surfactants because they are easily removable, nontoxic, biodegradable and relatively cheap.

2.6.4 Mechanisms formation of mesoporous materials

2.6.4.1 Liquid crystal templating mechanism

A liquid crystal templating (LCT) mechanism was proposed by the Mobil researchers that firstly reported for M41S material. The variation of surfactant concentration plays a significant role to control the structure. Figure 2.9 shows the possible way the LCT mechanism for hexagonal MCM-41 [38].
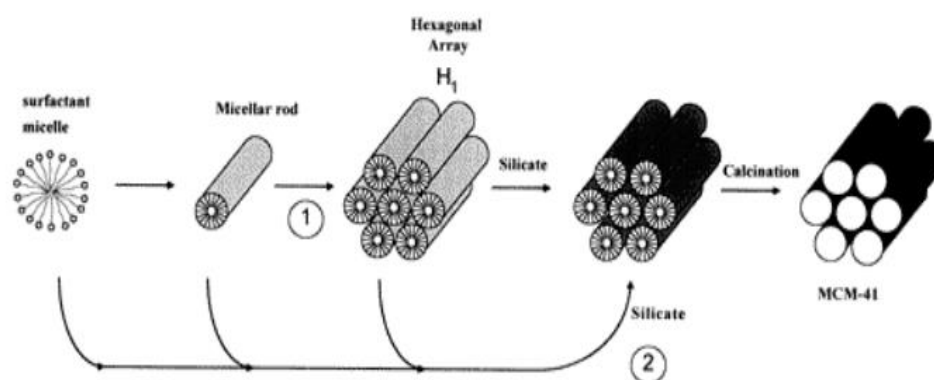
Figure 2.9 The possible ways for the LCT mechanism in MCM-41 synthesis [38]

2.6.4.2 Folding sheet formation

The interaction of ammonium surfactant into hydrated sodium silicate, which composed of singled-layered silica sheet call kanemite, produced the lamellar to hexagonal phase in FSM-16. After surfactants were ion exchanged into the layer structure, the silicates sheets were folded around the surfactants and condensed into hexagonal mesostructured. Folding sheet formation is illustrated in Figure 2.10.
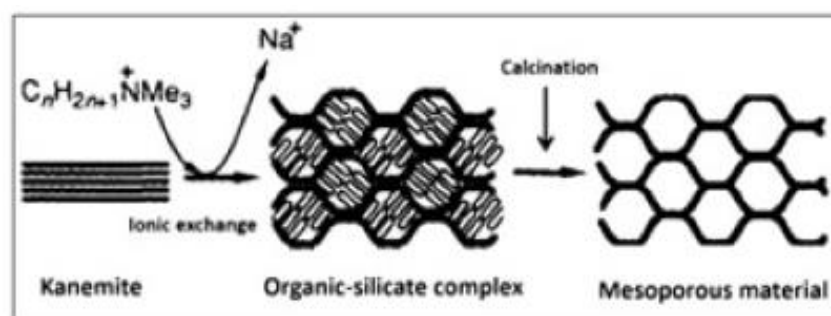
Figure 2.10 Folding Sheet Mechanism of FSM-16

2.6.4.1 Hydrogen bonding interaction

Hydrogen bonding interaction is the neutral templating produces mesoporous materials with thicker walls and higher thermal stability as compared to the LCT derived silicates. Figure 2.11 shows the shaded lobes on the surfactant head groups are electron lone pairs that participate in H bonding with framework silanols [40].
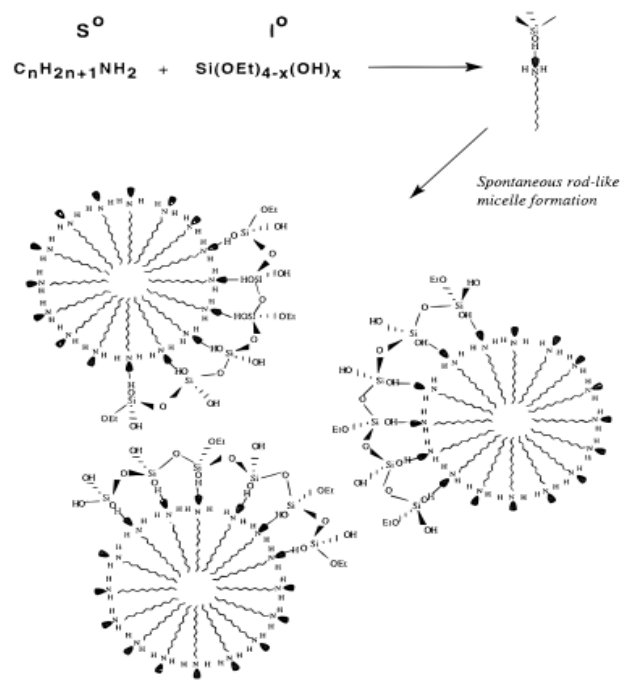
Figure 2.11 H-bonding in HMS formation.

2.6.5 Synthesis strategy of mesoporous material using block–copolymer as structure directing agent

The synthesis of mesoporous material are done in extreme (alkaline) pH condition and the obtained materials have pore size in range of 15 to 100 Å only. However, by this mean, two limitations occur;

(a) The lower stability of the obtained materials ; due to the thinner pore wall of materials (8-13 Å)

(b) Difficult to expending the pore size; the ionic surfactants give a limited pore size. The only way to expand the pore size is in employing swelling agent.

Therefore, the block copolymer has been used to solve these problems. The properties of block copolymer can be continuously tuned by adjusting solvent composition, molecular weight, or type of polymer. Typical block copolymer used as templates are shown in figure 2.12.
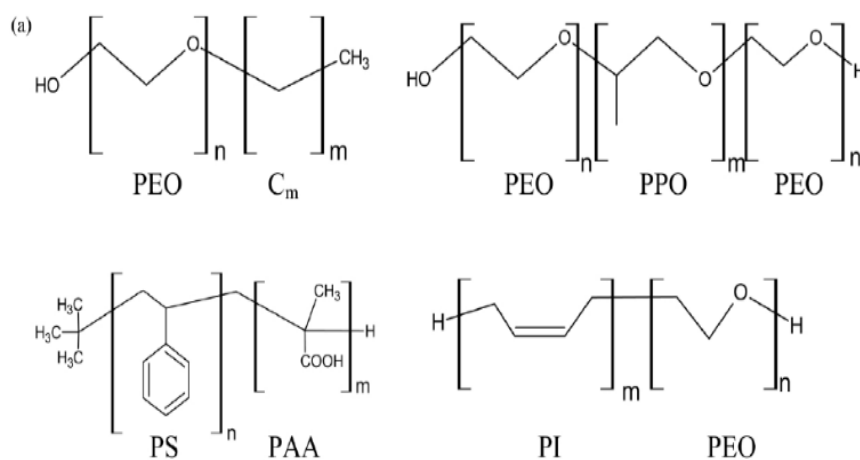
Figure 2.12 Block Copolymer templates used in mesostructure generation

Some advantages of using these block copolymer are:

(1) The thicker wall thickness (about 15-40 Å), enhancing hydrothermal and thermal stability of materials

(2) Pore diameter can be tuned easier by vary type or concentration of polymer.

(3) Easies to remove from mineral framework by thermal treatment or solvent.

Interaction between block copolymer template and inorganic species, calls hybrid interphase (HI), is particularly important, and especially in PEO-PPO based one. Different possible interactions take place at the HI are schematized in Figure 2.13
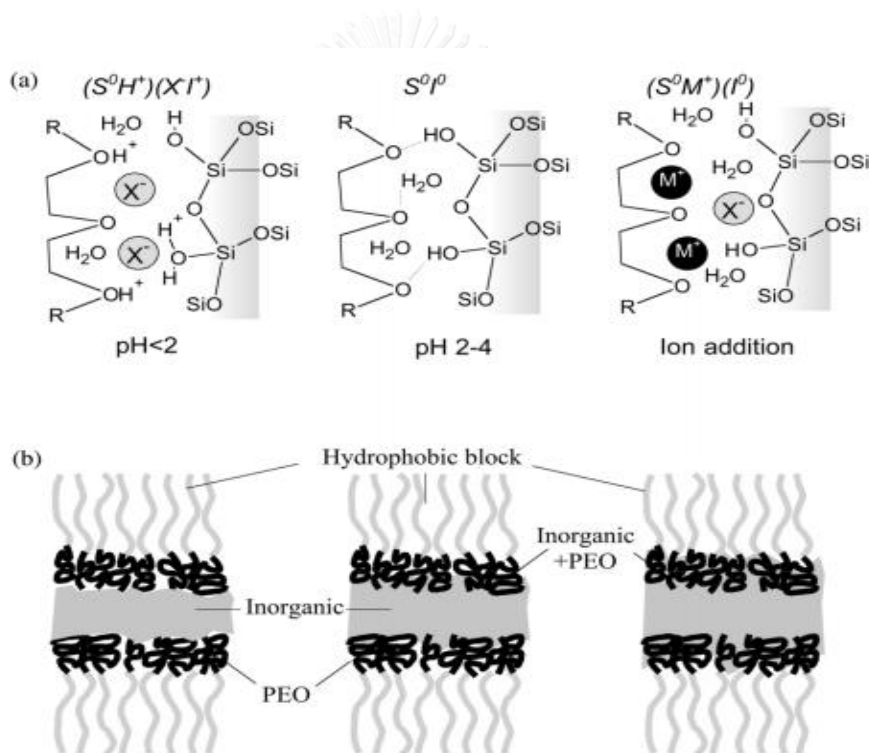
Figure 2.13 Different possible interactions take place at the hybrid interphase [41]

2.7 Zeolite beta

2.7.1 Structure of zeolite beta

Beta zeolite is aluminosilicate microporous material with BEA framework type that was first synthesized in 1967. The framework structure is illustrated in Figure 2.15. According to its structure, beta zeolite consists of an intergrowth of two distinct structures termed Polymorphs A and B, as shown in Figure 2.14. Both polymorphs has 12 membered ring openings 0.76 X 0.64 nm with a three dimensional channel system. Because zeolite beta has strong acidic sites, it is widely used as solid acid catalyst in various chemical and petrochemical processes [42].
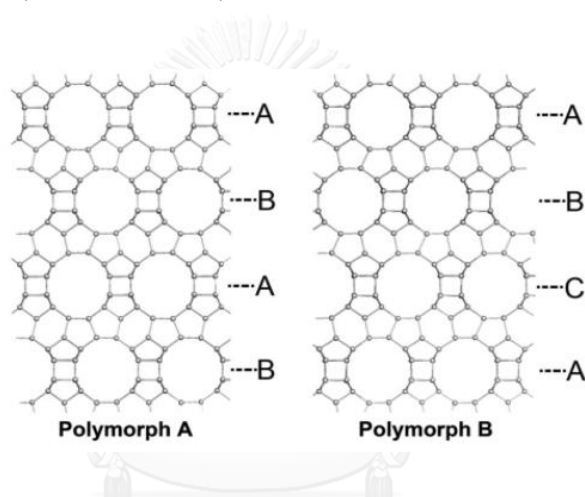
Figure 2.14 Structures of polymorph A and polymorph B of zeolite Beta [43]
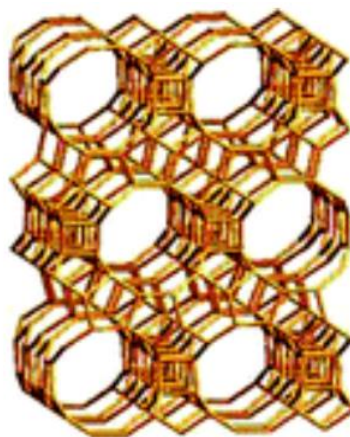
Figure 2.15 Framework of beta zeolite [44]

2.8 MCM-41

2.8.1 Structure and properties of MCM-41

MCM-41, Mobil composition of matter No.41, is the mesoporous which was developed by Molbil Oil Corporation. It is uniform arranged into hexagonal, honeycomb-like lattice, as shown in Figure 2.15 [3]. Because MCM-41 has high surface area (1000 m^2/g) and high pore volume with a sharp pore distribution, it is widely use as catalyst supports. However, MCM-41 has low acidity and low thermal stability. The Table 2.6 shows comparisons of three well know mesoporous material, MCM-41, SBA-15 and MCA in their characteristic properties [45].

Figure 2.15 Hexagonal of one-dimensional cylindrical pores of MCM-41

Table 2.6 Comparisons of three well know mesoporous material, MCM-41, SBA-15 and MCA in their characteristic properties [46], [47]

properties	MCM-41	SBA-15	MCA
Pore size (Å)	20-100	46-300	34.9
Pore volume (mL/g)	>0.7	0.8-1.23	0.82
Surface area (m^2/g)	>1000	690-1040	456
Wall thickness (Å)	10-15	31-64	9.4

2.8.2 Synthesis of MCM-41

In typically procedure of MCM-41 production consist of hydrolysis and condensation of a silicate source (Tetraethyl orthosilicate (TEOS)) and an aqueous surfactant solution (Cetyltrimethylammonium bromide (CTAB)). This stage leads to a silica framework which builds around the surfactant micelles which are referred to as 'as-synthesized' mesosilica. After this stage, as-synthesized mesosilica is removed the surfactant template to form porous by solvent extraction, calcination or microwave digestion. A possible mechanisms of the formation of MCM-41 is given in Figure 2.16. [48].
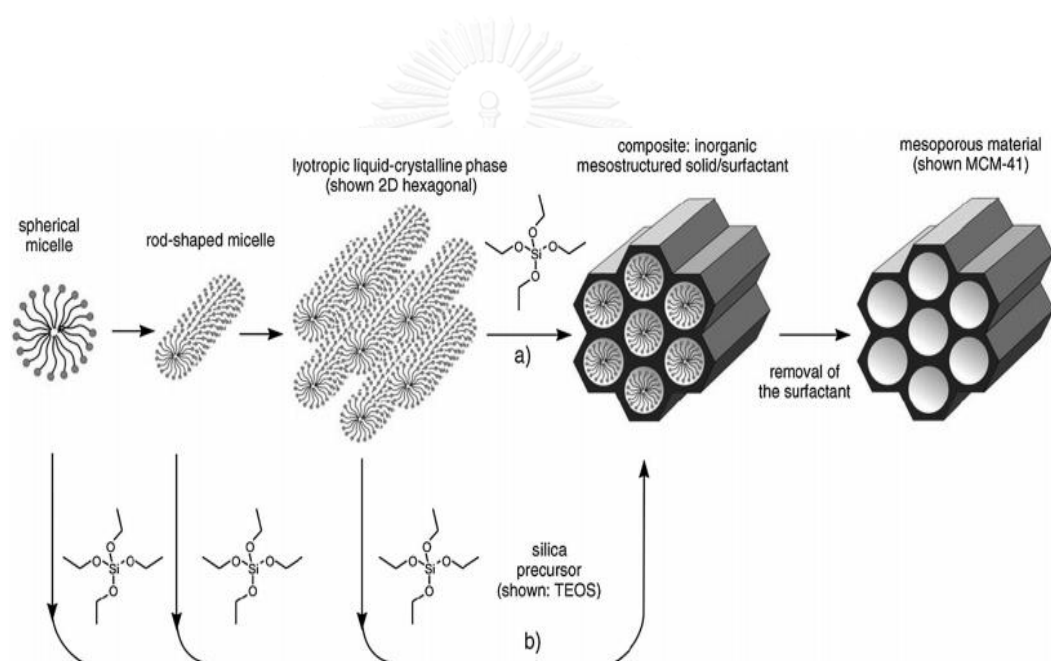
Figure 2.16 A possible mechanisms of the formation of MCM-41

2.9 Modification of catalyst

There are two strategies to incorporate organic group onto silica surface which are direct synthesis and post synthesis.

2.9.1 Direct synthesis

Direct synthesis consists of the co-condensation of siloxane and organo-siloxane precursors in the presence of corresponding structure-directing agent. Figure 2.17 illustrate the preparation of sulfonic acid modified mesostructured material. The incorporation of the organic precursor and the formation of the mesoporous material occur in a single synthetic step. After synthesis, there are two technique that usually used for remove the template within the pores to create porosity which are calcination and extraction. Calcination the synthetic material will destroy the incorporated organic functional groups. Extraction technique can be most effectively accomplished by solution [49].
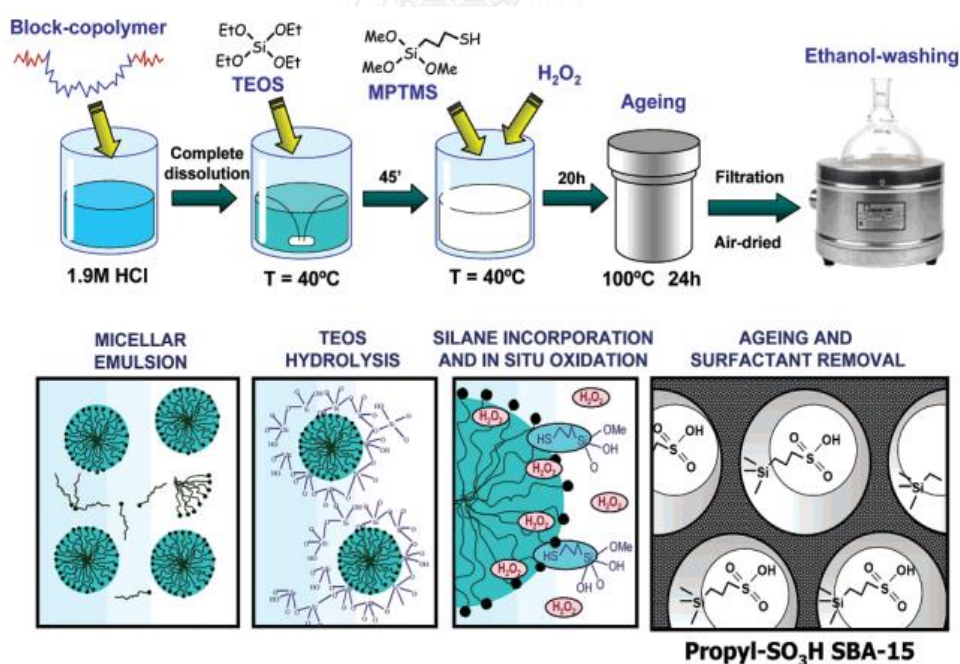
Figure 2.17 In-situ oxidation synthesis strategy for the preparation of sulfonic-acid-modified mesostructured materials [49]

2.9.2 Post synthesis (Grafting method)

Grafting procedure based on modification of the silica surface with organic groups though silylation reaction occurring on isolated (SI-OH) and germinal ($=Si(OH)_2$) silanol groups using tricholro- or trialkylmethoxy- organosilane and silyamines as organic precursors. Synthesis of sulfonic functionalized MCM-41 by post synthesis is shown in Figure 2.18. In typical procedure, calcined MCM-41 is refluxed with a silating agent such as 3-mercaptopropyltrimethoxysilane (MPTMS) in nonpolar solvent like toluene to immobilize thiol groups on the surface. Then, thiol functionalities are oxidized by hydrogen peroxide. The advantage of this procedure is good preservation of the mesostructured after post–modification [50].
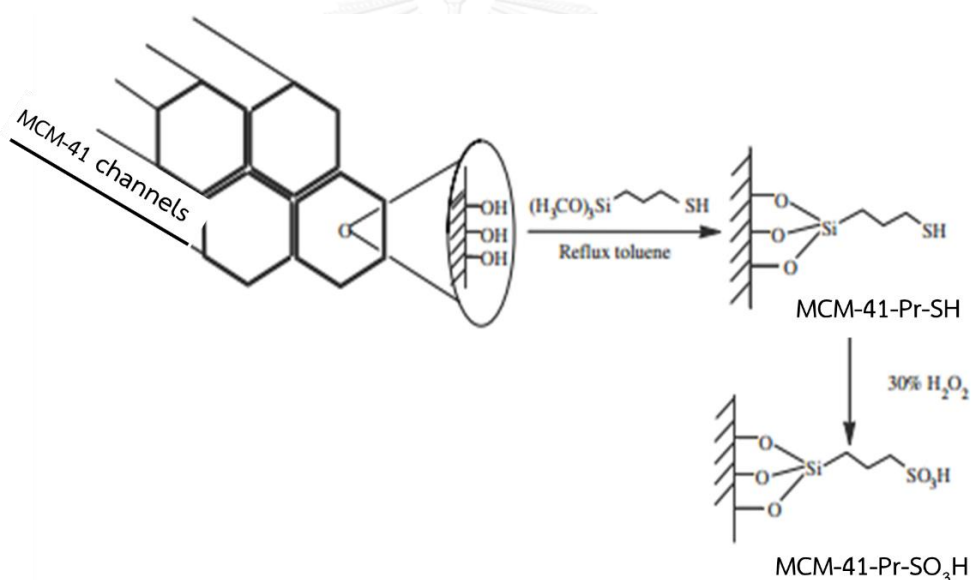
Figure 2.18 Synthesis of propyl-sulfonic acid functionalized MCM-41 [50]

The different between the two methods mainly involves the location of the organic functional group on the resulting silica material. The functional groups of grafted material only exhibited on the surface while the co-condensed material contained the groups on the surface and within the walls of silica framework.
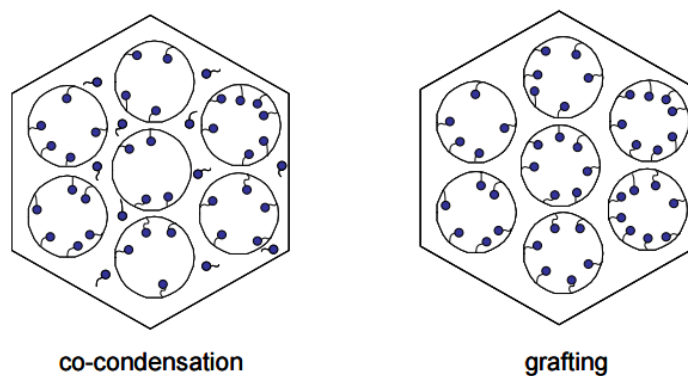
Figure 2.19 Comparison between co-condensation and grafting methods [50]

2.10 Amberlyst -15

Amberlyst-15 is ion exchange resin that having strongly acidic sulfonic group based on polystyrene. The structure is shown in Figure 2.20. Amberlyst-15 is brown-gray solid having particle size between 0.60-0.85 nm with maximum operating temperature of 120°C. In the past decade, Amberlyst-15 has been used in various acid catalyzed reactions because of its excellent source of strong acid. Moreover, it is safe to use, easy to measure, and readily removed at the end of the reaction. [51].
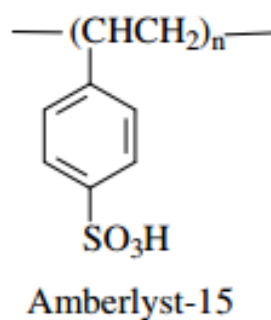
Figure 2.20 Structure of amberlyst-15 [52]

2.11 Characterization of materials

2.11.1 X-ray powder diffraction

X-ray diffraction is a common technique to study the atomic spacing and crystal structures. Moreover, it can be used for the study of component in samples. The fundamental principle of X-ray diffraction based on constructive interference of monochromatic X-rays and a crystalline sample. Basically, X-rays which was shoot to the sample which is making the diffraction of the radii at various angles. Figure 2.21 shows diffraction of x-ray by regular planes of atoms. The relationship between angle of incidence, the wavelength of the incident X-rays and spacing between the crystal lattice planes of atoms is known as Bragg's Law, expressed as:

$$n\lambda = 2d \sin\theta$$

Normally, Conversion of the diffraction peaks to d-spacing allows identification of the mineral because each mineral has a set of unique d-spacing. Typically, this is achieved by comparison of d-spacing with standard reference patterns [53], [54].
.
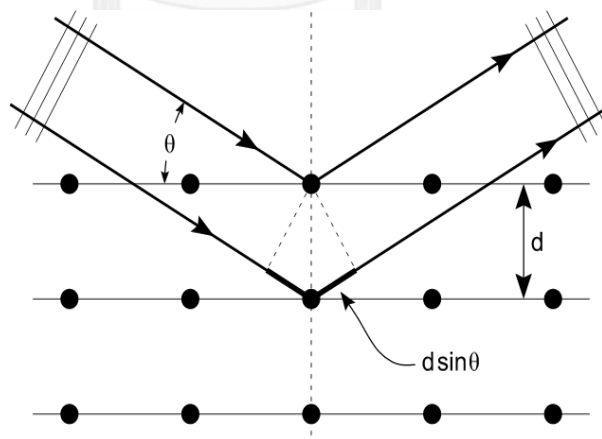
Figure 2.21 Diffraction of x-ray by regular planes of atoms [54]

2.11.2 Nitrogen adsorption-desorption technique

Nitrogen adsorption-desorption technique is gas adsorption analysis that use nitrogen as probe molecules. Normally, this technique is widely used for porosity and surface area measurements. Moreover, it also used for determination of pore size distribution of solid catalysts. The fundamental principle of this technique base on the process of adsorption that takes place on a solid surface, and adsorption processes between a solid (adsorbent) and a gas (adsorbate) at 77 K [55].

In typical adsorption, adsorption isotherms can be classify as one of 6 types, as shown in the table 2.7.

Relative pressure (p/p_0)
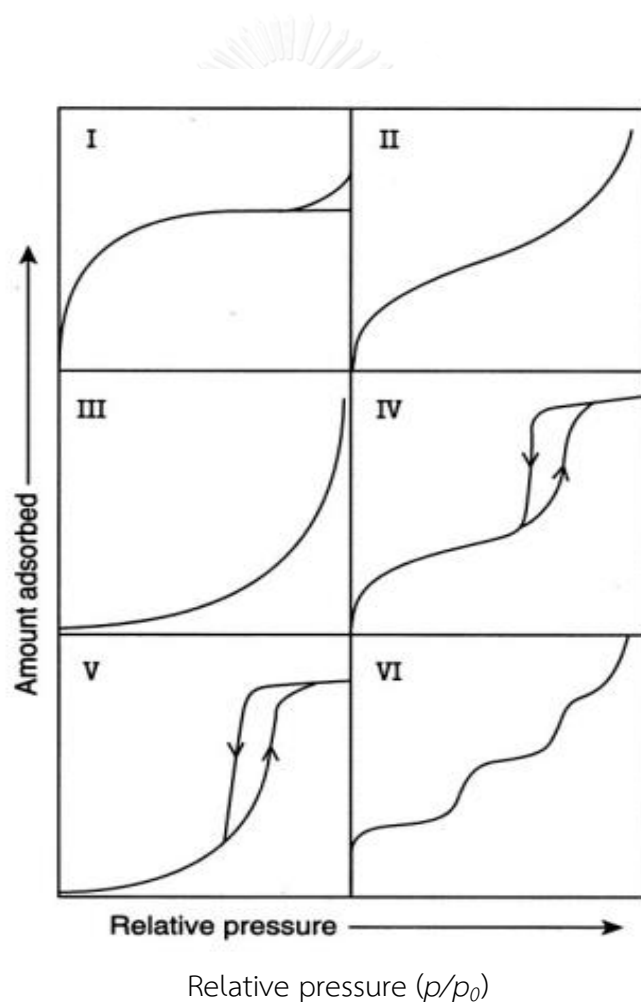
Figure 2.22 IUPAC classification of adsorption isotherms [56]

The Brunauer, Emmett and Teller (BET) is the most common method to determine the surface area of porous materials. The fundamental principle base on adsorption (physisorption) and desorption of nitrogen gas on materials' porous. There are 2 functions of BET method which are analysis and degas sample. Adsorption isotherm was measured when the sample was adsorbed nitrogen gas and degassed. BET equation is used for calculation specific surface area by using obtained adsorption data.

The data are treated according to the Brunauer, Emmett and Teller (BET) adsorption isotherm equation:

$$\frac{1}{\left[V_a\left(\frac{P_0}{P}-1\right)\right]} = \frac{C-1}{V_mC} \times \frac{P}{P_0} + \frac{1}{V_mC}$$

Table 2.7 Features of adsorption isotherms

type	features		Sample-Adsorptive example
	Interaction between sample surface and adsorbate	porosity	
I	Relatively strong	microporous	Activated carbon -nitrogen
II	Relatively strong	Nonporous	Oxide-Nitrogen
III	weak	nonporous	Carbon- Water vapor
IV	Relatively strong	mesoporous	Silica-Nitrogen
V	weak	mesoporous	
		microporous	Activated carbon-water vapor
VI	Relatively strong sample surface has an even distribution of energy	Nonporous	Graphite-krypton

2.11.3 Scanning electron microscope

Scanning electron microscopy (SEM), a type of electron microscope, is widely used to study morphology such as surface, size, and shape of particles. Moreover, it can be used to provide elemental identification and quantitative compositional information (EDX). According to principle of SEM, it uses a focused beam of high-energy electrons to generate a variety of signals at the surface of solid specimens to produce 3D image of a sample. The resolution of the SEM reaches 10-20 Å for high performance equipment [57]. The component of SEM is shown in Figure 2.23.
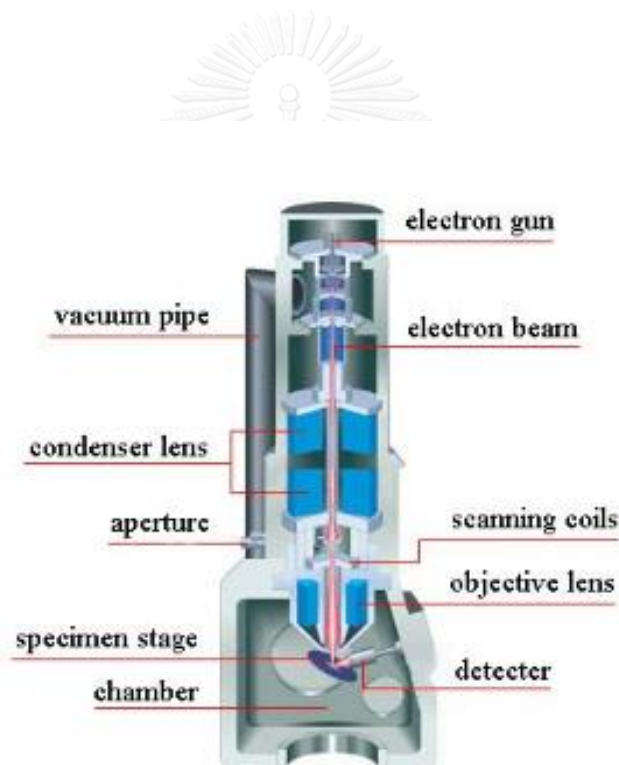
Figure 2.23 Scanning electron microscope [58]

2.12 Solketal and its application.

2.12.1 Proposed reaction mechanism

The proposed reaction mechanism of acid catalyzed of acetalization of glycerol with acetone was shown in Figure 2.24. Firstly, the carbonyl group of acetone is protonated by the acid sites in catalyst forming a carbocation. Then, the hydroxyl group of glycerol attacks the carbocation to form hemi-acetal intermediate. After that, the middle hydroxyl group of glycerol undergoes cyclization with water elimination to from solketal (give membered ring). While, the terminal hydroxyl group of glycerol attack on tertiary carbon atom with water elimination to from six membered ring [22].
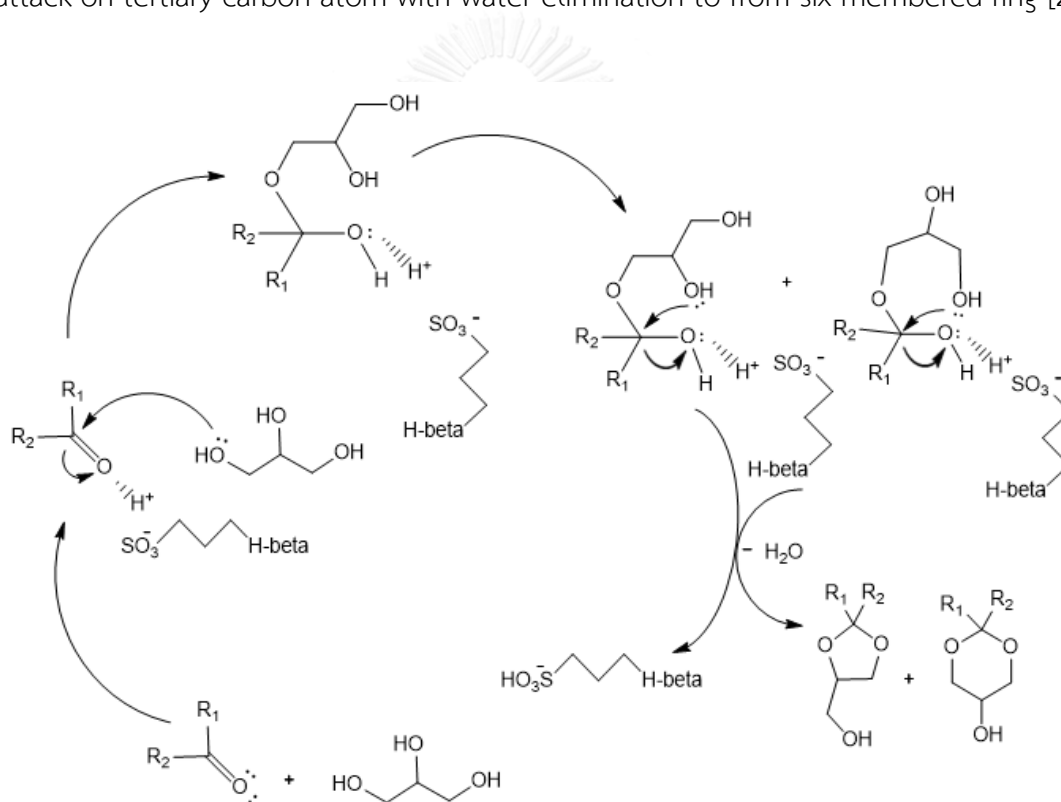
Figure 2.24 Mechanism for acetalization of glycerol with acetone

2.12.2 Application of solketal

Solketal ((2,2-Dimethyl-1,3-dioxolan-4-yl)methanol) is synthesized from acetalization of glycerol with acetone. It is a protected form of glycerol with an isopropylideneacetal group joining two neighboring hydroxyl groups. Solketal contains a chiral center on the center carbon of the glycerol backbone [59]. Solketal is a colourless and odourless liquid, completely soluble in water and stable under normal temperature and pressures. Due to its low toxicity, it has been reported that solketal is utilized for the additive in fuel and anti-knocking which increase the octane and cetane numbers, reduce coke and decrease in harmful emissions when blended with diesel [4], [5]. In addition, this compound can be used as plasticizer in polytrimethylene terephthalate and polyurethane process [6]. Furthermore, solketal can be used in perfume and cosmetic industries [7]
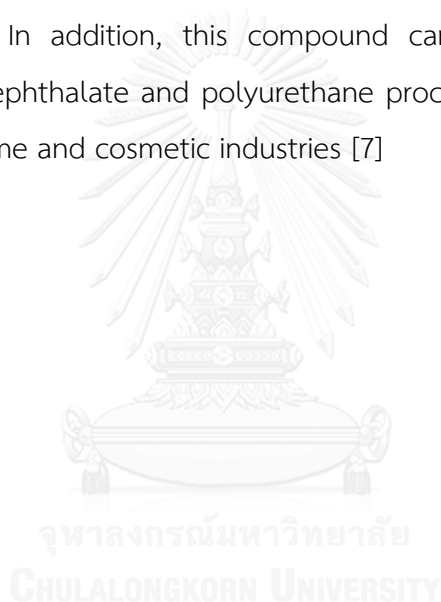
CHAPTER 3

EXPERIMENTS

3.1 Instrument and apparatus

3.1.1 X-ray diffraction

Powder X-ray diffraction pattern of synthesized catalysts were identified with a Rigaku D/MAX-2200 Ultima⁺ X-ray diffractometer equipped using Cu target X-ray tube (40 kV, 30 mA). For MCM-41 and sulfonated MCM-41, the samples were scanned at 2-theta angle in the range of 0.70 to 3.00 degree with 1.00 degree/min of scan speed. While, in case of commercial beta and sulfonated beta were scanned at 2-theta angle in the range of 5.0 to 50.00 degree with 1.00 degree/min of scan speed.

3.1.2 Specific surface area

Specific surface area, N_2 adsorption-desorption isotherms and pore size distribution of catalysts were determined by a BEL Japan, BELSORP mini28SP instrument. Before measurement, the unmodified catalysts and sulfonated catalysts and were pretreated at $400^{\circ}C$ and $150^{\circ}C$ for 3 h, respectively.

3.1.3 Nuclear magnetic resonance spectrometer (Solid state ^{13}C NMR)

The solid state C13-NMR spectra were obtained with Bruker DRX 400 spectrometer equipped with a magic-angle spin probe using a 4-mm ZrO_2 rotor.

3.1.4 Fourier transform infrared spectroscopy (FTIR)

Fourier transform infrared spectroscopy was performed in range of 400-4000 cm^{-1} with 4 cm^{-1} resolution on a Nicolet 6700 instrument. Prior to FTIR measurement, the powder samples were vacuum-dried at $100^{\circ}C$ for 30 min and embedded in KBr pellet.

3.1.5 Scanning electron microscope (SEM)

The morphology of synthesized materials was analyzed by JSM-5410 LV scanning electron microscope with 15 kV of acceleration. All sample were coated with sputter gold under vacuum for conductivity.

3.1.6 Gas chromatography

To preparation of sample for analysis, 0.5 g of reaction mixture from acetalization of glycerol was mixed with 1 g of 0.20 M n-dodecane as internal standard and 2 mL of dimethylformamide (DMF) as solvent. The mixture solution was analyzed using a Varian CP 3800 gas chromatograph equipped with a 30 m length x 0.32 mm inner diameter VF-maxs and flame ionization detector. The column oven-heating program used for 0.1 uL liquid sample is shown in Figure 3.5. Qualitative analysis of liquid product was identified with GC-MS technique.
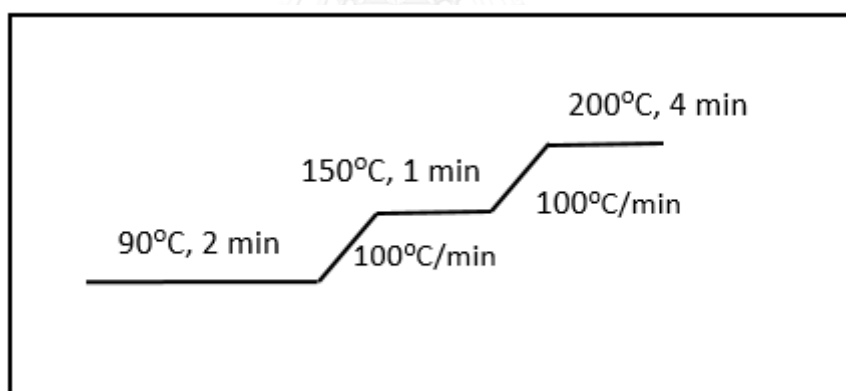
Figure 3.1 The column heating program for acetalization of glycerol with acetone

3.2 Chemicals

1. Cetyltrimethylammonium bromide, CTAB (Sigma-Aldrich, 95%)

2. Ammonium hydroxide solution, (Sigma-Aldrich, ≥25% NH_3 in H_2O)

3. Tetraethyl orthosilicate, TEOS (Fluka, 98%)

4. (3-mercaptopropyl)trimethoxysilane, MPTMS (Aldrich, 95 %)

5. Hydrogen peroxide (Merck, 30%)

6. Sulfuric acid (Merck, 95-97 %)

7. Toluene (CARLO ERBA, 99.5%)

8. Ethanol (Merck, 99%)

9. Glycerol (Aldrich, 99.5%)

10. Acetone (Aldrich, 99.5%)

11. Cyclohexanone (CARLO ERBA, 99%)

12. Cyclooctanone (Aldrich, 99%)

13. Cyclododecanone (Sigma-Aldrich, 99%)

14. Benzaldehyde (Merck, 99%)

15. n-dodecane (Merck, 99%)

16. Dimethylformamide (RCl Labscan, 99.8%)

17. Sodium hydroxide (Merck, 99%)

18. Sodium chloride (CARLO ERBA, 99%)

19. Amberlyst-15 in dry (Rohm & Hass, France)

20. Zeolite beta (ZEOCHEM, Si/Al = 15)

21. Zeolite ZSM-5 (ZEOCHEM, Si/Al = 14.1)

22. Deionized water

23. Phenolphthalein

3.3 Synthesis of catalysts

3.3.1 Synthesis of MCM-41

Mesoporous silica MCM-41 was synthesized by hydrothermal method, reported by Zeid et al [60]. The gel mole composition was 1.0 TEOS: 1.43 NH_4OH: 0.15 CTAB: 1.57 H_2O. In typical experiment, 7.20 g of CTAB was dissolved in 360 g of DI water and added into 400 mL round bottom flask. Then, 30.6 g of 25% ammonium was dropped into solution and stirred at room temperature for 10 min. Subsequently, TEOS was dropped and stirred at room temperature for 18 h. After stirred, the milky solution was filtrated, washed with mixture of DI water and ethanol (800ml/200ml) for several times and dried at 60°C. Then the solid product was calcined at 550°C for 5 h to remove template.
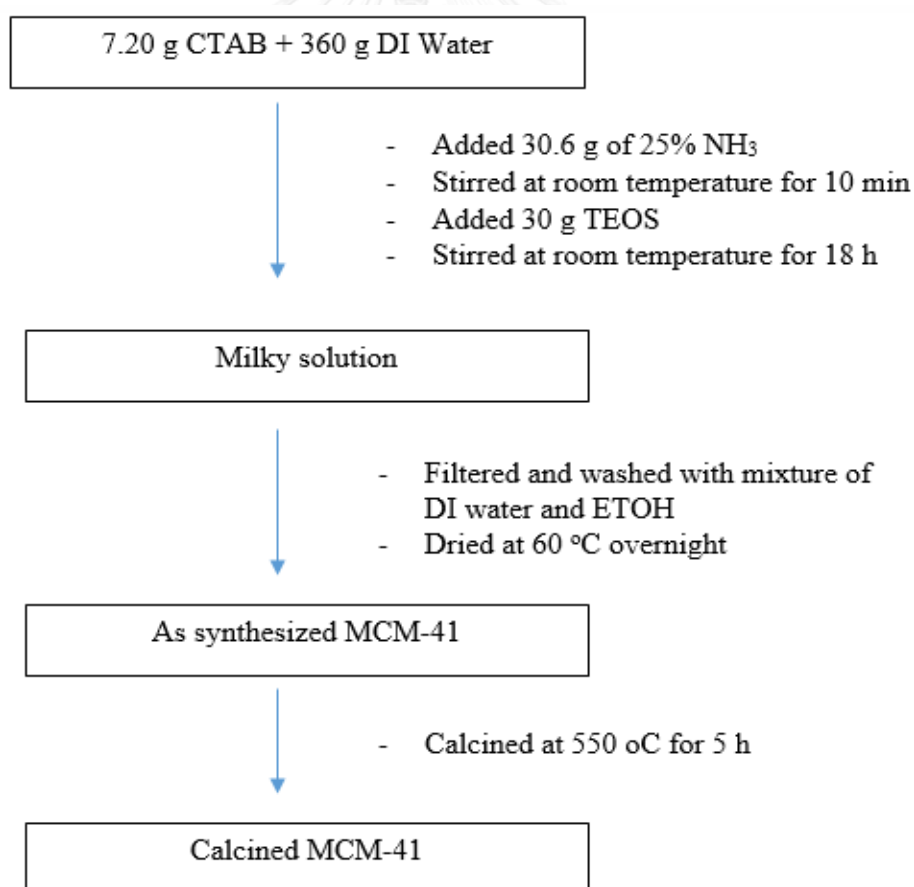
Figure 3.2 Diagram of MCM-41 synthesis

3.3.2 Synthesis propyl sulfonic functionalized catalysts

Propyl sulfonic functionalized catalysts were synthesized by grafting method using MPTMS as sulfonic functionalized. In typical experiment, 3.0 g of unmodified catalysts was added into the mixture solution of 5.301 g MPTMS and 50 ml toluene. Then, the mixture solution was stirred at $60^{\circ}C$ for 6 h. Subsequently, the mixture solution was filtered, washed with toluene and dried $60^{\circ}C$ overnight. Then, the solid product was added into 30 ml of 30% H_2O_2 and refluxed at $60^{\circ}C$ for 24 h. After reflux, the solid product was filtered, washed with deionized water. Then, the solid product was added into 50 g of 0.2 M H_2SO_4 and stirred for 2 h. The solid product was filtered, washed with deionized water, dried at $60^{\circ}C$ overnight [61].
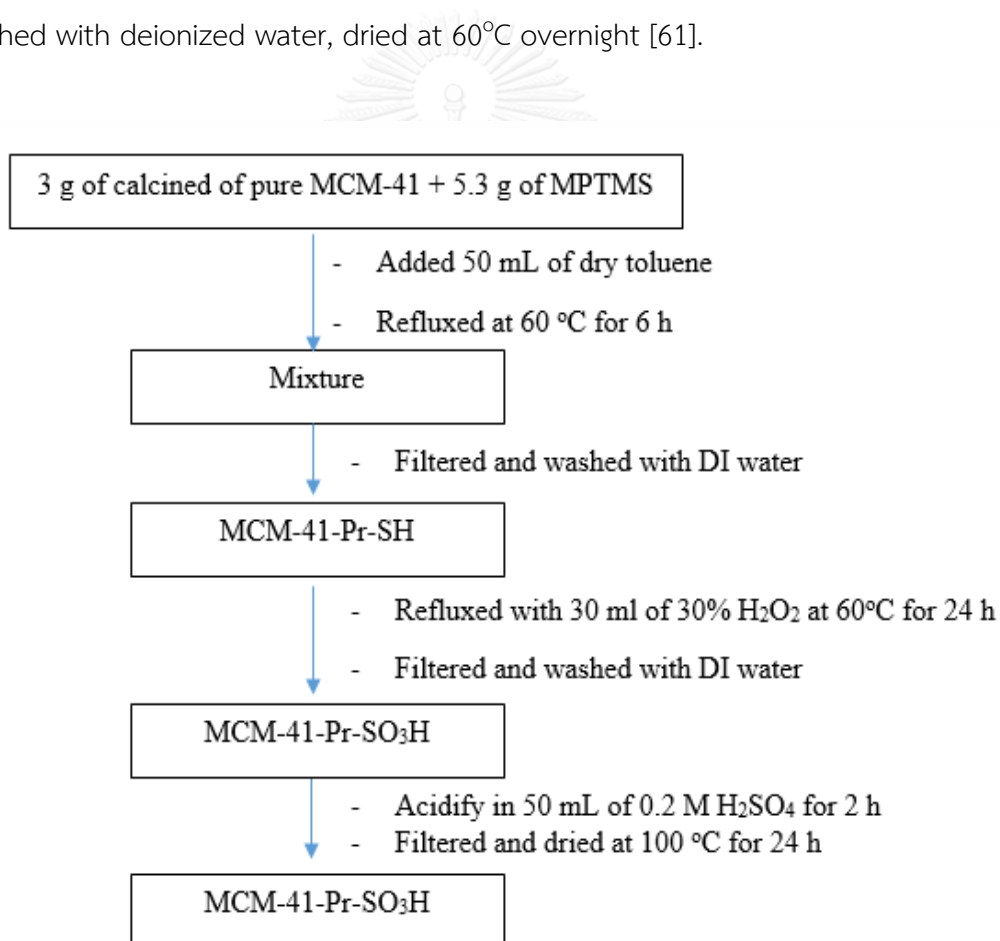
Figure 3.3 Diagram of propyl sulfonic acid functionalized mesoporous silica synthesis

3.4 Acid-base titration

The acid capacities of catalysts were quantified using 2 M NaCl solution as the ion exchange agent. Approximately 0.05 g of catalyst was exchanged with 15 mL of the salt (NaCl) solution and allowed to equilibrate for 30 min at room temperature. After that, the sample solution was titrated with 0.01M NaOH solution using phenolphthalein as indicator.
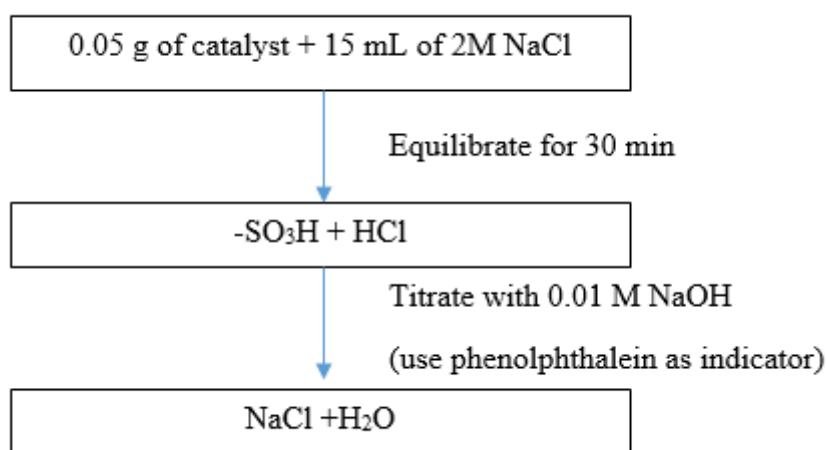
Figure 3.4 Diagram for acid-base titration

3.5 Procedure in solketal synthesis

Solketal preparation was carried out in stirred batch reactor with acetone to glycerol mole ratio of 2:1. In the typical experiment, 5 g of glycerol and 8 mL of acetone were taken in a 25 mL round bottom flask with 0.25 g of pre-activated catalysts (5wt% referred to glycerol mass). The reaction mixture was magnetically stirred at room temperature for 1h. After that, the reaction mixture was centrifuged to separate out the catalysts from the liquid phase.
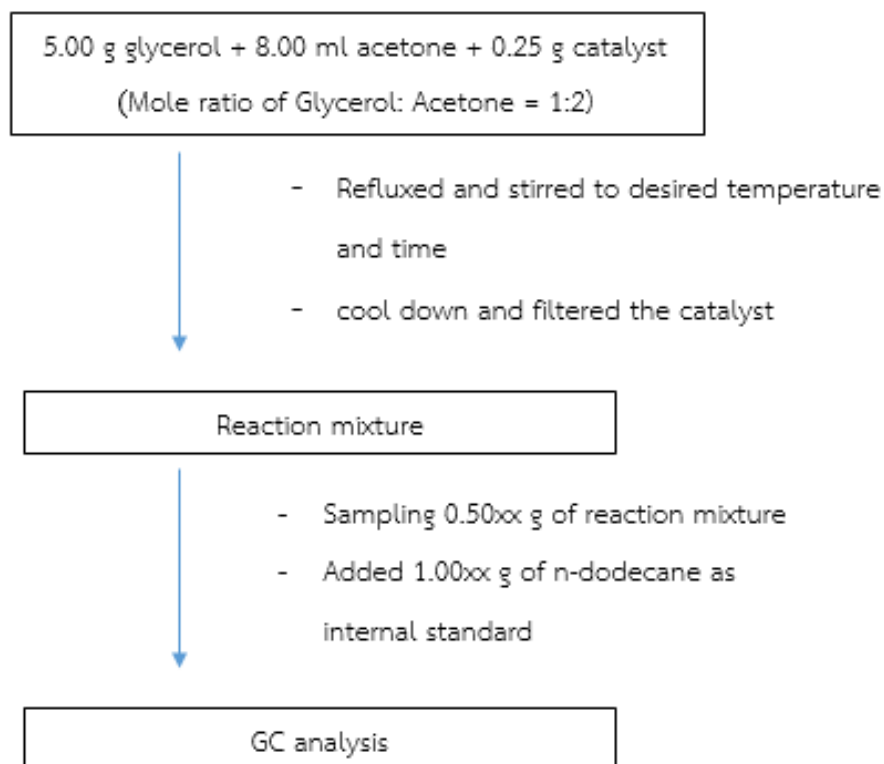
Figure 3.5 Diagram for solketal synthesis and analysis

3.6 Parameters affecting solketal synthesis

3.6.1 Effect of catalytic type

Catalytic activities of H-beta-Pr-SO$_3$H were compared with sulfonated mesoporous catalysts (MCM-41-Pr-SO$_3$H, SBA-15-Pr-SO$_3$H, and MCA-Pr-SO$_3$H) and sulfonated microporous catalysts (MCM-22-Pr-SO$_3$H and ZSM-5-Pr-SO$_3$H) and commercial catalysts (H-beta, H-ZSM-5, and Amberlyst-15).

3.6.2 Effect of reaction temperature

The reaction was studied at different reaction temperature of 32, 60, 100 and 120°C.

3.6.3 Effect of reaction time

In this work, the reaction time was varied to 0.5, 1.0, 2, 4 and 8 h.

3.6.4 Effect of glycerol/ acetone mole ratio

The mole ratio of glycerol to acetone was varied to 1:1, 1:2, 1:4, 1: 8, 1:10 and 1:12.

3.6.5 Effect of catalyst loading

The catalytic loading was varied from 0 to 10 wt% based on weight of glycerol.

3.7 Standard solution and calibration solution

3.7.1 Glycerol standard solution

3.7.1.1 Stock standard solution

To prepared glycerol 1.0 M as stock standard solution, a 2.30 g of glycerol was accurately weight in a 25 mL volumetric flask and made up to the mark with dimethylformamide.

3.7.1.2 Working standard solution

The concentration of 0.5 M, 0.2 M, 0.1 M and 0.05 M glycerol as working standard solution were prepared by dilution of the standard solution using pipette and made up to the mark with dimethylformamide.

3.7.2 Solketal standard solution

3.7.2.1 Stock standard solution

To prepared glycerol 1.0 M as stock standard solution, a 2.30 g of solketal was accurately weight in a 25 mL volumetric flask and made up to the mark with dimethylformamide.

3.7.2.2 Working standard solution

The concentration of 0.5 M, 0.2 M, 0.1 M and 0.05 M solketal as working standard solution were prepared by dilution of the standard solution using pipette and made up to the mark with dimethylformamide.

3.7.3 Internal standard

For determine of glycerol conversion, solketal selectivity and solketal yield, 0.20 M of n-dodecane was used as internal standard. A 0.85 g of n-dodecane was accurately weight approximately in a 25 mL volumetric flask and fill with dimethylformamide.

3.7.4 Preparation and analysis of the calibration solution

To preparation of sample for analysis, 0.5 g of reaction mixture from acetalization of glycerol was mixed with 1 g of 0.25M n-dodecane as internal standard and 2 mL of dimethylformamide (DMF) as solvent. The mixture solution was analyzed using a Varian CP 3800 gas chromatograph equipped with a 30 m length x 0.32 mm inner diameter VF-maxs and flame ionization detector. The values of %glycerol conversion, % solketal selectivity and % solketal yield were calculated based on the following equations:

$$\text{Yield (\%)} = \frac{moles\ of\ solketal\ formed}{initial\ mole\ og\ glycerol} \times 100 \qquad (1)$$

$$\text{Conversion (\%)} = \frac{Initial\ moles\ of\ glycerol - Final\ mole\ of\ glycerol}{initial\ mole\ of\ glycerol} \times 100 \qquad (2)$$

$$\text{Selectivity (\%)} = \frac{moles\ of\ solketal\ formed}{initial\ mole\ og\ glycerol - Final\ moles\ of\ glycerol} \times 100 \qquad (3)$$

3.8 Reuse of catalysts

The spent H-beta-pr-SO$_3$H catalyst from acetalization reaction at same condition (reaction time = 1 h, temperature = 32°C, catalyst weight = 1.25 wt% based on glycerol) was reused by washed and stirred with acetone at room temperature for 2 h three times. The reused catalyst was dried at 70°C for overnight.

3.9 Acetalization of glycerol with other carbonyl compounds

Cyclohexanone, cyclooctanone, cyclododecanone and benzaldehyde was used as carbonyl compounds for synthesis other acetals. The reaction was performed in 100 mL Parr reactor with stirred of 350 rpm for 1 h. For cyclohexanone, cyclooctanone and benzaldehyde, the reaction was carried out at 100°C under reaction condition of carbonyl/glycerol mole ratio of 1:2 with pre-activated catalyst 50 mg. While, for cyclododecanone, the reaction was carried out at 120°C under reaction condition of carbonyl/glycerol mole ratio of 1:1 with pre-activated catalyst 50 mg. After completion of the reaction, the catalyst was centrifuge out of solution. Then, the mixture solution were separated by separated funnel. The products were confirmed by GC-MS. The glycerol conversion was calculated from standard glycerol calibration cure and the selectivity of 1, 3 dioxalane was calculated from the proportion of peak areas.

CHAPTER 4

RESULTS AND DISCUSSION

4.1 The physic-chemical properties of propyl sulfonic functionalized beta catalyst (H-beta-pr-SO$_3$H)

4.1.1 X-ray diffraction results

The XRD patterns of commercial beta and sulfonated beta are shown in Figure 4.1a and 4.1b, respectively. Both of catalysts revealed the characteristic peak at 2θ = 6.2, 21.13 and 22.30 indicating a well-defined diffraction pattern corresponding to the Beta zeolite structure [22]. However, the intensity peak at 6.2 of the sulfonated beta dramatically decreased as compared with the commercial parent beta. The reason is due to a pure crystalline beta zeolite and sulfonated beta derivative.
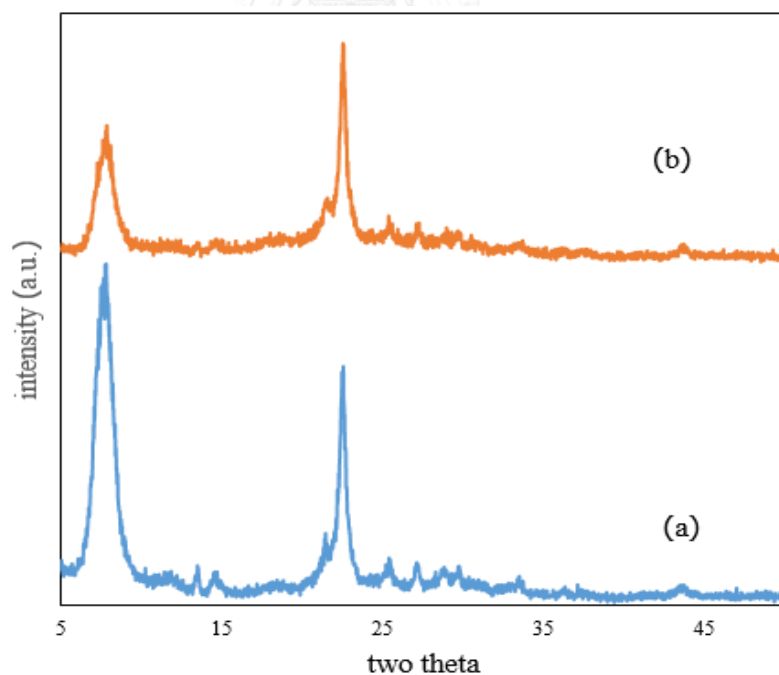
Figure 4.1 X-ray diffraction of (a) H-beta and (b) H-beta-Pr-SO$_3$H

4.1.2 Nitrogen adsorption/desorption isotherm

The N_2 adsorption-desorption isotherms of commercial beta and sulfonated beta catalysts were presented in Figure 4.2a and 4.2b, respectively. The isotherms of these samples exhibited type I according to the IUPAC classification, which indicates mainly microporous materials. The specific surface area, total pore volume and pore size distribution were calculated from N_2 adsorption-desorption at -77K using BET method and MP method, respectively, whilst the internal surface area was obtained from t-plot equation (see Table 4.1). The commercial beta was found to have a BET surface area of 555 m^2/g with internal surface of 517 m^2/g and pore diameter of 0.7 nm. After sulfonic functionalization, sulfonated beta had a BET surface area as 351 m^2/g with internal surface of 304 m^2/g and pore diameter of 0.7 nm. The specific surface area and internal surface area were decreased after sulfonic functionalization because of the incorporation of propyl-sulfonic group ($-Pr-SO_3H$) inside the microporous structure and outside the surface at the same time. The acidity of catalysts was determined by titration with NaOH and the results were listed in Table 4.1. As expected, sulfonated beta gave acid amount (1.07 mmol H^+g^{-1}) higher than commercial beta (0.78 mmol H^+g^{-1}) because of the increasing of Brønsted acid site in sulfonic groups.

Table 4.1 Textural and acid properties H-Beta andH-Beta-Pr-SO₃H

Catalyst	S^a_{BET} (m^2/g)	External surface area[b] (m^2/g)	Internal surface area[c] (m^2/g)	Total pore volume[d] (cm^3/g)	dp[d] (nm)	Acid amount[e] (mmol/g)
H-beta	555	38	517	0.29	0.70	0.78
H-beta-Pr-SO₃H	351	28	304	0.16	0.70	1.07

[a] Calculate from BET method.

[b] Calculate from t-plot

[c] Internal surface area = (total surface area (from *t-plot*) –(external surface area (from *t-plot*)).

[d] Calculated from the MP method for microporous material.

[e] Determined by acid titration
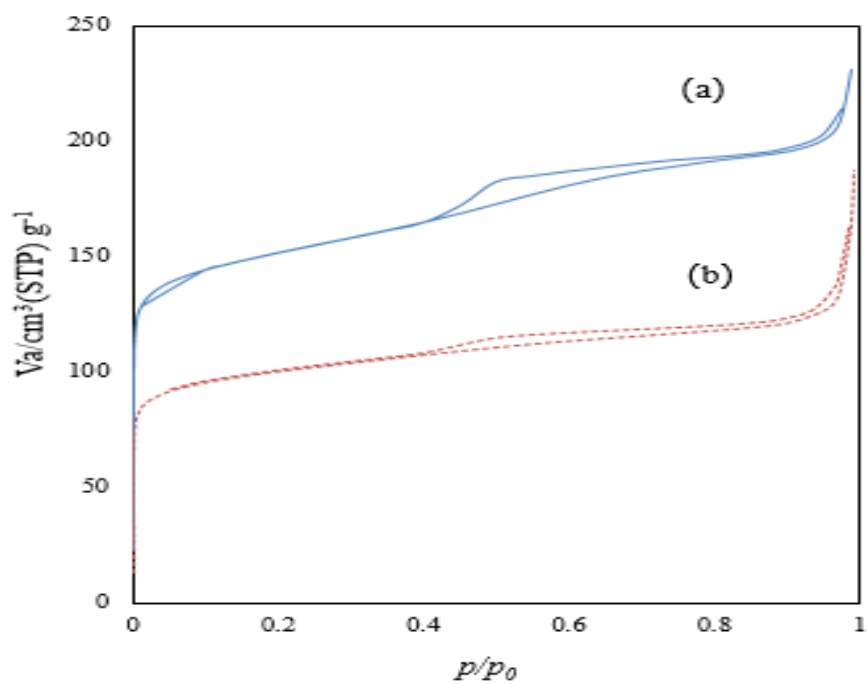
Figure 4.2 The comparison of nitrogen adsorption-desorption of (a) H-beta and (b) H-beta-Pr-SO$_3$H
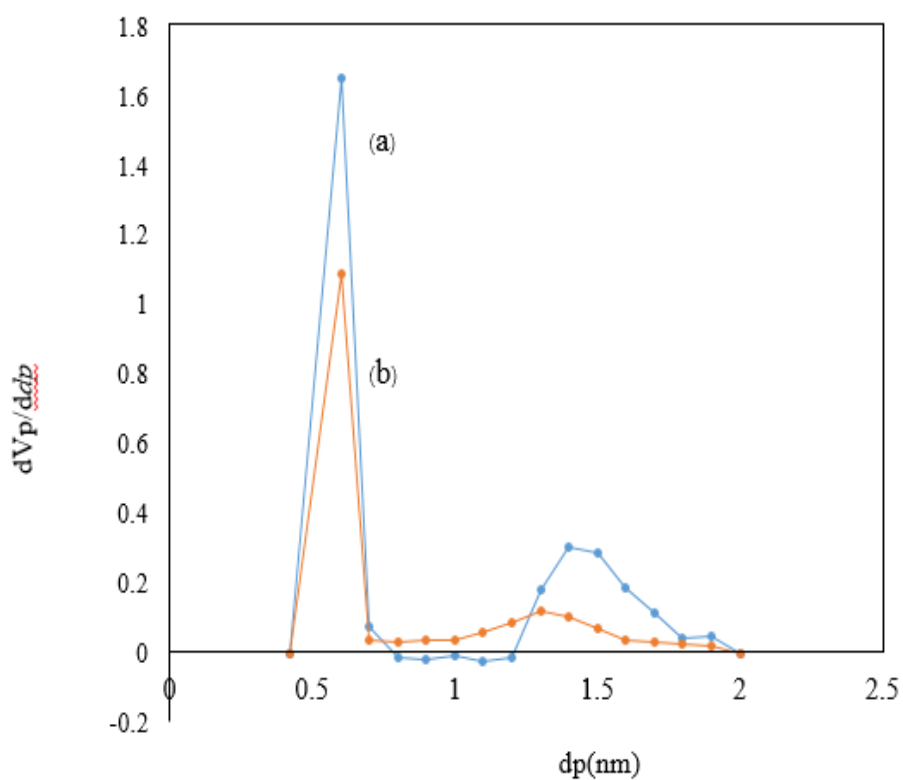
Figure 4.3 BJH-pore size distribution of (a) H-beta and (b) H-beta-SO$_3$H

4.1.3 Scanning electron microscope

The SEM images of commercial beta at x10,000 and x30,000 magnification were illustrated in figure 4.4 a-1 and a-2, respectively. While, sulfonated beta at x10,000 and x30,000 magnification were illustrated in figure 4.4 b-1 and b-2, respectively. It can be seen that both of them were uniform spherical shape aggregated particle.
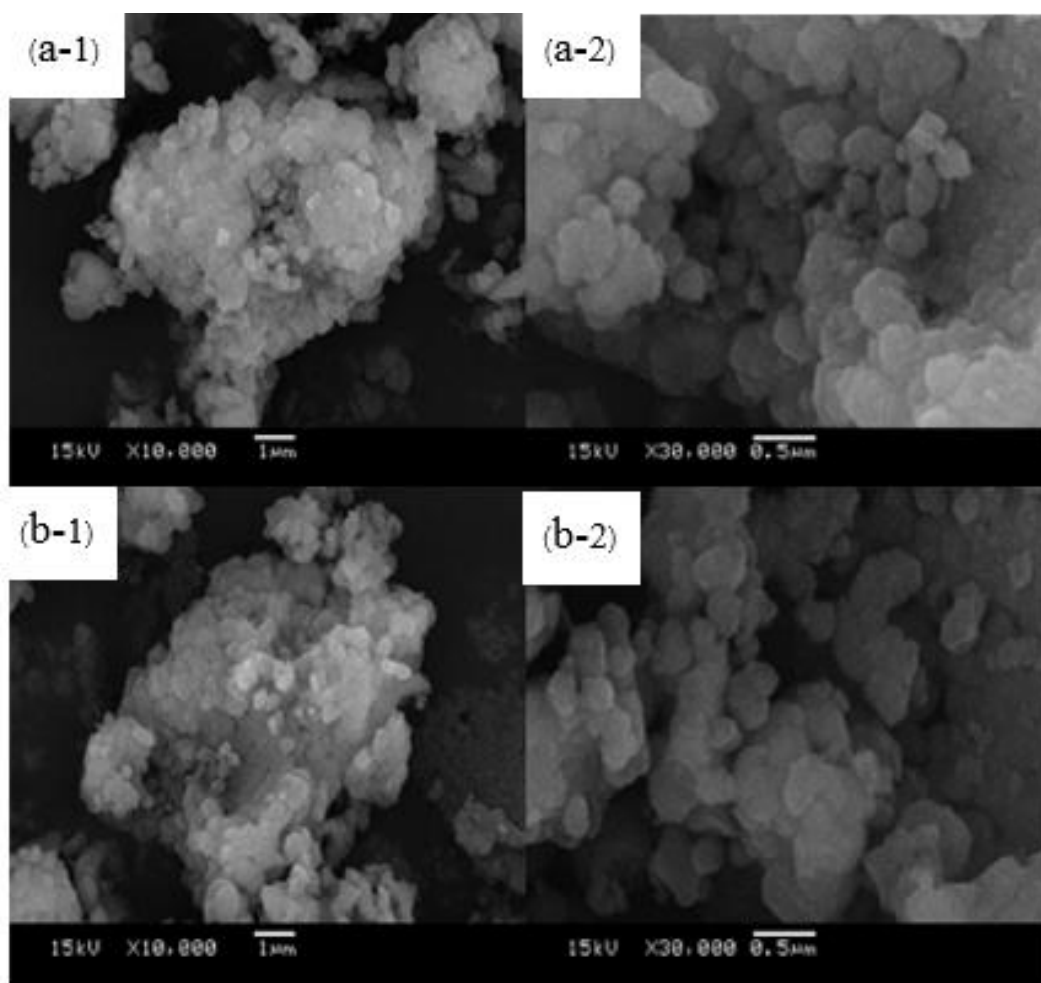
Figure 4.4 SEM images of commercial beta zeolite ((a-1) x10000 and (a-2) x30000) and H-beta-Pr-SO$_3$H ((b-1) x10000 and (b-2) x30000)

4.2 The physico-chemical properties of propyl sulfonic functionalized MCM-41 catalyst

4.2.1 X-ray diffraction results

From the Figure 4.5, X-ray powder diffraction pattern of MCM-41 and sulfonic functionalized MCM-41 showed very intense peak at 2Θ = 2.34 and two weak peaks at 2Θ = 4.06 and 4.74 indexed to (100), (110) and (200) diffractions, respectively. These peaks of the synthesized material indicated the well-ordered hexagonal structure [17]. In comparison with MCM-41, the intensity diffraction peaks of sulfonic functionalized MCM-41 were decreased because of decreasing of crystallinity. Moreover, the diffraction peak was slightly shift to lower angle (higher d-spacing) after fictionalization due to organic group incorporated to MCM-41. However, the results still exhibited the mesoporous structure after post-modification.
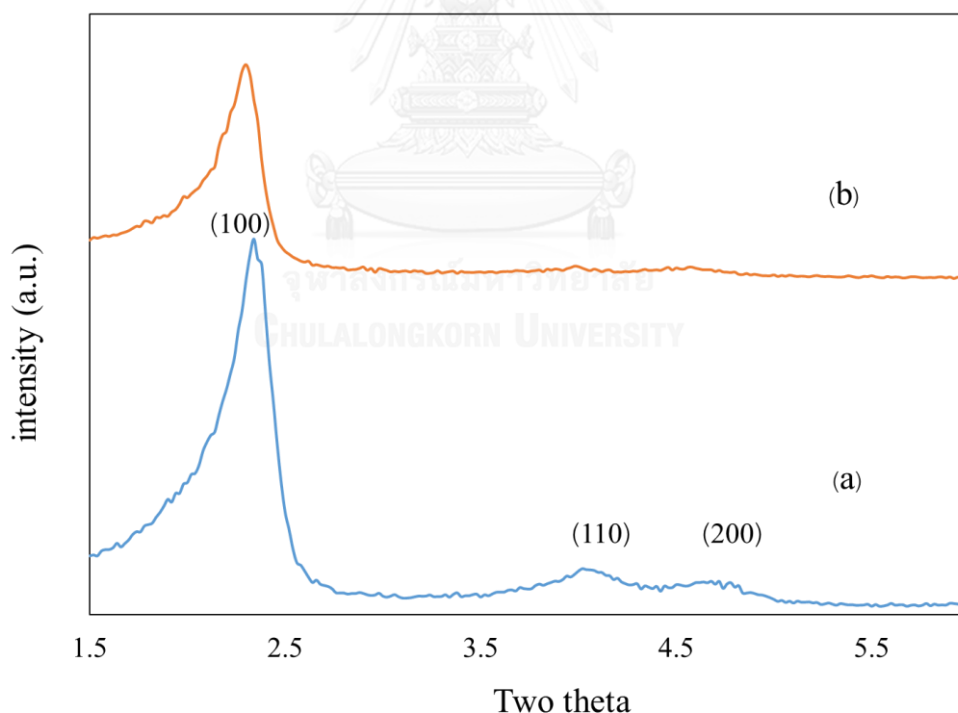
Figure 4.5 X-ray diffraction of (a) MCM-41 and (b) MCM-41-Pr-SO₃H

4.2.2 Nitrogen adsorption/desorption

The Figure 4.6 illustrates nitrogen adsorption-desorption isotherms of MCM-41 and sulfonated MCM-41. Both of samples exhibited characteristic type IV isotherm according to IUPAC classification, indicating the mesoporous materials. After propyl-sulfonic functionalization, the isotherms was slightly shift to lower relative pressure and had lower adsorption volume, indicating that the sulfonated MCM-41 have a smaller pore diameter and lower surface area than unmodified MCM-41.

The specific surface area, total pore volume and pore diameter of samples were calculated from N_2 adsorption–desorption results using the standard BET method and the BJH equation, respectively. As shown in Table 4.2, MCM-41 was found to have the specific surface area of 1023 m^2/g, with total pore volume of 0.46 cm^3/g and a pore diameter of 2.44 nm (24.4 Å). After the sulfonic functionalization, the specific surface area and total pore volume were reduced to 766 m^2/g and 0.41 cm^3/g, respectively. The decrease in specific surface area, internal surface area, external surface area and pore volume after sulfonic functionalization revealed that the propyl-sulfonic groups incorporated both into the external surface and internal surface at the same time [21].

Table 4.2 Textural and acid properties MCM-41 and MCM-41-Pr-SO$_3$H

catalyst	$S^a{}_{BET}$ (m^2/g)	Internal surface area[c] (m^2/g)	External surface area[b] (m^2/g)	Total pore volume[d] (cm^3/g)	dp[d] (nm)	Acid amount (mmol/g)
MCM-41	1023	1017	40	0.46	2.44	0.46
MCM-41-Pr-SO$_3$H	766	730	32	0.41	2.44	1.17

[a] Calculate from BET method.

[b] Calculate from t-plot

[c] Internal surface area = (total surface area (from *t-plot*) –(external surface area (from *t-plot*)).

[d] Calculated from the BJH method for mesoporous material.

[e] Determined by acid titration
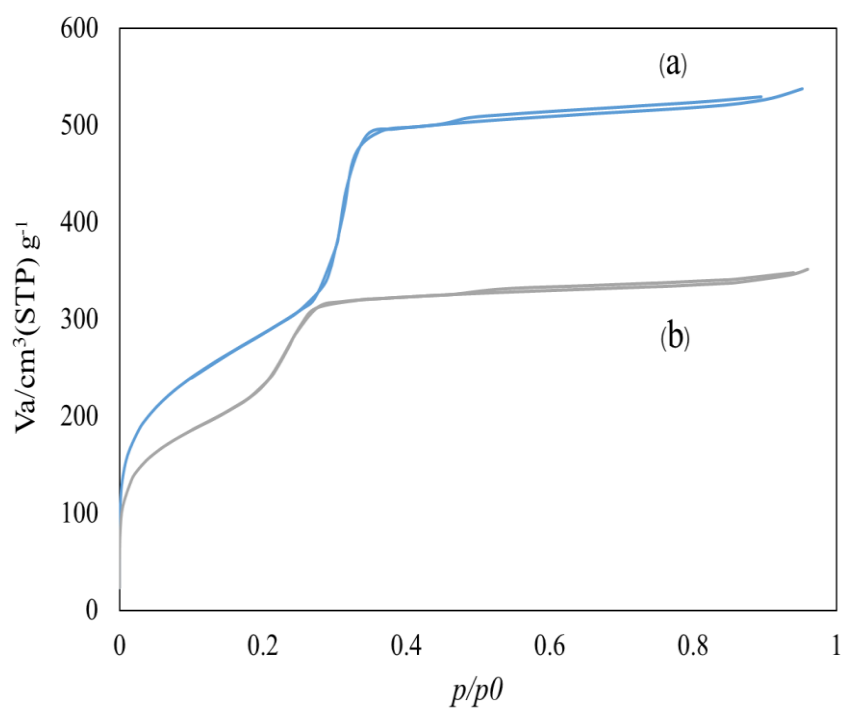
Figure 4.6 Nitrogen adsorption-desorption isotherm of (a) MCM-41
and (b) MCM-41-Pr-SO$_3$H
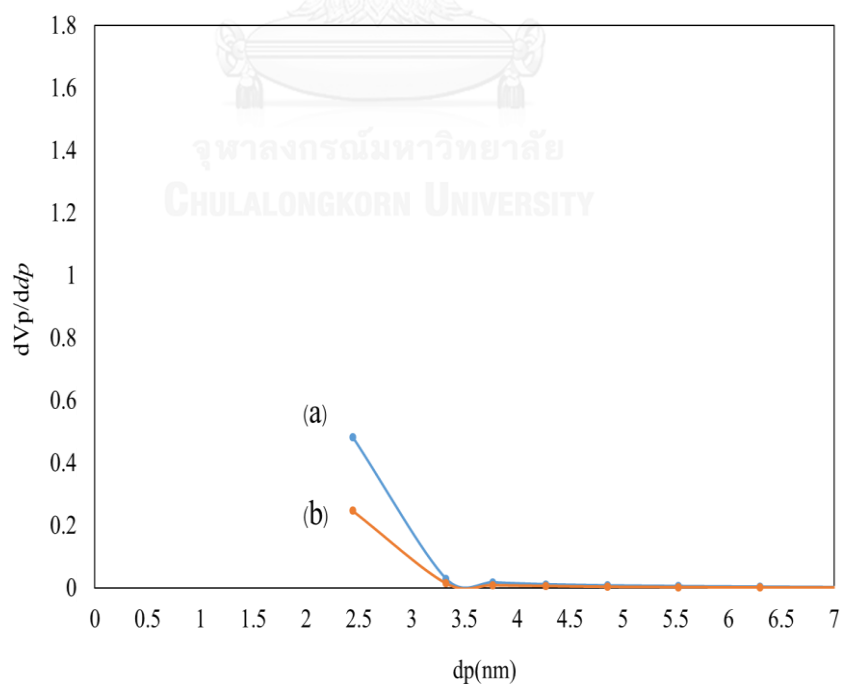
Figure 4.7 BJH-pore size distribution of (a) MCM-41 and (b) MCM-41-Pr-SO$_3$H

4.2.3 Scanning electron microscope

The Figure 4.8 showed SEM images of MCM-41 and sulfonated MCM-41 at x10,000 and x 30,000 magnification. MCM-41 had spherical aggregated particles, while its functionalized MCM-41 still exhibited the same particle shape but was more aggregated.
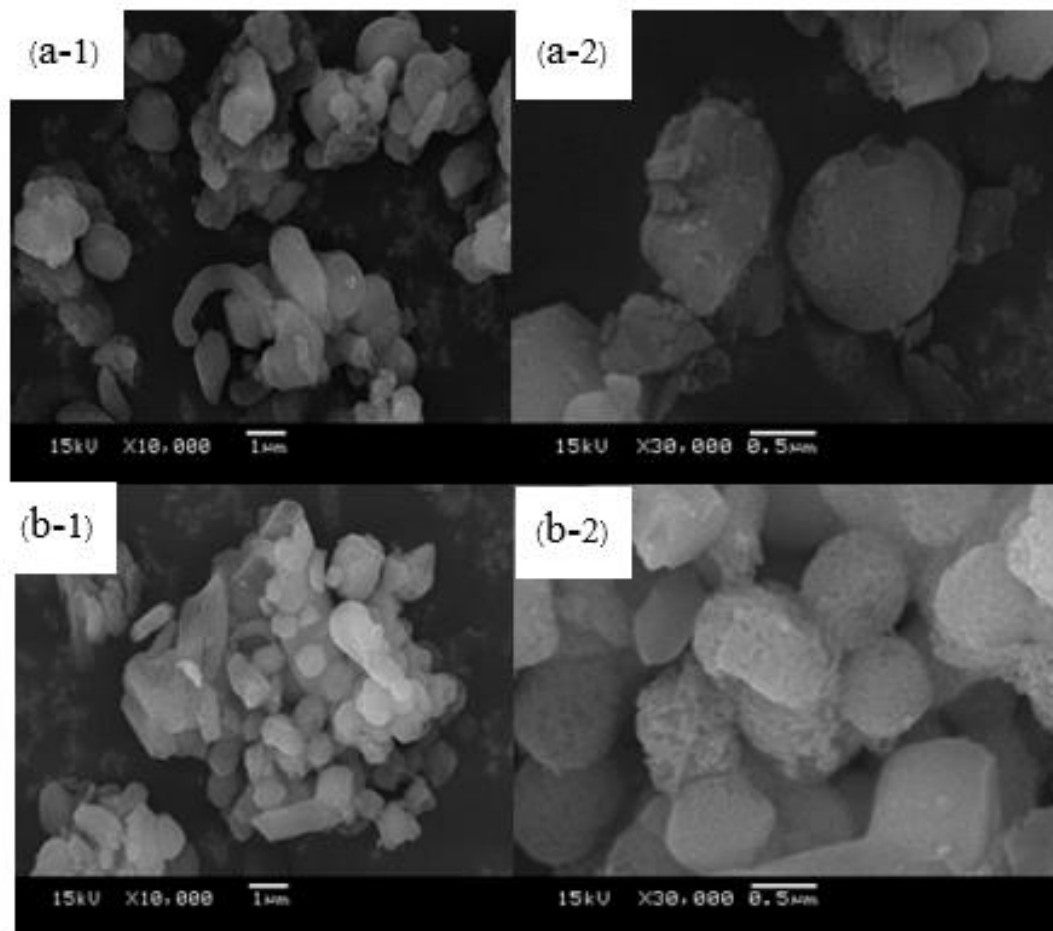
Figure 4.8 SEM images of MCM-41 ((a-1) x10000 and (a-2) x30000) and MCM-41-Pr-SO$_3$H ((b-1) x10000 and (b-2) x30000)

4.3 Fourier transform infrared spectroscopy patterns (FT-IR)

The FT-IR spectra in the range 400-4000 cm^{-1} of the unmodified beta zeolite, mesoporous MCM-41 and propyl sulfonic beta zeolite, MCM-41 catalysts were shown in Figure 4.9. All samples exhibited the 4 characteristic peaks of tetrahedral silicon oxide at 467 cm^{-1} (Si-O-Si and O-Si-O, bending vibration), 800 cm^{-1} (Si-O-Si, symmetric vibration), 962 cm^{-1} (Si-O bending vibration) and 1090 cm^{-1} (Si-O-Si, asymmetric vibration). In addition, the characteristic peak of water were appeared at 1648 cm^{-1} and 3400 cm^{-1}. In case of propyl sulfonic functionalized catalysts, the IR spectra showed the strong band characteristic peak of sulfonic group at 1400 cm^{-1} and 1200 cm^{-1} (S=O asymmetric stretching vibration), indicating the propyl sulfonic groups were successful grafted on the Beta and MCM-41 surface [47].
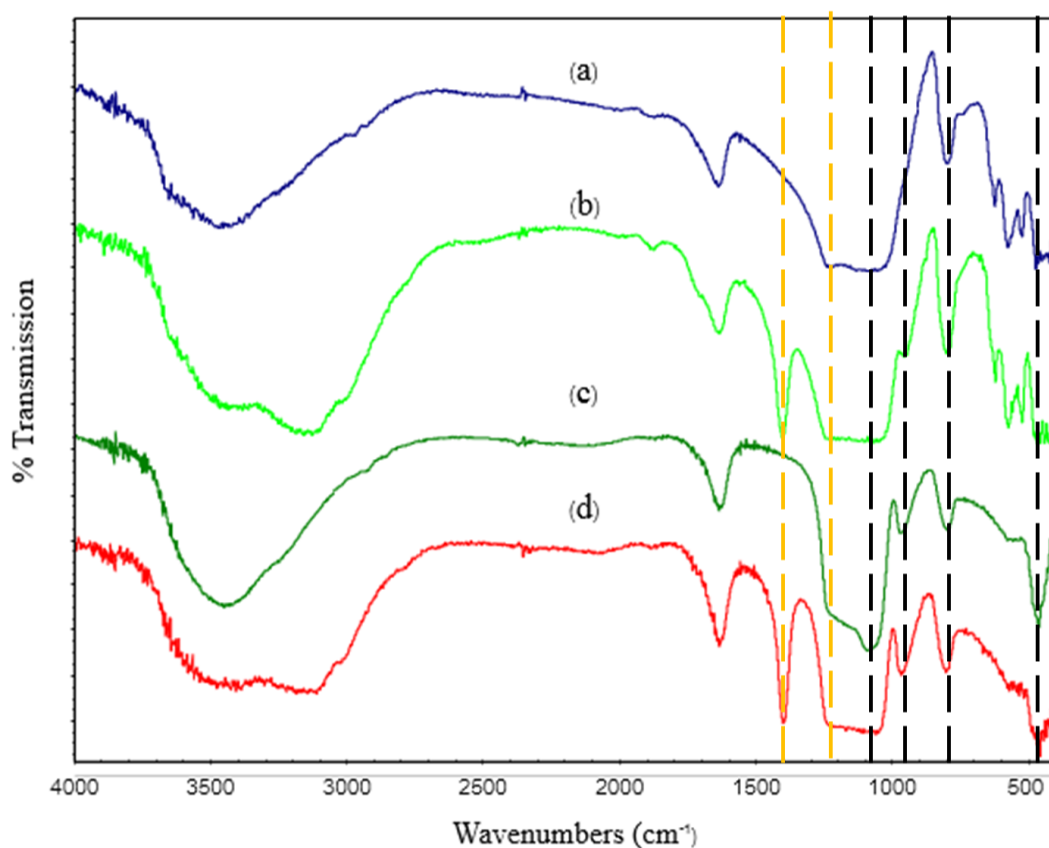
Figure 4.9 FTIR spectra of (a) commercial H-beta, (b) H-beta-Pr-SO$_3$H, (c) MCM-41 and(d) MCM-41-Pr-SO$_3$H

4.4 ^{13}C-MAS-NMR spectra

The propyl sulfonic groups on MCM-41 and H-beta were confirmed by solid state ^{13}C-MAS-NMR, as shown in Figure 4.10a and 4.10b, respectively. The ^{13}C–NMR spectra of MCM-41-Pr-SO$_3$H exhibited signal at 10.9, 17.8 and 53.7 ppm that were derived from the ^{1}C, ^{2}C and ^{3}C carbon atoms of Si-^{1}CH$_2$-^{2}CH$_2$-^{3}CH$_2$-SO$_3$H, respectively. In addition, the signal at 64.9 ppm was appeared that might be the carbon atom from residual surfactant. The ^{13}C-NMR spectra of H-beta-Pr-SO$_3$H performed signal at 11.5, 17.9 and 53.8 ppm indicating to the ^{1}C, ^{2}C and ^{3}C methylene carbon atoms of Si-^{1}CH$_2$-^{2}CH$_2$-^{3}CH$_2$-SO$_3$H, respectively. Thus, it could be concluded that the propyl sulfuric groups were grafting into the silica materials [62].

Chemical Shift / ppm
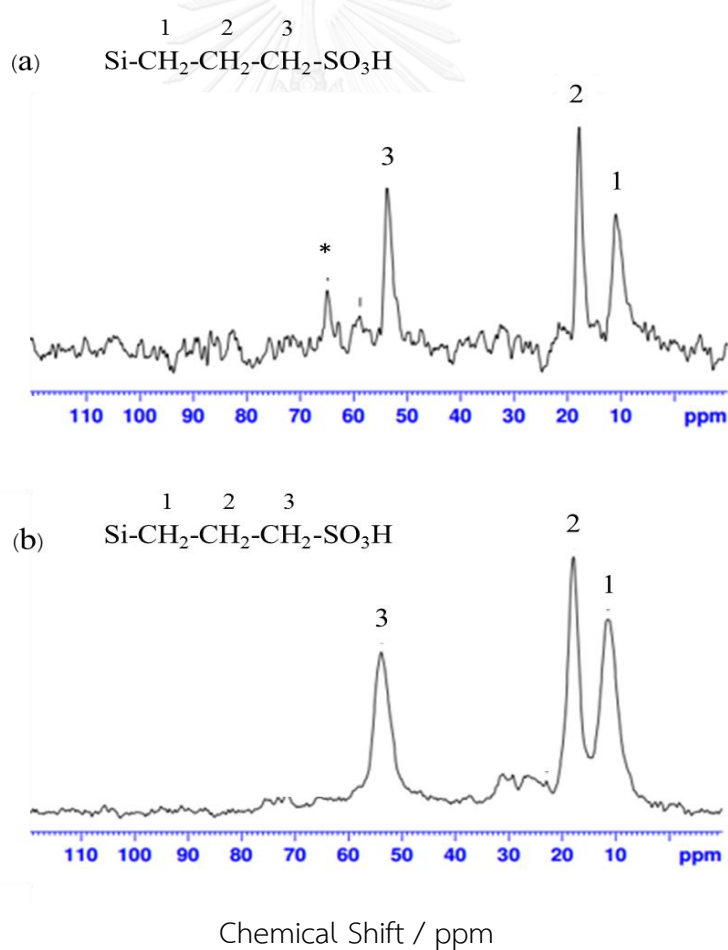
Figure 4.10 ^{13}C-MAS-NMR spectra of (a) MCM-41-Pr-SO$_3$H and (b) H-beta-Pr-SO$_3$H

4.5 Catalytic activity

The acetalization of glycerol with acetone gave two isomers acetal products, including 2, 2 dimethyl-1, 3-dioxolane-4-methanol or solketal (five membered ring) and 2, 2-dimethyl-1, 3- dioxolan-5-ol (six membered ring), as illustrated in Scheme 4.1. The formation of products was further confirmed by GC-MS as shown in appendix.
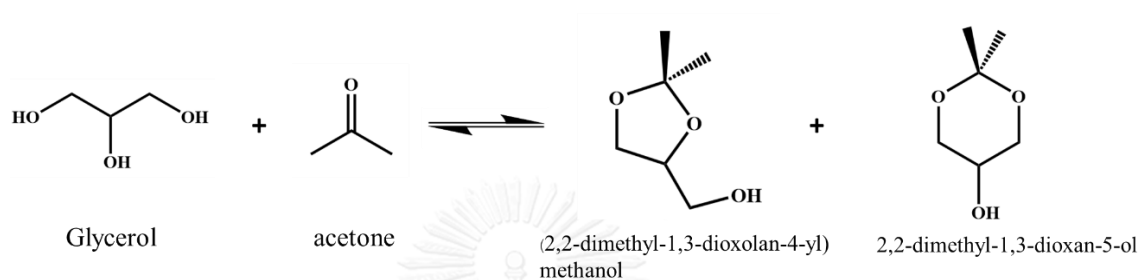
Scheme 4.1 Acetalization of glycerol with acetone

4.5.1 Screening of catalyst in acetalization of glycerol with acetone

To screen catalysts in acetalization of glycerol with acetone, the propyl-sulfonic functionalized of mesoporous materials (SBA-15-Pr-SO$_3$H, MCM-41-Pr-SO$_3$H, and MCA-Pr-SO$_3$H), propyl-sulfonic functionalized of microporous materials (ZSM-5-Pr-SO$_3$H, MCM-22-Pr-SO$_3$H, H-beta-Pr-SO$_3$H) and commercial catalysts (ZSM-5, H-beta, Amberlyst-15) were used for screening in this reaction.The performance of all catalysts are also listed in Table 4.3. At room temperature, all the screened catalysts were compared in their performances with glycerol to acetone mole ratio of 1:2 at catalyst loading of 5wt% based on glycerol without solvent for 1 h. To investigate blank runs before catalytic activity studies, the reaction without catalyst showed very low glycerol conversion (<0.01%) with the disappearance of solketal peak.

Table 4.3 Acetalization of glycerol with acetone over micro/mesoporous sulfonated aluminosilicate

Catalyst	Acidity (mmol H$^+$/g)	Acetalization of glycerol with acetone		
		Glycerol conversion %	Solketal Selectivity %	Solketal Yield %
Blank	-	0.0	0.0	0.0
Microporous materials				
H-beta	0.64	58.4	99	57.8
H-beta-Pr-SO$_3$H	1.07	61.5	99	60.9
H-ZSM-5	0.60	31.4	99	31.1
H-ZSM-5-Pr-SO$_3$H	0.77	36.9	99	36.5
H-MCM-22	0.96	34.0	97	33.0
MCM-22-Pr-SO$_3$H	1.17	37.6	93	37.2
Mesoporous materials				
SBA-15-Pr-SO$_3$H	0.87	51.4	99	50.9
MCM-41-Pr-SO$_3$H	1.17	51.7	99	51.2
MCA-Pr-SO$_3$H	0.79	58.8	97	58.3
Ion exchange resin				
Amberlyst-15	4.53	58.3	99	57.1

Reaction condition: Temperature = 32°C, glycerol: acetone mole ratio = 1:2, catalyst weight= 5 wt% based on glycerol, time = 1 h.

Figure 4.11 Acetalization of glycerol with acetone over micro/mesoporous sulfonated aluminosilicate

4.5.2 Comparison of catalytic activity in solketal preparation over Microporous materials

As comparing the activity over microporous materials, the pure zeolite, SiO_2/Al_2O_3 ratios approximate 28, (commercial ZSM-5, commercial H-beta, and prepared H-MCM-22) and sulfonated zeolites were used for catalyzing for this reaction at same condition. In order to investigate the effect of structure of zeolites on solketal preparation, the physical properties of both of zeolite and sulfonated zeolites were characterized using nitrogen adsorption-desorption isotherm, as showed in Table 4.4. From the results, the specific surface area and total pore volume decreased in following order: H-beta > H-MCM-22 > HZSM-5. All of sulfonated zeolites had pore diameter smaller than 2 nm indicating microporous materials. According to their microporous structure, the small pore zeolite ZSM-5 has 10 membered ring with multi-dimensional [63], while the medium pore beta zeolite has 12 membered ring pore opening in three directions [22]. MCM-22 has two non-connected pore systems, one with 12-ring pores and the other having 10 ring pores [64]. The structures of ZSM-5, Beta, and MCM-22 were exhibited in the Table 4.5.

Table 4.4 Textural and acid properties of sulfonic functionalized microporous

catalyst	S^a_{BET} (m²/g)	Internal surface area (m²/g)	External surface area (m²/g)	Total pore volume (cm³/g)	dp (nm)	Acid amount (mmol/g)
H-beta	555	517	38	0.29	0.7	0.78
H-beta-Pr-SO₃H	351	304	28	0.16	0.6	1.07
H-MCM-22	540	527	74	0.18	0.7	0.96
H-MCM-22-Pr-SO₃H	453	449	65	0.15	0.6	1.17
H-ZSM-5	360	351	46	0.12	0.6	0.60
H-ZSM-5- Pr-SO₃H	326	319	31	0.12	0.6	0.77

[a] Calculate from BET method.

[b] Calculate from t-plot

[c] Internal surface area = (total surface area (from *t-plot*) –(external surface area (from *t-plot*)).

[d] Calculated from the MP method for microporous material.

[e] Determined by acid titration

Table 4.5 Structure of zeolites [65]

Catalyst	Dimension of membered ring	Structure
H-ZSM5	10 MR [100] 10MR 5.1 X5.5 Å	MFI framework
H-Beta	12 MR [100] 12MR 6.6 X6.7 Å [001] 12MR 5.6 X5.6 Å	BEA framework
H-MCM-22	10 and 12 MR [100] 10MR 4.0 X 5.5 Å [001] 10MR 4.1 X 5.1 Å External cup 7.1X7.0 Å	MWW framework

To compare the activity of unmodified zeolites, HZSM-5 and H-MCM-22 (see Table 4.6) resulted in low glycerol conversion (31.4% and 34.0%, respectively) which could be attributed to diffusion limitation caused by small pore size restriction. While, H-beta gave high glycerol conversion (58%) which was caused by high surface area and appropriate pore size distribution with multi-dimensional.

Based on the experimental results, all of the sulfonated zeolite gave glycerol conversion and solketal yield higher than pure zeolites. It was caused by the increasing of Brønsted acid sites on propyl sulfonic group.

Table 4.6 The catalytic activity of zeolites and sulfonated zeolites over acetalization of glycerol with acetone

Catalyst	Acidity (mmol H$^+$/g)	Acetalization of glycerol with acetone		
		Glycerol conversion %	Solketal Selectivity %	Solketal Yield %
H-beta	0.64	58.4	99	57.8
H-beta-Pr-SO$_3$H	1.07	61.5	99	60.9
H-ZSM-5	0.60	31.4	99	31.1
H-ZSM-5-Pr-SO$_3$H	0.77	36.9	99	36.5
H-MCM-22	0.96	34.0	97	33.0
MCM-22-Pr-SO$_3$H	1.17	37.6	93	37.2

Reaction condition: temperature = 32°C, glycerol: acetone mole ratio = 1:2, catalyst weight= 5 wt% base on glycerol, time = 1 h

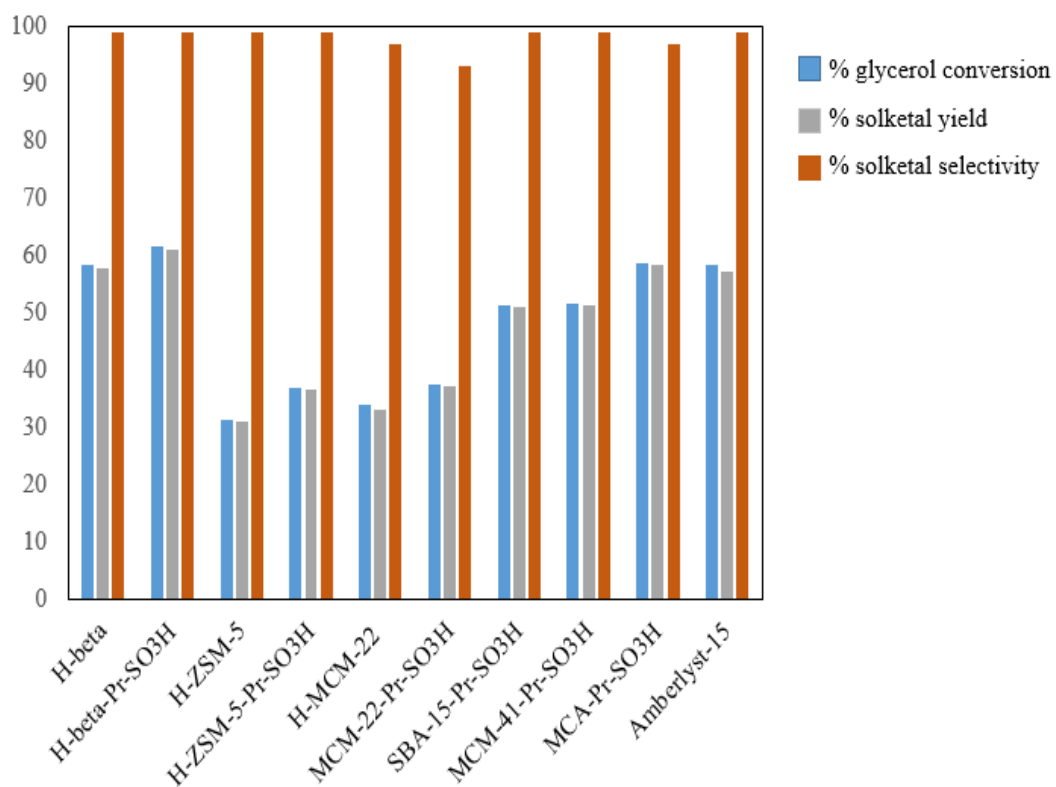**4.5.3 Comparison of catalytic activity in solketal preparation over Mesoporous materials**

To compare catalytic activity of mesoporous material, sulfonated of MCM-41, SBA-15 and MCA were used for this reaction. According to their mesoporous structures, they has high surface area and large pore (2-50 nm). The textural properties were showed in Table 4.7. From the nitrogen adsorption-desorption results, the specific surface area and total pore volume decreased in following order: MCM-41-Pr-SO$_3$H > SBA-15-Pr-SO$_3$H > MCA-Pr-SO$_3$H. All of them showed pore diameter between 2 and 50 nm indicating mesoporous materials. Moreover, pore diameter decreased in following order: SBA-15-Pr-SO$_3$H> MCA-Pr-SO$_3$H > MCM-41-Pr-SO$_3$H. Figure 4.12 presents the mesoporous structure of MCM-41, SBA-15 and MCA. Based on their structural studied, MCM-41 (pore diameter 2.4 nm) and SBA-15 (pore diameter 8.2 nm) have 2D hexagonal array of cylindrical channels, while MCA (the cubic la-3d mesoporous silica, pore diameter 5.1 nm) has 3D cubic structure [47], [46]. The catalytic activity of sulfonated mesoporous was displayed in Table 4.8. The MCA-Pr-SO$_3$H exhibited better performance than MCM-41 and SBA-15, respectively. It was caused by the diffusion in three dimensional is more effective than two dimensional. While, MCM-41-Pr-SO$_3$H showed the catalytic activity better than SBA-15-Pr-SO$_3$H due to its high surface area and acidity (1.17 H$^+$mmol/g).
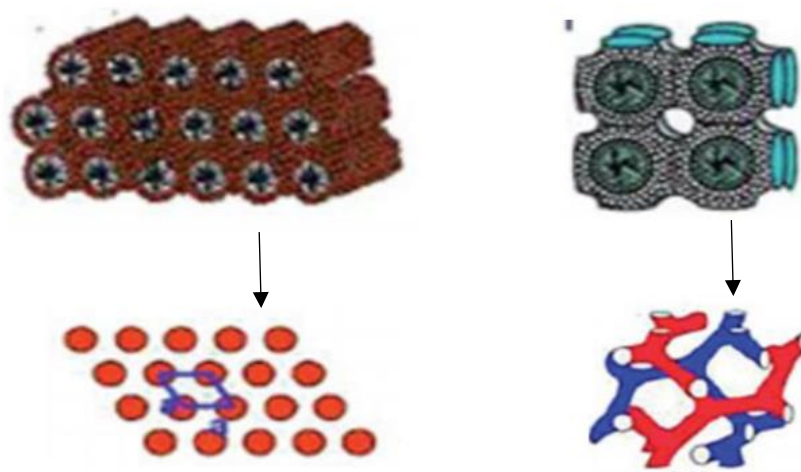
(a) hexagonal periodicity in two dimension   (b) cubic *la3d* periodicity in three dimension

Figure 4.12 Structures of mesoporous silica materials: (a) MCM-41 (hexagonal), (b) MCM-48 (Cubic) [46]

Table 4.7 Textural and acid properties sulfonic functionalized mesoporous

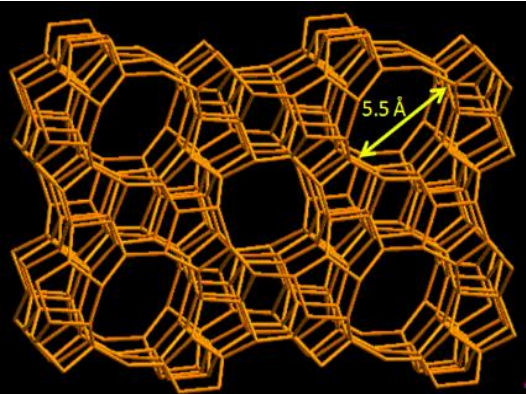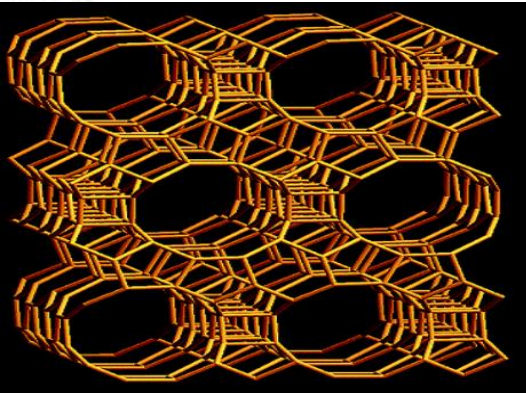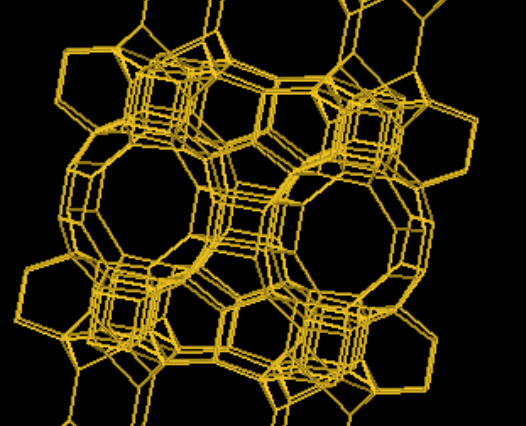| catalyst	S^a_{BET} (m²/g)	Internal surface area[c] (m²/g)	External surface area[b] (m²/g)	Total pore volume[d] (cm³/g)	dp^d (nm)	Acid amount (mmol/g)
MCM-41-Pr-SO₃H	766	730	32	0.41	2.44	1.17
SBA-15-Pr-SO₃H	726	661	59	1.01	8.19	0.87
MCA- Pr-SO₃H	706	686	14	0.74	5.14	0.79

[a] Calculate from BET method.

[b] Calculate from t-plot

[c] Internal surface area = (total surface area (from t-plot) –(external surface area (from t-plot)).

[d] Calculated from the BJH method.

[e] Determined by acid titration.

Table 4.8 The catalytic activity of sulfonated mesoporous catalyst over acetalization of glycerol with acetone

Catalyst	Acidity (mmol H$^+$/g)	Acetalization of glycerol with acetone		
		Glycerol conversion %	Solketal Selectivity %	Solketal Yield %
SBA-15-Pr-SO$_3$H	0.87	51.4	99	50.9
MCM-41-Pr-SO$_3$H	1.17	51.7	99	51.2
MCA-Pr-SO$_3$H	0.79	58.8	97	58.3

Reaction condition: temperature = 32°C, glycerol: acetone mole ratio = 1:2, catalyst weight= 5 wt% based on glycerol, time = 1 h.

To study the effect of types of catalysts on solketal selectivity, the catalytic activity results revealed the same solketal selectivity (97-99 % of solketal selectivity). Therefore, types of catalysts had no result on solketal selectivity, but had direct results on solketal yield.

According to the above results, sulfonated mesoporous performed the higher glycerol conversion than sulfonated microporous material, except H-beta and sulfonated H-beta, which caused by the reactants and products were diffusion easier through mesoporous. However, H-beta-Pr-SO$_3$H seems to be an efficient catalyst for acetalization of glycerol with acetone compared to other heterogeneous catalysts for this reaction because of its high acidity and appropriate pore sizes. Thus, H-beta-Pr-SO$_3$H was chosen to study the influence of reaction temperature, time, glycerol/acetone mole ratio and catalyst loading in this reaction without solvent.

4.5.4 Effect of reaction temperature

The effect of reaction temperature was studied at various temperature ranging from 32°C to 120°C under the condition of H-beta-Pr-SO$_3$H catalyst weight 5wt% based on glycerol, glycerol/acetone mole ratio = 1:2, time = 1 h, as represented in Table 4.9. The results exhibited that reaction at room temperature (32°C) gave the highest conversion (61.5%) and solketal yield (60.9%). Moreover, the glycerol conversions slightly decreased with increasing temperature, indicating the acetalization reaction is exothermic [66]. At the different temperatures studied, similar values of selectivity to solketal (99%) obtained. This result indicated that the effect of reaction temperature has no significant influence on the solketal selectivity.

Table 4.9 Influence of reaction temperature on acetalization of glycerol with acetone over the H-beta-Pr-SO$_3$H catalyst

Temperature (°C)	Acetalization of glycerol with acetone		
	Glycerol conversion %	Solketal Selectivity %	Solketal Yield %
32	61.5	99	60.9
65	59.6	99	59.0
100	58.8	99	58.2
120	51.5	99	51.4

Reaction condition: catalyst = H-beta-Pr-SO$_3$H, catalyst weight = 5wt% based on glycerol, glycerol/acetone mole ratio = 1:2, time = 1 h
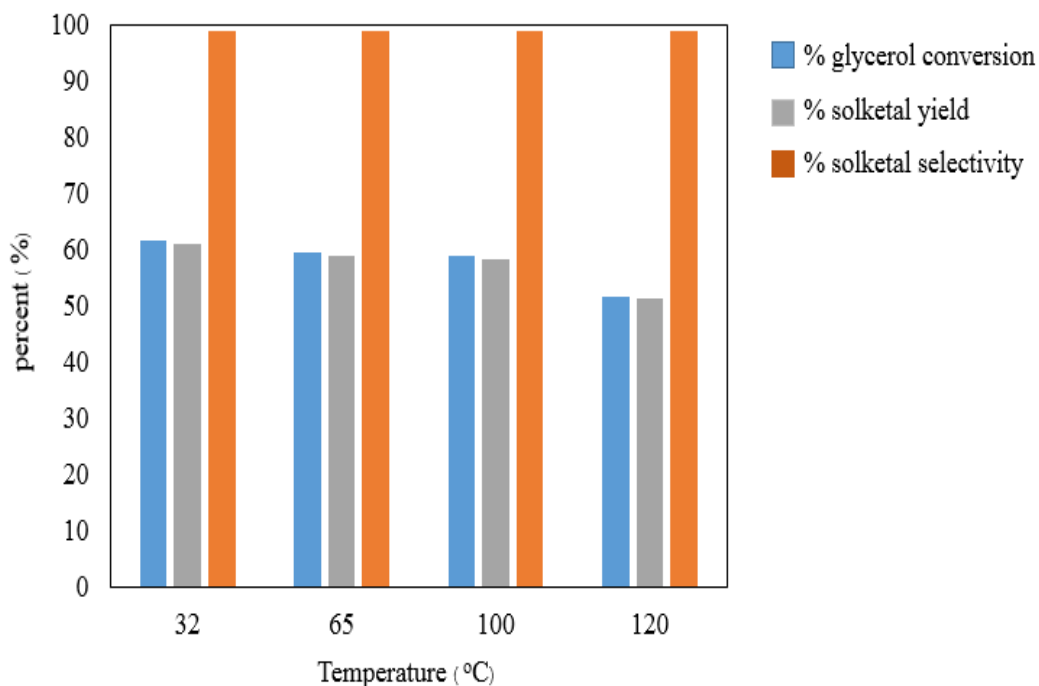
Figure 4.13 Influence of reaction temperature on acetalization of glycerol with acetone over H-beta-Pr-SO$_3$H

4.5.5 Effect of reaction time

The effect of reaction time was studied at room temperature over 5 wt% of H-beta-Pr-SO$_3$H catalyst based on glycerol. The reaction time was varied from 30 min to 480 min. From the Table 4.10, the glycerol conversion were found to be 44.6 %, 61.5%, 59.4 %, 59.6 % and 63.2% for 30, 60, 120, 240 and 480 min, respectively. It can be observed that the conversion of glycerol increased with reaction time and remains constant at 60 min. In addition, solketal selectivity was constrain at 60 min. According to this results, it can be assumed that the acetalization of glycerol with acetone achieves the equilibrium state at 60 min.

Table 4.10 Influence of reaction time on acetalization of glycerol with acetone over the H-beta-Pr-SO$_3$H catalyst

Reaction time (min)	Acetalization of glycerol with acetone		
	Glycerol conversion %	Solketal Selectivity %	Solketal Yield %
30 (0.5h)	44.6	79	35.2
60 (1h)	61.5	99	60.9
120 (2h)	59.4	99	61.3
240 (4h)	59.6	99	63.8
480 (8 h)	63.2	99	62.6

Reaction condition: catalyst = H-beta-Pr-SO$_3$H, catalyst weight 5wt% based on glycerol, glycerol/acetone mole ratio = 1:2, temperature = 32°C.
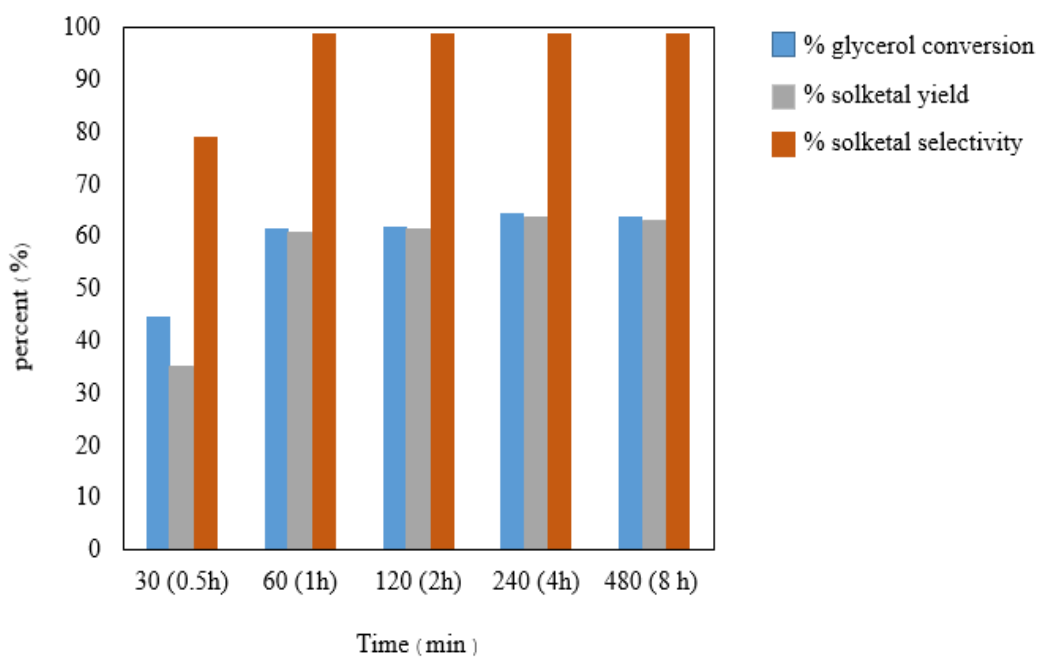
Figure 4.14 Influence of reaction time on acetalization of glycerol with acetone over H-beta-Pr-SO$_3$H at room temperature

4.5.6 Effect of glycerol to acetone mole ratio

The effect of reactants mole ratio of glycerol to acetone was studied at room temperature, for 1 h and 2.5 wt% of H-beta-Pr-SO₃H catalyst based on glycerol. The mole ratio of glycerol to acetone was varied from 1:1 to 1:12 as shown in Table 4.11. The conversion of glycerol significantly increased with increase in mole ratio from 1:1 to 1:10 because of increasing in accessibility of acetone to glycerol [22]. However, the glycerol conversion at glycerol to acetone mole ratio of 1:12 (83.9 %) was less than glycerol to acetone mole ratio of 1:10 (86.8%) that possibly caused by over flood of acetone. Thus, glycerol to acetone mole ratio of 1:10 was found to be optimum for converted glycerol to solketal due to solvation effect. Considering the selectivity, solketal selectivity was equal and maintained at 99%.

Table 4.11 Influence of mole ratio of reactants on acetalization of glycerol with acetone over the H-beta-Pr-SO₃H catalyst

Mole ratio (glycerol: acetone)	Acetalization of glycerol with acetone		
	Glycerol conversion %	Solketal Selectivity %	Solketal Yield %
1:1	43.2	99	42.8
1:2	61.5	99	60.9
1:4	76.3	99	75.5
1:8	83.2	99	82.4
1:10	86.8	99	85.9
1:12	83.9	96	80.5

Reaction condition; catalyst = H-beta-Pr-SO₃H, catalyst weight 5wt% based on glycerol, temperature = 32°C, time = 1 h.
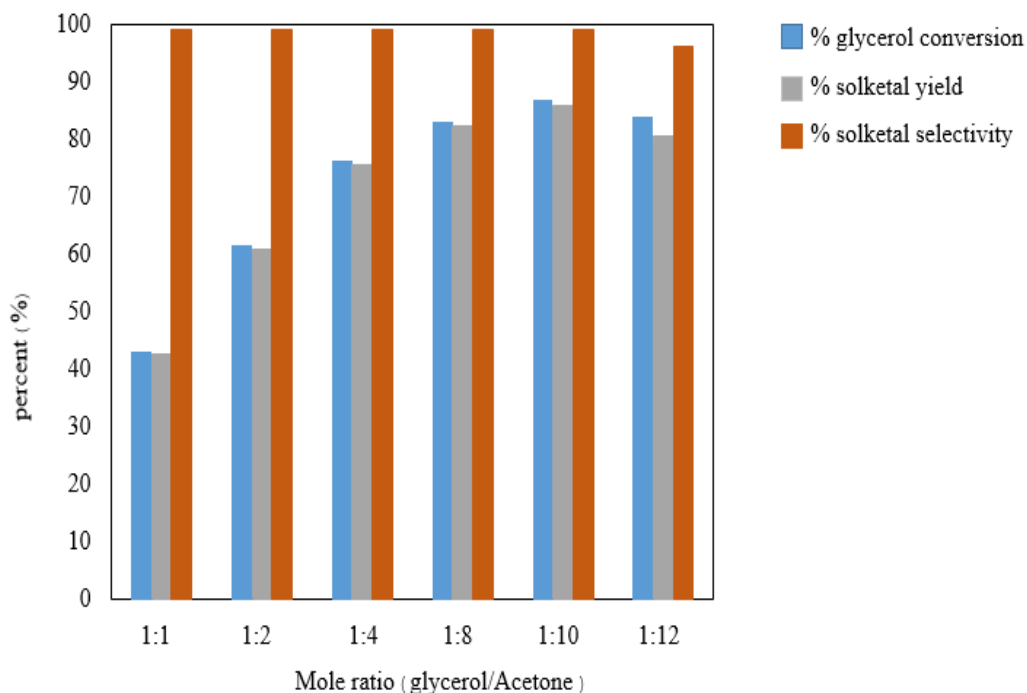
Figure 4.15 Influence of reactant mole ratio on acetalization of glycerol with acetone over H-beta-Pr-SO$_3$H at room temperature.

4.5.7 Effect of catalyst loading

The effect of catalyst loading was studied at room temperature for 1 hour by loading H-Beta-Pr-SO$_3$H at different catalyst amount from 0 to 10 wt% based on glycerol with glycerol to acetone mole ratio of 1:4 and 1:10, as shown in Table 4.12. Although the catalyst amount was increased, there was very little change in glycerol conversion and solketal yield for both of reactant mole ratios. It can be observed that H-Beta-Pr-SO$_3$H catalyst showed good conversion of glycerol even at low catalyst amount that may cause by the optimal number of acid sites on H-beta-Pr-SO$_3$H catalyst. On the other hands, glycerol conversion dramatically increased with increasing glycerol to acetone mole ratio from 1:4 to 1:10 at catalysts loading of 2.5 wt% (referred to glycerol). Thus, the catalyst loading had an impact on glycerol conversion less than the reactant mole ratio. However, catalyst loading of 2.5 wt% gave the highest solketal yield.

Table 4.12 Influence of catalyst weight on acetalization of glycerol with acetone over the H-beta-Pr-SO₃H catalyst

Catalyst weight % based on glycerol	glycerol/acetone mole ratio = 1:4			glycerol/acetone mole ratio = 1:10		
	Glycerol conversion %	Solketal Selectivity %	Solketal Yield %	Glycerol conversion %	Solketal Selectivity %	Solketal Yield %
0.00	0.0	0.0	0.0	0.00	0.00	0.00
1.25	77.1	99	76.3	90.1	99.0	89.3
2.50	78.9	99	78.1	90.8	99.0	89.9
5.00	76.3	99	75.5	86.8	99.0	85.9
10.00	76.3	99	75.6	86.0	97.6	83.9

Reaction conditions; catalyst= H-beta-Pr-SO₃H, temperature = 32°C, time = 1 h.
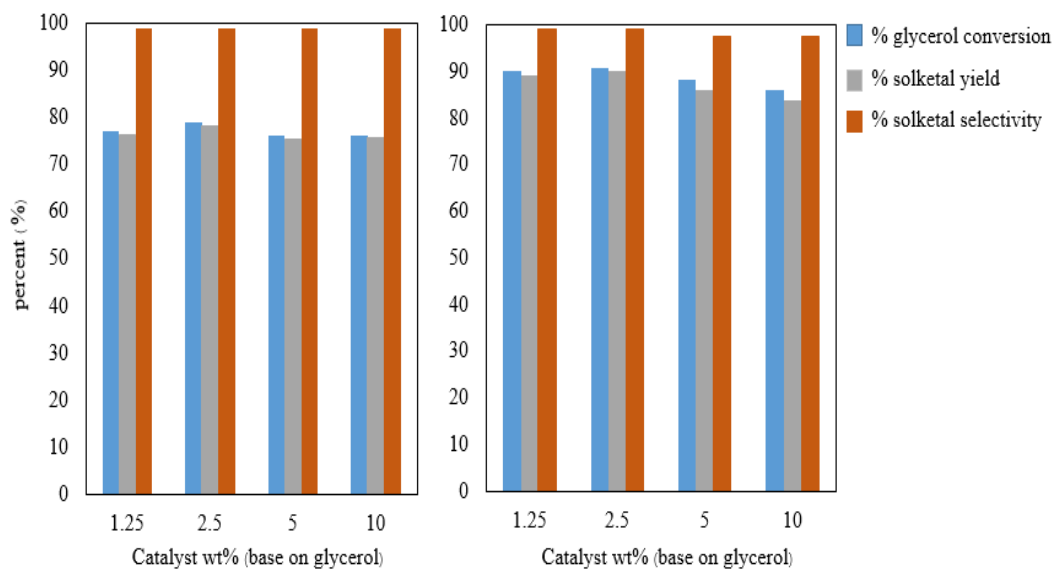
Figure 4.16 Influence of catalysts weight on acetalization of glycerol with acetone over H-beta-Pr-SO$_3$H

From this study the parameter on acetalization of glycerol with acetone that gave highest solketal yield (89.9%) with excellent solketal selectivity (99%) was room temperature (32°C), glycerol: acetone mole ratio = 1:10, catalyst weight= 2.5 wt% based on glycerol at reaction time = 1 h.

4.6 Reused of catalyst

In order to study the stability of catalysts, H-beta-Pr-SO$_3$H was chosen because of its high performance for acetalization of glycerol with acetone. In this research, H-beta-Pr-SO$_3$H was reused for third runs under optimized condition (temperature = 32°C, glycerol: acetone mole ratio = 1:10, catalyst weight = 2.5 wt% based on glycerol, time = 1 h). The used catalyst was washed with acetone for three times and dried at 70°C overnight prior to reutilization in the next batch. Moreover, all of used H-beta-Pr-SO$_3$H catalysts were characterized by X-ray diffraction, nitrogen adsorption-desorption and acid titration.

4.6.1 Characterization of used catalysts.

The XRD patterns of fresh and used H-beta-Pr-SO$_3$H catalysts were presented in Figure 4.17. From the results, the XRD pattern of all reused catalysts still revealed the characteristic peak of beta zeolite as same the fresh catalyst with very small change in intensity.

The SEM images of used 1st, used 2nd and used 3rdof H-beta-Pr-SO$_3$H catalysts at x10,000 and x30,000 magnification were represented in Figure 4.19. The morphology of all catalysts still remained uniform spherical aggregated particles.
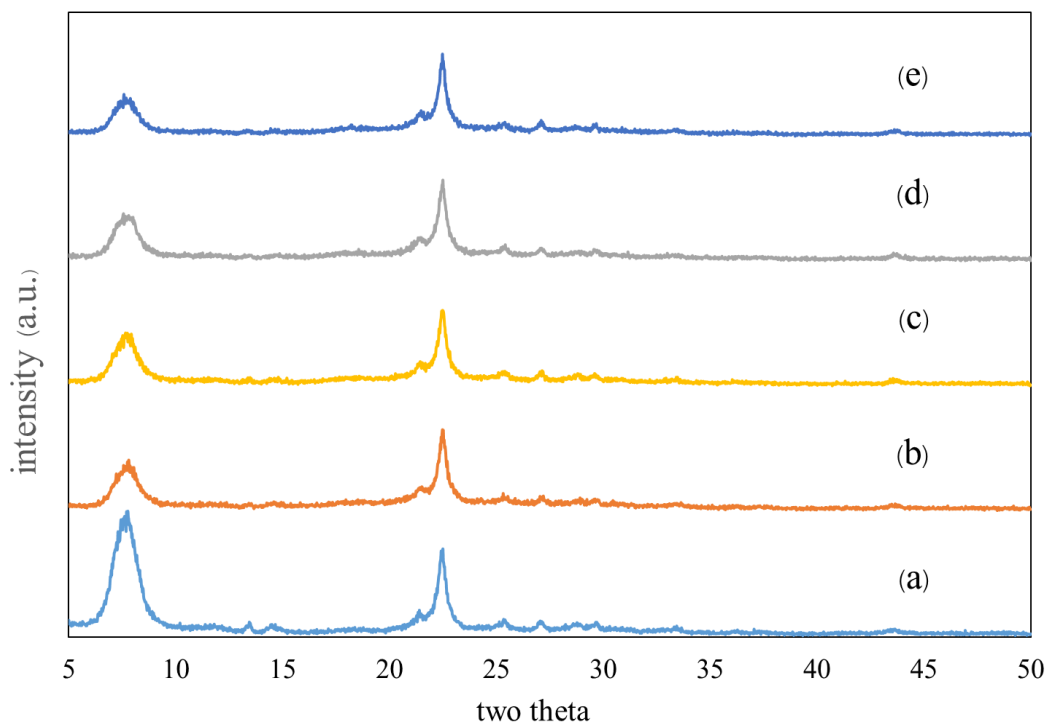
Figure 4.17 X-ray diffraction pattern of (a) commercial H-beta (b) fresh H-beta-Pr-SO$_3$H (c) used 1st H-beta-Pr-SO$_3$H (d) used 2nd H-beta-Pr-SO$_3$H and (e) used 3rd H-beta-Pr-SO$_3$H

The nitrogen adsorption-desorption isotherm of those catalysts were presented in Figure 4.18. The isotherm of all catalysts exhibited type I according to microporous materials. Even though they showed the similar isotherm shape the volume of nitrogen adsorptions of reused catalyst slightly decreased after the respective catalytic testing. Table 4.13 showed textural properties of fresh and used H-beta-Pr-SO$_3$H. After using catalysts, the specific surface area of used catalyst decreased from 351 to 192 m^2/g for the third runs, which reduced about 34 % as compared to the fresh one. Because organic molecule remained inside microporous pore. Moreover total pore volume and external surface area also slightly decreased after using catalysts liked total specific surface area.
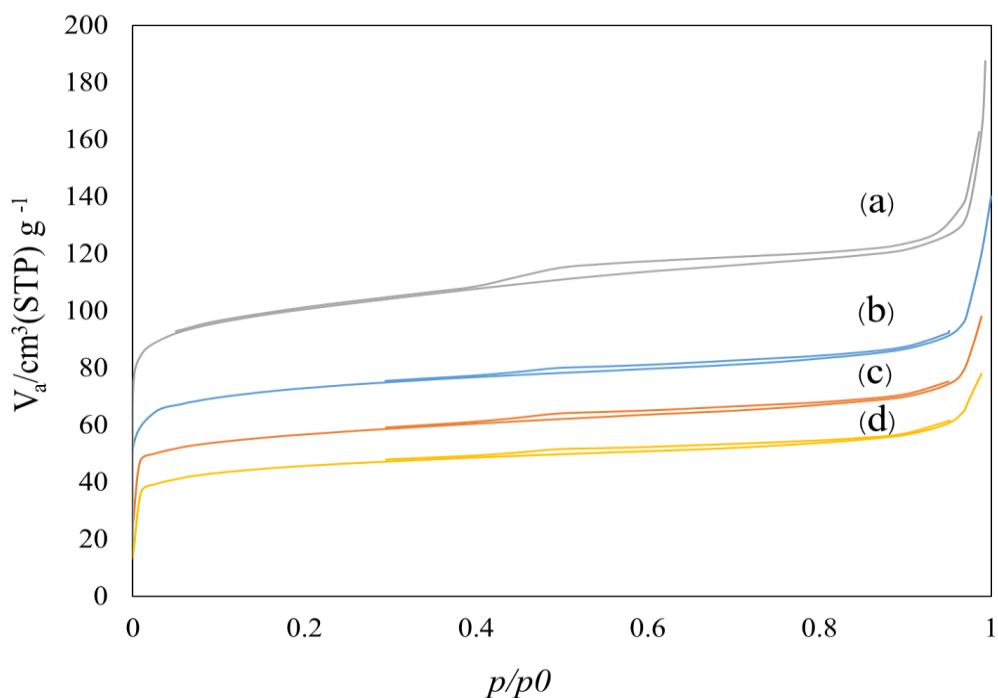
Figure 4.18 Nitrogen adsorption-desorption isotherm of (a) fresh (b) used 1st(c) Used 2nd and (d) Used 3rdH-beta-Pr-SO$_3$H

Table 4.13 Textural properties and acid amount

catalyst	S^a_{BET} (m^2/g)	Internal surface area[b] (m^2/g)	External surface area[c] (m^2/g)	Total pore volume[d] (cm^3/g)	dp^d (nm)	Acid Amount (mmol/g)
Fresh	351	304	28	0.16	0.7	1.07
After 1st run	275	252	24	0.12	0.7	1.07
After 2nd run	212	194	19	0.09	0.7	1.05
After 3rd run	192	189	12	0.09	0.7	1.04

[a] Calculate from BET method.

[b] Calculate from t-plot

[c] Internal surface area = (total surface area (from *t-plot*) –(external surface area (from *t-plot*)).

[d] Calculated from the MP method for microporous material.

[e] Determined by acid titration
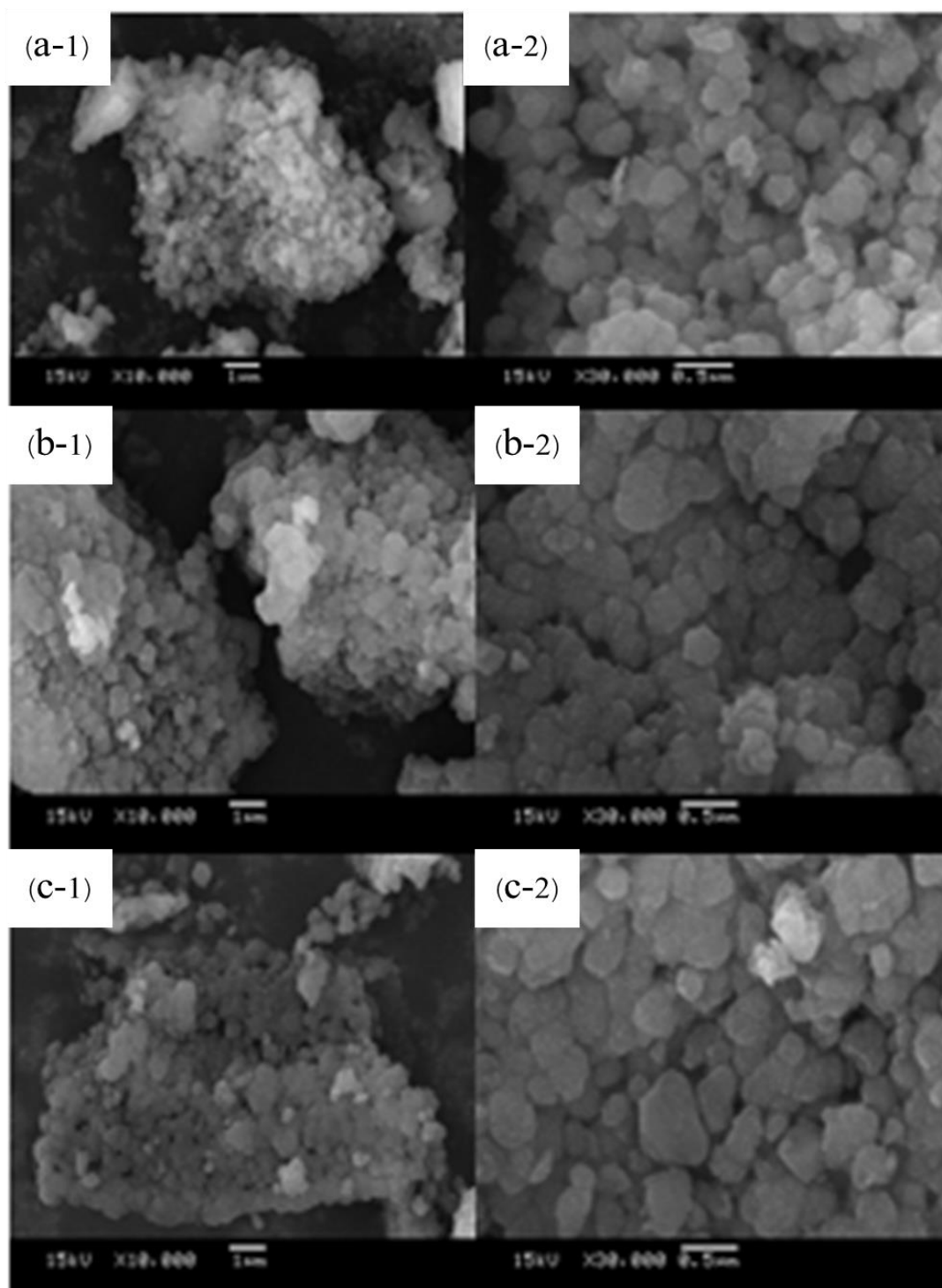
Figure 4.19 SEM images of (a) used 1st ((a-1) x1000, (a-2) x3000)), (b) used 2nd ((b-1) x1000, (b-2) x3000)), and (c) used 3^{s} ((c-1) x1000, (c-2) x3000)) H-beta-Pr-SO$_3$H

4.6.2 Catalytic activity of used catalysts

To investigate the stability of H-beta-Pr-SO$_3$H, it was tested in solketal synthesis under the optimal condition. From the catalytic activity results, solketal yield and glycerol conversion slightly decreased from 90.8% to 80.8% without considerable change in solketal selectivity after the third run which was reduced about 9.9% yield as compared to the fresh one. The reduction in solketal yield and glycerol conversion may be caused by reducing of acid site in sulfonic group and coke formation, which corresponding to the results, as shown in Table 4.14.

Table 4.14 The catalytic activity of reused H-beta-Pr-SO$_3$H test under the optimized reaction condition

Reused catalyst	Acetalization of glycerol with acetone		
	Glycerol conversion %	Solketal Selectivity %	Solketal Yield %
Fresh	90.8	99	89.9
first	85.2	99	84.3
second	84.8	99	83.9
third	80.8	99	80.0

Optimal condition: temperature = 32°C, glycerol: acetone mole ratio = 1:10, catalyst weight= 2.5 wt% based on glycerol, time = 1 h.
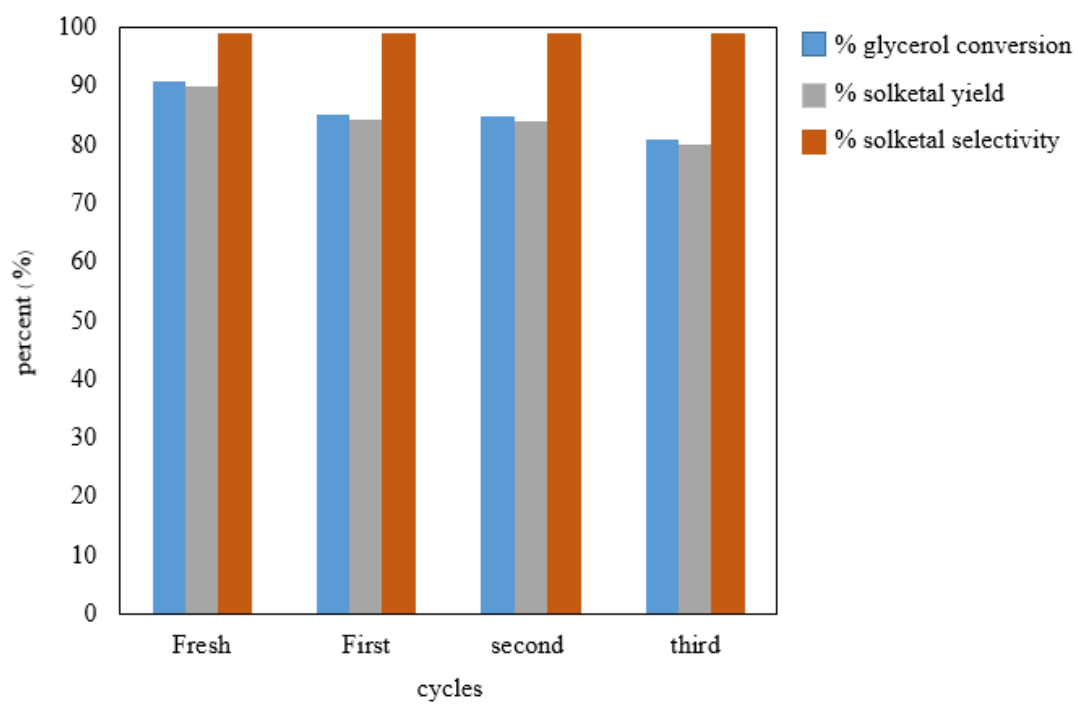
Figure 4.20 Catalyst reused test under the optimized reaction condition
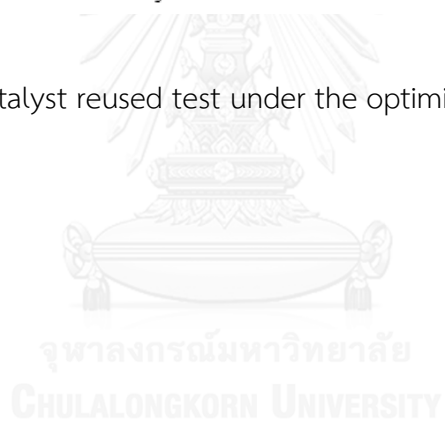
4.7 Acetalization of glycerol with other carbonyl compounds

To study effect of pore size and pore structure of microporous and mesoporous materials, we also studied the acetalization of glycerol with other carbonyl compounds such as cyclohexanone, cyclooctanone, cyclododecanone and benzaldehyde over sulfonated microporous and mesoporous materials.

4.7.1 Acetalization of glycerol with cyclohexanone

The reaction of glycerol with cyclohexanone gave two acetal products, which are 1,3 dioxalane(1,4-dioxaspiro [4,5] decan-2-ylmethnol) and 1,3 dioxane(1,5 - dioxaspiro [5,5] undecan-3-ol), as shown in Scheme 4.2. Moreover, the other products, which are (A) [1, 1'- bi(cylohexylidiene)]-2-one (B) 2-cyclohexenylcyclohexanone and (C) 1'-hydroxybi(cyclohexan)-2-one, appeared in this reaction (Figure 4.21). All of products were analyzed by GC-MS, as seen in appendix.
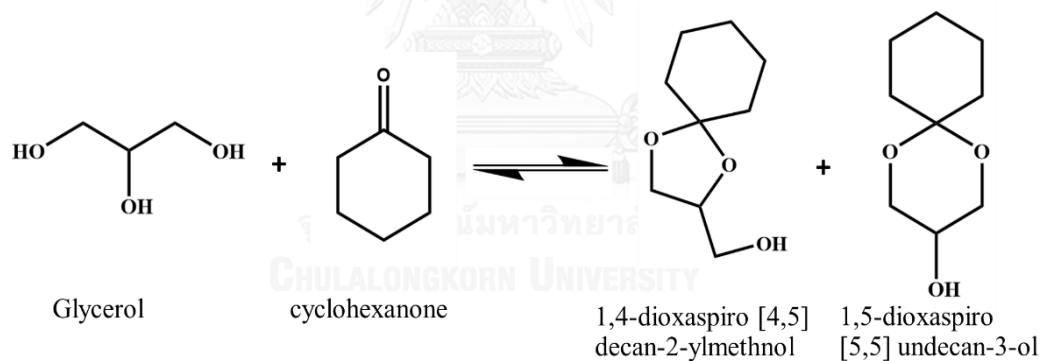
Scheme 4.2 Acetalization of glycerol with cyclohexanone
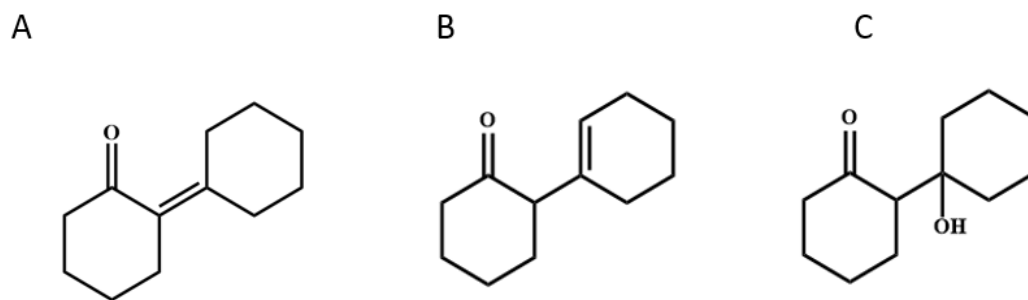
Figure 4.1 Other products (A) [1, 1'- bi(cylohexylidiene)]-2-one
(B)2-cyclohexenylcyclohexanone and (C) 1'-hydroxybi(cyclohexan)-2-one

To screen catalysts for this reaction, the reaction of glycerol with cyclohexanone was carried out over 25 mg of pre-activated catalysts under solvent free condition with glycerol to cyclohexanone mole ratio of 1:2 for 1h. Table 4.15 represents the performance of various catalysts such as sulfonated mesoporous, sulfonated microporous and commercial catalysts on this reaction. The results revealed the decreasing of glycerol conversion in following order; MCM-41-Pr-SO$_3$H> H-beta-Pr-SO$_3$H> SBA-15-Pr-SO$_3$H > MCA-Pr-SO$_3$H> Amberlyst-15 > MCM-22-Pr-SO$_3$H> HZSM-5-Pr-SO$_3$H. Blank run (in an absence of catalyst) gave glycerol conversion 25% under the same condition. As compared catalytic activity between microporous and mesoporous catalysts, it can be seen that, for microporous catalyst, H-beta-Pr-SO$_3$H showed the highest activity (90.27 % of glycerol conversion with 94.5 % of 5 membered ring selectivity), while, for mesoporous catalysts, MCM-41-Pr-SO$_3$H showed highest activity (93.56 % of glycerol conversion with 93.5 % of 5 membered ring selectivity). The interesting results were that sulfonated mesoporous catalysts showed activity better than microporous materials, except H-beta-Pr-SO$_3$H catalyst. Among the various catalysts, the highest glycerol conversion was obtained from MCM-41-Pr-SO$_3$H, with acidity of 1.17 mmol H$^+$/g. The reason for this high conversion was diffusion of molecule products to appropriated pore size and high acidic properties. Moreover, all of sulfonated catalysts also gave glycerol conversion higher than unmodified catalysts, as expected, due to the increasing of acid site on propyl sulfonic groups. Although,

Amberlyst-15 displayed highest H^+ as 4.53 mmol/g, the activity was less than sulfonated mesoporous. The reason was low surface area with nonporous materials.

From the experiment as shown in Table 4.15, it can be found that the selectivity of five membered ring, six membered ring and other products was found in the range of 80-95 %, 2-12% and 2-8%, respectively. The other products may be occurred from aldol condensation reaction of cyclohexanone by acid catalysts [67], [68].

Table 4.15 Acetalization of glycerol with cyclohexanone over micro/mesoporous sulfonated aluminosilicate

catalyst	Acidity (mmol H^+/g)	% glycerol conversion	% 5 membered	%6 membered	Other products
Catalyst free	-	24.5	78.5	14.9	6.6
Microporous materials					
H-beta	0.64	83.4	95.0	2.1	2.9
H-beta-Pr-SO₃H	1.07	90.3	94.4	2.2	3.4
H-MCM-22	0.90	73.2	95.5	2.1	2.4
MCM-22-Pr-SO₃H	1.17	84.7	94.6	2.2	3.2
H-ZSM-5	0.60	70.3	95.4	2.0	2.3
H-ZSM-5-Pr-SO₃H	0.77	77.2	94.7	2.2	3.1
Mesoporous materials					
MCM-41	0.56	34.5	80.1	11.5	8.5
MCM-41-Pr-SO₃H	1.17	93.6	95.1	2.1	3.1
SBA-15	0.67	32.3	81.0	12.5	6.5
SBA-15-Pr-SO₃H	0.87	90.0	93.5	2.5	4.0
MCA-Pr-SO₃H	0.97	87.5	94.1	2.3	3.6
Ion exchange resin					
Amberlyst-15	4.53	85.9	93.8	2.2	4.0

Reaction condition: temperature = 100°C, glycerol: acetone mole ratio = 1:2, catalyst weight =25 mg, time = 1 h.

4.7.2 Acetalization of glycerol with cyclooctanone

The reaction of glycerol with cyclooctanone was studied over sulfonated H-beta, MCM-41 and commercial Amberlyst-15. This reaction was carried out over 25 mg of catalysts with glycerol to cyclooctanone mole ratio of 1:2 for 1 h under solvent free condition. The synthesis products mixture, confirmed by GC-MS (see appendix), contained two isomeric products, a five membered cyclic 1,3 dioxalane(1,4 dioxaspiro[4.7]dodecan-2-ylmethanol) and a six membered cyclic1,3 dioxane(1,5 dioxaspiro[5.7]tridecan-3-ol), as depicted in Scheme 4.3.
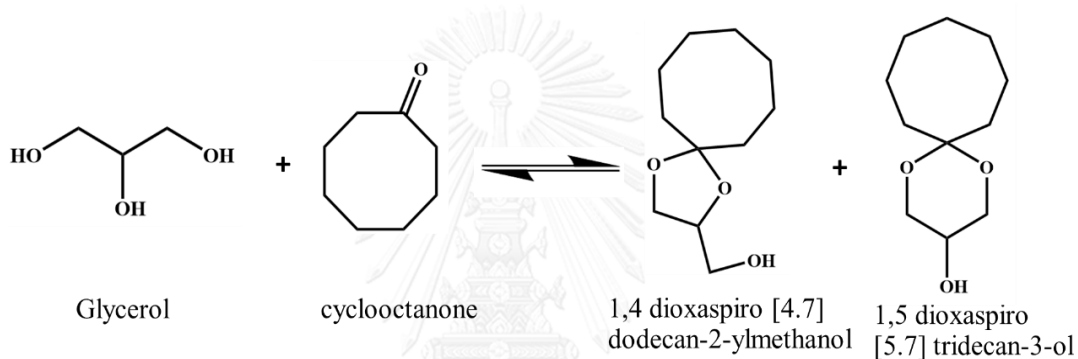
Scheme 4.3 Acetalization of glycerol with cyclooctanone

The result in Table 4.16 indicated that the highest glycerol conversion was obtained from MCM-41-Pr-SO$_3$H, resulting in 57.6 % of glycerol conversion with 96.6% selectivity of five membered cyclic acetal. All of catalysts showed selectivity of fived membered ring in high range (92-98%). The glycerol conversion was decreased in following order; MCM-41-Pr-SO$_3$H> H-beta-Pr-SO$_3$H> H-beta > Amberlyst-15, which was similar to the reaction of cyclohexanone result.

Table 4.16 Acetalization of glycerol with cyclooctanone using sulfonated catalyst and commercial catalyst

catalyst	%glycerol conversion	% selectivity of 5 membered ring	% selectivity of 6 membered ring
H-beta	47.0	97.7	2.3
H-beta-Pr-SO$_3$H	54.3	97.2	2.9
MCM-41-Pr-SO$_3$H	57.6	96.6	3.4
Amberlyst-15	44.9	92.4	7.6

Reaction condition: temperature = 100°C, glycerol: acetone mole ratio = 1:2, catalyst weight=25 mg, time = 1 h

4.7.3 Acetalization of glycerol with cyclododecanone

Scheme 4.4 Acetalization of glycerol with cyclododecanone

The reaction of glycerol with cyclododecanone was studied over sulfonated H-beta, MCM-41 and commercial beta zeolite, Amberlyst-15. This reaction was carried out over 25 mg of catalysts at 120°C with glycerol to cyclododecanone mole ratio of 1:1 for 1 h with DMF as solvent. The synthesis products, confirmed by GC-MS (see appendix), was a five membered ring (1,4 dioxaspiro[4,11]hexadecane-2-ylmethanol), as depicted in Scheme 4.4.

From the results as represented in Table 4.17, the highest glycerol conversion was obtained from MCM-41-Pr-SO$_3$H, resulting in 2.5 % of glycerol conversion with 100 % selectivity of five membered cyclic acetals. All of catalysts showed selectivity of fived membered ring in 100% selectivity. The glycerol conversion was decreased in following order; MCM-41-Pr-SO$_3$H > H-beta-Pr-SO$_3$H > H-beta > Amberlyst-15, which was constantly similar to the reaction of cyclohexanone and cyclooctanone.
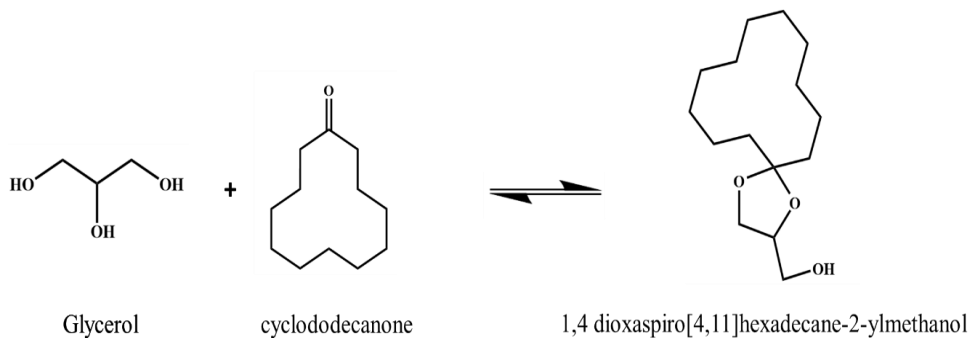
Table 4.17 Acetalization of glycerol cyclododecanone using sulfonated catalyst and commercial catalyst

catalysts	%glycerol conversion	% selectivity of acetal
H-beta	1.2	100
H-beta-Pr-SO$_3$H	1.9	100
MCM-41-Pr-SO$_3$H	2.5	100
Amberlyst-15	2.1	100

Reaction condition: temperature = 120°C, glycerol: cyclododecanone mole ratio = 1:1, DMF as solvent 20 mL, catalyst weight=25 mg, time = 1 h.

4.7.4 Acetalization of glycerol with benzaldehyde

The reaction of glycerol with benzaldehyde was studied over sulfonated H-beta, MCM-41 and commercial Amberlyst-15. This reaction was carried out over 25 mg pre-activated catalysts at 100°C with glycerol to benzaldehyde mole ratio of 1:2 for 1 h without solvent. The synthesis products mixture, confirmed by GC-MS, contained two isomeric products, a five membered cyclic 1,3 dioxalane, [2-phenyl-1,3-dioxolane-4-ylmethanol], and a six membered cyclic, 1,3-dioxane[2-phenyl-1,3-dioxane-5-ol] , as depicted in Scheme 4.5.

Glycerol   cyclooctanone   (2-phenyl-1,3-dioxolane   2-phenyl-1,3-
                                          -4-yl) methanol   dioxane-5-ol

Scheme 4.5 Acetalization of glycerol with benzaldehyde
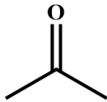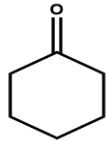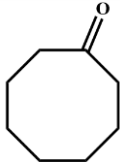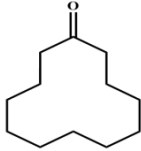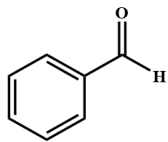
The results of acetalization of glycerol with benzaldehyde using sulfonated catalyst and commercial catalyst are displayed in Table 4.18. It can be seen that sulfonated catalyst exhibited higher glycerol conversion than commercial, as expected. The highest glycerol conversion of 80.2% was obtained from H-beta-Pr-SO$_3$H, while the lowest glycerol conversion was obtained from Amberlyst-15 with similar selectivity of 5 membered ring (59-60%).
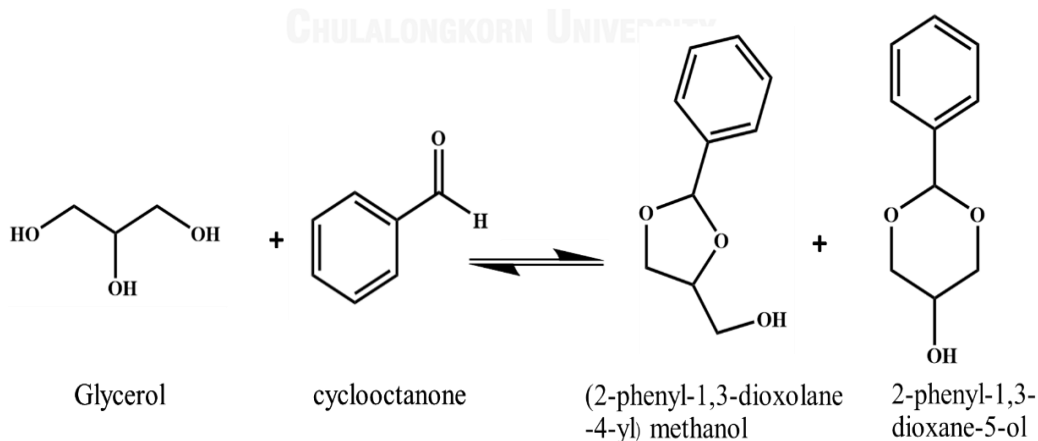
Table 4.18 Acetalization of glycerol with benzaldehyde using sulfonated catalyst and commercial catalyst

catalyst	%glycerol conversion	% selectivity of 5 membered ring	% selectivity of 6 membered ring
H-beta	77.1	60.3	39.7
H-beta-Pr-SO$_3$H	80.2	60.4	39.6
MCM-41-Pr-SO$_3$H	78.0	53.6	46.4
Amberlyst-15	70.6	59.7	40.3

Optimal condition: temperature = 100°C, glycerol: acetone mole ratio = 1:2, catalyst weight = 25 mg, time = 1 h.

Table 4.19 Summarize of glycerol conversion of acetalization of glycerol with other aldehyde/ketone

Reactant	Catalyst	% glycerol conversion	% 5 membered ring	% 6 membered ring
a (acetone)	Amberlyst-15	58.3	99.0	1.0
	H-beta	58.4	99.0	1.0
	H-beta-Pr-SO$_3$H	61.5	99.0	1.0
	MCM-41-Pr-SO$_3$H	51.7	99.0	1.0
b (cyclohexanone)	Amberlyst-15	85.9	93.8	2.2
	H-beta	83.4	95.0	2.1
	H-beta-Pr-SO$_3$H	90.3	94.4	2.2
	MCM-41-Pr-SO$_3$H	93.6	93.5	2.5
b (cyclooctanone)	Amberlyst-15	44.9	92.4	7.6
	H-beta	47.0	97.7	2.3
	H-beta-Pr-SO$_3$H	54.3	97.2	2.8
	MCM-41-Pr-SO$_3$H	57.6	96.7	3.3
c (cyclododecanone)	Amberlyst-15	2.1	100.0	0.0
	H-beta	1.2	100.0	0.0
	H-beta-Pr-SO$_3$H	1.9	100.0	0.0
	MCM-41-Pr-SO$_3$H	2.5	100.0	0.0
b (benzaldehyde)	Amberlyst-15	70.6	59.7	40.3
	H-beta	77.1	60.3	39.7
	H-beta-Pr-SO$_3$H	80.2	60.4	39.6
	MCM-41-Pr-SO$_3$H	78.0	53.6	46.4

[a] Reaction condition: temperature = 32°C, glycerol: ketone mole ratio = 1:2, catalyst weight = 5 wt% based on glycerol, time = 1 h.

[b] Reaction condition: temperature = 100°C, glycerol: ketone or aldehyde mole ratio = 1:2, catalyst weight = 25 mg, time = 1 h.

[c] Reaction condition: temperature = 120°C, glycerol: cyclododecanone mole ratio = 1:1, DMF as solvent 20 mL, catalyst weight = 25 mg, time = 1 h.

To study effect of pore size of catalysts on various carbonyl compound reactants, the structural size (length x wide) were determined using Hyperchem program, as show in Figure 4.22.

Table 4.19 summarized glycerol conversion of acetalization of glycerol with aldehyde or ketone. For cyclohexanone, cyclooctanone and cyclododecanone, MCM-41-Pr-SO$_3$H was found to be active than other catalysts but, for acetone, H-beta-Pr-SO$_3$H was found to be more active. Even though products from acetalization of glycerol with acetone, which was less steric hindrance compare to that cyclooctanone and cyclododecanone, can diffuse out of pore of all porous materials, H-beta-Pr-SO$_3$H gave the highest glycerol conversion because it has multi-dimensional with appropriated pore size (6 Å). Meanwhile, products of acetalization of glycerol with cyclohexanone, cyclooctanone and cyclododecanone can diffuse out of the pores of MCM-41-Pr-SO$_3$H (hexagonal, 2 dimensional, 24 Å) but cannot diffuse out of the pores of H-beta-Pr-SO$_3$H because of the restriction of molecular size (see Figure 4.22) [17].

Even though commercial Amberlyst-15 had high acid amount, the lower yield was presence in this catalyst. This reason might be due to its low surface area with nonporous material. Therefore, the reaction was occurred only on external surface area. In case of beta zeolite, the sulfonated beta showed better activity than un-sulfonated beta, indicating the Brønsted acid site on sulfonic group played an important role on this reaction.

(2,2-dimethyl-1,3-dioxolan-4-yl)methanol

w x l = 3.14 Å x 5.93 Å
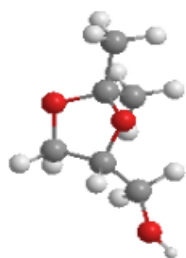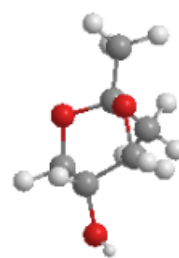
2,2-dimethyl-1,3-dioxan-5-ol

w x l = 4.32 Å x 5.91 Å
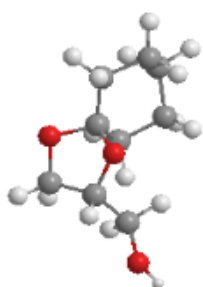
1,4-dioxaspiro[4.5]decan-2-ylmethanol

w x l =   4.05 Å x 7.36 Å
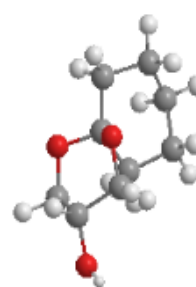
1,5-dioxaspiro[5.5]undecan-3-ol

w x l   =   5.00 Å x 7.45 Å

1,4-dioxaspiro[4.7]dodecan-2-ylmethanol

w x l =   5.51 Å x 8.74 Å
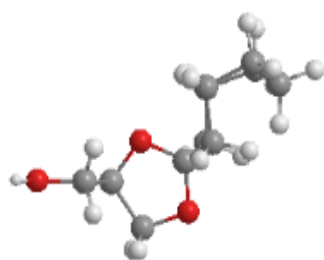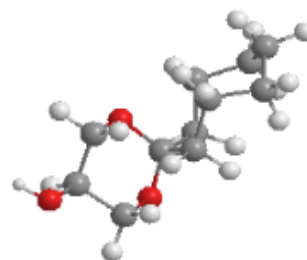
1,5-dioxaspiro[5.7]tridecan-3-ol

w x l =   5.68 Å x 8.91 Å

Figure 4.22 The structural size of products by Hyper program
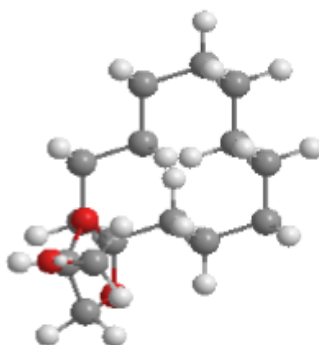
1,4-dioxaspiro[4.11]hexadecane-2-ylmethanol

w x l = 6.41 Å x 10.99 Å
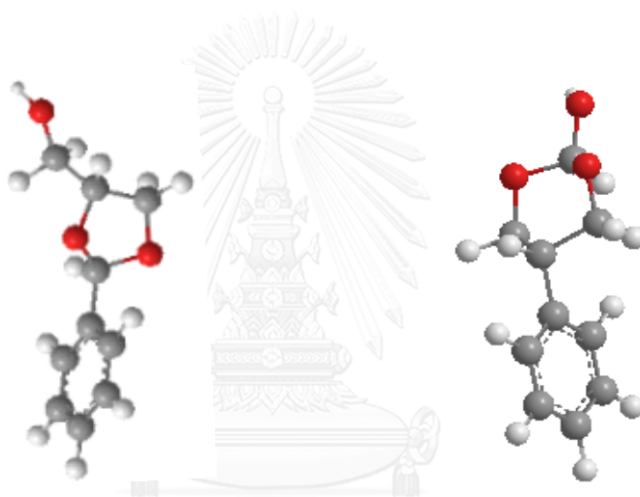
(2-phenyl-1,3-dioxolan-4-yl)methanol

w x l =   4.32 Å x 9.42 Å

2-phenyl-1,3-dioxan-5-ol

w x l = 4.34 Å x 9.83 Å

Figure 4.22 The structural size of products by Hyper program (cont.)

For each catalyst, the conversion of glycerol with carbonyl compound decreased in the order of cyclohexanone >benzaldehyde > acetone >cyclooctanone > cyclododecanone. It can be seen that the catalytic activity deceased when the steric hindrance of the reactant increased, indicating the steric factor may be important to account for different in their conversion [69]. The decreasing in conversion may be attributed to geometrical hindrance posed by eight and twelve ring conformations. Hence it may also be inferred that in addition to the rate determining step of carbonium ion, the steric factor and reactivity of ketone are also important factor when acetalization is carried out in heterogeneous catalyst [25].

All of acetalization of glycerol with ketones gave excellent selectivity to five-membered ring (94-99%), Moreover, according to the studied parameter, there were no change in solketal selectivity. The reason might be the five-membered ring was more stable than the six- membered ring isomer because of repulsively interact with the two hydrogen atoms in the other axial positions of the six-membered ring [70], as shown in Figure 4.23A. For example as shown in Figure 4.24, 3D structure of products from acetalization of glycerol with acetone exhibit that six membered ring has more repulsive than five membered ring.

In case of acetalization of glycerol with benzaldehyde, the results showed a moderate selectivity. This is due to low difference of stability between five-membered ring and six membered ring, which has no repulsive interact between hydrogen atom and phenyl group [71], [72], as shown in Figure 4.23B. Therefore, the regioselectivity is the reason for five membered ring selection on acetalization of glycerol with ketones.
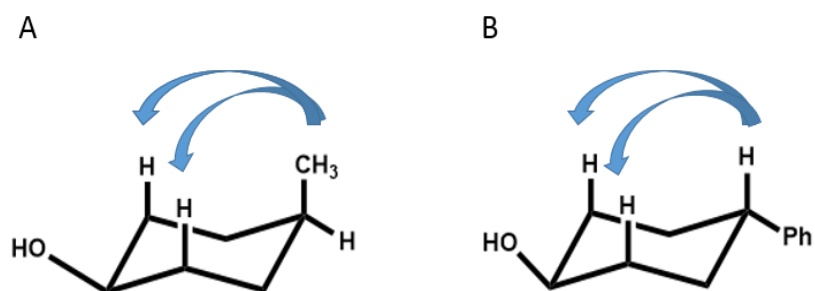
Figure 4.23 Comparison of repulsive of H atom on six membered ring of (A) 2,2 – dimethyl-1,3-dioxan-5-ol and (B) 2-phenyl-1,3-5-ol
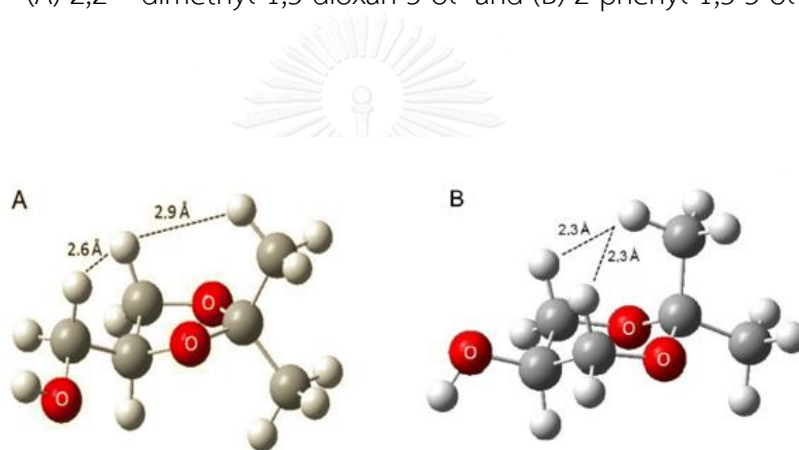
Figure 4.24 3D structure of the (A) (2,2-dimethyl-1,3-dioxolan-4yl)methanol (five-membered ring isomer) and (B) 2,2-dimethyl-1,3-dioxan-5-ol (six-membered ring isomer) [70].

Table 4.20 lists glycerol acetalization with acetone under various experimental conditions, relative data from previous reports to compare the catalytic activity with this present work. From previous researches, heteropolyacids, which was reported by Ferreira [11], exhibited the best catalytic activity (98 %glycerol conversion).However, this performance was obtained at high temperature (70°C) and longer reaction time (3 h). Moreover, the catalytic activity of heteropolyacids was decreased after the fourth run about 10%. For this present work, although H-beta-Pr-SO$_3$H gave lower glycerol conversion, this reaction was carried under milder condition with giving higher solketal selectivity.

To compare glycerol acetalization with cyclohexanone and cyclooctanone with previous researches (see Table 4.21), H-beta-Pr-SO$_3$H and MCM-41-Pr-SO$_3$Hform this work were also gave high glycerol conversion with excellent 5 membered ring acetal selectivity. Moreover, this work is a novels research for investigates acetalization of glycerol with cyclododecanone. Nevertheless, in case of glycerol acetalization with benzaldehyde (see Table 4.22), this H-beta-Pr-SO$_3$H catalyst was interestingly developed to give higher activity.

Table 4.20 Glycerol acetalization with acetone under various experimental conditions, relative data from previous reports

Rank	catalysts	Glycerol/ketone Mole ratio	T (°C)	Time (h)	%Glycerol conversion	%Solketal selectivity	%Solketal yield%	REF
				Acetalization of glycerol with acetone				
1	Heteropolyacid	1:6	70	3	98	97	95	[11]
2	Promoted metaloxide	1:6	RT	1.5	98	97	95	[12]
3	Amberlyst-15	1:2	70	1h	95	-	-	[16]
4	H-beta-Pr-SO$_3$H	1:10	32	1	91	99	90	This work
5	40 wt% MoPO/SBA-15	1:3	RT	2	90	98	88	[14]
6	H-beta	1:2	70	1	85	99	86	[22]
7	p-toluene sulfonic	1:6	RT	12	83	-	-	[8]
8	SnCl$_2$	1:4	25	1	81	98	79	[10]
9	Sulfuric acid	1:4	75	15 min	69	-	-	[9]
10	Fe/Al-SBA-15	1:1	100	8	58	99	57	[73]

- no report

Table 4.21 Glycerol acetalization with cyclohexanone and cyclooctanone under various experimental conditions, relative data from previous reports

Rank	catalysts	Glycerol/ketone Mole ratio	T (°C)	Time (h)	%Glycerol conversion	%Selectivity of 5 membered ring	REF
				Acetalization of glycerol with cyclohexanone			
1	MCM-41-Pr-SO$_3$H	1:2	100	1	94	97	This work
2	Clay	1:2	60	1	92	98	[25]
3	Microwave	1:2	140	15 min	90	99	[74]
4	H-beta-Pr-SO$_3$H	1:2	100	1	90	97	This work
5	[Cp*IrCl$_2$]$_2$	1:3	40	2	76	97	[24]
				Acetalization of glycerol with cyclooctanone			
1	MCM-41-Pr-SO$_3$H	1:2	100	1	57	97	This work
2	H-beta-Pr-SO$_3$H	1:2	100	1	54	97	This work
3	Clay	1:2	60	1	23	98	[25]

Table 4.22 Glycerol acetalization with benzaldehyde under various experimental conditions, relative data from previous reports

Rank	catalysts	Glycerol/aldehyde Mole ratio	T (°C)	Time (h)	%Glycerol conversion	%Selectivity of 5 membered	REF
		Acetalization of glycerol with benzaldehyde					
1	microwave	1:2	140	15 min	95	56	[74]
2	Clay	1:2	60	1	81	60	[25]
3	Amberlyst-36	1:1.1	RT	8	81	59	[75]
4	H-beta -Pr-SO$_3$H	1:2	100	1	80	60	This work
5	MCM-41-Pr-SO$_3$H	1:2	100	1	78	54	This work
6	RHA-SO$_3$H	1:2	120	8	78	67	[76]
7	Fe Al-SBA-15	1:1	100	4	70	84	[73]
8	MoO$_3$/SiO$_2$	1:1.1	100	16	70	30	[77]

CHAPTER 5

CONCLUSION

Propyl sulfonic functionalized beta zeolites and mesoporous silica MCM-41 were successfully synthesized by grafting method. The MPTMS was used as propyl-thiol precursor and hydrogen peroxide (H_2O_2) was used as oxidizing agent. All sulfonated catalysts were characterization by X-Ray powder diffraction, nitrogen adsorption desorption, acid-titration, SEM, FT-IR and ^{13}C-MAS-NMR. After sulfonic acid functionalization, both catalysts exhibited higher acid amount and a bit lower specific surface area. Moreover, FT-IR and ^{13}C-MAS-NMR spectra also confirmed that the propyl-sulfonic group was interoperated into the surface of materials.

For acetalization of glycerol with acetone, H-beta-Pr-SO$_3$H was found to be the best performance with excellent solketal selectivity and still gave high glycerol conversion after the third runs. Moreover, under optimal condition (Temperature = 32°C, glycerol: acetone mole ratio = 1:10, catalyst weight = 2.5 wt% based on glycerol, time = 1 h, without solvent), glycerol conversion could reach to 90 %. Whereas, for acetalization of glycerol with cyclohexanone, cyclooctanone, and cyclododecanone, MCM-41-Pr-SO$_3$H was found to be more active than H-beta-Pr-SO$_3$H, H-beta and Ambelyst-15 because bulky reactant easily diffusion into large pore of MCM-41-Pr-SO$_3$H. In selectivity, for ketone, all catalyst revealed excellent five membered ring selectivity, whereas, a moderate selectivity of five membered ring and six membered ring was found in acetalization of glycerol with benzaldehyde due to the regioselectivity.

The suggestion for future work.

1. Modified mesoporous silica by grafting method with other organno sulfonic acid such as aryl-sulfonic acid.

2. Study effect of bulkier reactant such as Pentaerythritol over H-beta-Pr-SO_3H and MCM-41-Pr-SO_3H catalyst in order to study reaction mechanism.

3. Study effect of solvent on acetalization of glycerol with acetone.

REFERENCES

[1]   Marcacci, S. Global Biofuels Market Could Double To $185.3 Billion By 2021. 2012.

[2]   Johnson, D.T. and Taconi, K.A. The glycerin glut: Options for the value-added conversion of crude glycerol resulting from biodiesel production. Environmental Progress 26(4) (2007): 338-348.

[3]   de Lima, A.L., Ronconi, C.M., and Mota, C.J. Heterogeneous basic catalysts for biodiesel production. Catalysis Science & Technology 6(9) (2016): 2877-2891.

[4]   Priya, S.S., Selvakannan, P.R., Chary, K.V.R., Kantam, M.L., and Bhargava, S.K. Solvent-free microwave-assisted synthesis of solketal from glycerol using transition metal ions promoted mordenite solid acid catalysts. Molecular Catalysis 434 (2017): 184-193.

[5]   Mota, C.J.A., Da Silva, C.X.A., Rosenbach, N., Costa, J., and Da Silva, F. Glycerin derivatives as fuel additives: The addition of glycerol/acetone ketal (solketal) in gasolines. Energy and Fuels 24(4) (2010): 2733-2736.

[6]   Selifonov, S. Glycerol levulinate ketals and their use. 2011, Google Patents.

[7]   García, J.I., García-Marín, H., and Pires, E. Glycerol based solvents: synthesis, properties and applications. Green Chemistry 16(3) (2014): 1007-1033.

[8]   Suriyaprapadilok, N. and Kitiyanan, B. Synthesis of Solketal from Glycerol and Its Reaction with Benzyl Alcohol. Energy Procedia 9 (2011): 63-69.

[9]   Monbaliu, J.-C.M., et al. Effective production of the biodiesel additive STBE by a continuous flow process. Bioresource technology 102(19) (2011): 9304-9307.

[10]   Menezes, F.D., Guimaraes, M.D., and da Silva, M.r.J. Highly selective SnCl2-catalyzed solketal synthesis at room temperature. Industrial & Engineering Chemistry Research 52(47) (2013): 16709-16713.

[11]   Ferreira, P., Fonseca, I.M., Ramos, A.M., Vital, J., and Castanheiro, J.E. Valorisation of glycerol by condensation with acetone over silica-included heteropolyacids. Applied Catalysis B: Environmental 98(1–2) (2010): 94-99.

[12]   Reddy, P.S., Sudarsanam, P., Mallesham, B., Raju, G., and Reddy, B.M. Acetalisation of glycerol with acetone over zirconia and promoted zirconia catalysts under mild reaction conditions. <u>Journal of Industrial and Engineering Chemistry</u> 17(3) (2011): 377-381.

[13]   Nandan, D., Sreenivasulu, P., Sivakumar Konathala, L.N., Kumar, M., and Viswanadham, N. Acid functionalized carbon-silica composite and its application for solketal production. <u>Microporous and Mesoporous Materials</u> 179 (2013): 182-190.

[14]   Sudarsanam, P., Mallesham, B., Prasad, A.N., Reddy, P.S., and Reddy, B.M. Synthesis of bio–additive fuels from acetalization of glycerol with benzaldehyde over molybdenum promoted green solid acid catalysts. <u>Fuel processing technology</u> 106 (2013): 539-545.

[15]   Terrill, D.L., McMurray, B.D., Billodeaux, D.R., Little, J.L., and Howard, A.S. <u>Production of cyclic acetals or ketals using solid acid catalysts</u>. 2014, Google Patents.

[16]   Da Silva, C.X.A., Gonalves, V.L.C., and Mota, C.J.A. Water-tolerant zeolite catalyst for the acetalisation of glycerol. <u>Green Chemistry</u> 11(1) (2009): 38-41.

[17]   Rabindran Jermy, B. and Pandurangan, A. Al-MCM-41 as an efficient heterogeneous catalyst in the acetalization of cyclohexanone with methanol, ethylene glycol and pentaerythritol. <u>Journal of Molecular Catalysis A: Chemical</u> 256(1–2) (2006): 184-192.

[18]   Kim, J.H. <u>Brønsted acid catalyzed asymmetric acetalizations</u>. Universität zu Köln, 2015.

[19]   Margolese, D., Melero, J., Christiansen, S., Chmelka, B., and Stucky, G. Direct syntheses of ordered SBA-15 mesoporous silica containing sulfonic acid groups. <u>Chemistry of Materials</u> 12(8) (2000): 2448-2459.

[20]   Felice, V., Ntais, S., and Tavares, A.C. Propyl sulfonic acid functionalization of faujasite-type zeolites: Effect on water and methanol sorption and on proton conductivity. <u>Microporous and Mesoporous Materials</u> 169 (2013): 128-136.

[21]   Jeenpadiphat, S., Björk, E.M., Odén, M., and Tungasmita, D.N. Propylsulfonic acid functionalized mesoporous silica catalysts for esterification of fatty acids. Journal of Molecular Catalysis A: Chemical 410 (2015): 253-259.

[22]   Manjunathan, P., Maradur, S.P., Halgeri, A.B., and Shanbhag, G.V. Room temperature synthesis of solketal from acetalization of glycerol with acetone: Effect of crystallite size and the role of acidity of beta zeolite. Journal of Molecular Catalysis A: Chemical 396 (2015): 47-54.

[23]   Sandesh, S., Halgeri, A.B., and Shanbhag, G.V. Utilization of renewable resources: Condensation of glycerol with acetone at room temperature catalyzed by organic–inorganic hybrid catalyst. Journal of Molecular Catalysis A: Chemical 401 (2015): 73-80.

[24]   Crotti, C., Farnetti, E., and Guidolin, N. Alternative intermediates for glycerol valorization: iridium-catalyzed formation of acetals and ketals. Green chemistry 12(12) (2010): 2225-2231.

[25]   Pawar, R.R., Gosai, K.A., Bhatt, A.S., Kumaresan, S., Lee, S.M., and Bajaj, H.C. Clay catalysed rapid valorization of glycerol towards cyclic acetals and ketals. RSC Advances 5(102) (2015): 83985-83996.

[26]   https://en.wikipedia.org/wiki/Catalysis. Catalysis. 2017.

[27]   Hagen, J. industrial cataysis. New York :Weinheim Wiley (1999).

[28]   Zdravkov, B., Čermák, J., Šefara, M., and Janků, J. Pore classification in the characterization of porous materials: A perspective. Open Chemistry 5(2) (2007): 385-395.

[29]   Breck, D.W. Zeolite molecular sieves. Krieger, 1984.

[30]   Kulprathipanja, S. Zeolites in industrial separation and catalysis. John Wiley & Sons, 2010.

[31]   http://www.ch.ic.ac.uk/vchemlib/course/zeolite/structure.html. secondary building units. (2017).

[32]   Deka, R.C. Acidity in zeolites and their characterization by different spectroscopic methods. (1998).

[33]   Kondo, J.N., Nishitani, R., Yoda, E., Yokoi, T., Tatsumi, T., and Domen, K. A comparative IR characterization of acidic sites on HY zeolite by pyridine and

CO probes with silica–alumina and γ-alumina references. <u>Physical Chemistry Chemical Physics</u> 12(37) (2010): 11576-11586.

[34] Lercher, J.A. and Jentys, A. Catalytic properties of micro-and mesoporous nanomaterials. in <u>Dekker Encyclopedia of Nanoscience and Nanotechnology-Six Volume Set (Print Version)</u>: CRC Press, 2004.

[35] Kresge, C., Leonowicz, M., Roth, W., Vartuli, J., and Beck, J. Ordered mesoporous molecular sieves synthesized by a liquid-crystal template mechanism. <u>nature</u> 359(6397) (1992): 710-712.

[36] Beck, J.S. and Vartuli, J.C. Recent advances in the synthesis, characterization and applications of mesoporous molecular sieves. <u>Current Opinion in Solid State and Materials Science</u> 1(1) (1996): 76-87.

[37] Inagaki, S. and Fukushima, Y. Adsorption of water vapor and hydrophobicity of ordered mesoporous silica, FSM-16. <u>Microporous and Mesoporous Materials</u> 21(4-6) (1998): 667-672.

[38] Soler-Illia, G.J.d.A., Sanchez, C., Lebeau, B., and Patarin, J. Chemical strategies to design textured materials: from microporous and mesoporous oxides to nanonetworks and hierarchical structures. <u>Chemical reviews</u> 102(11) (2002): 4093-4138.

[39] Prasomsri, T., Jiao, W., Weng, S.Z., and Martinez, J.G. Mesostructured zeolites: bridging the gap between zeolites and MCM-41. <u>Chemical Communications</u> 51(43) (2015): 8900-8911.

[40] Tanev, P.T. and Pinnavaia, T.J. A neutral templating route to mesoporous molecular sieves. <u>Science</u> 267(5199) (1995): 865.

[41] Melosh, N., et al. Molecular and Mesoscopic Structures of Transparent Block Copolymer– Silica Monoliths. <u>Macromolecules</u> 32(13) (1999): 4332-4342.

[42] de AA Soler-Illia, G.J., Crepaldi, E.L., Grosso, D., and Sanchez, C. Block copolymer-templated mesoporous oxides. <u>Current Opinion in Colloid & Interface Science</u> 8(1) (2003): 109-126.

[43] Corma, A., et al. Synthesis and structure of polymorph B of zeolite beta. <u>Chemistry of Materials</u> 20(9) (2008): 3218-3223.

[44]   Tong, M., et al. Synthesis of chiral polymorph A-enriched zeolite Beta with an extremely concentrated fluoride route. Scientific reports 5 (2015).

[45]   Aprile, C., Corma, A., and Garcia, H. Enhancement of the photocatalytic activity of TiO 2 through spatial structuring and particle size control: from subnanometric to submillimetric length scale. Physical Chemistry Chemical Physics 10(6) (2008): 769-783.

[46]   Selvam, P., Bhatia, S.K., and Sonwane, C.G. Recent advances in processing and characterization of periodic mesoporous MCM-41 silicate molecular sieves. Industrial & Engineering Chemistry Research 40(15) (2001): 3237-3261.

[47]   Rath, D., Rana, S., and Parida, K. Organic amine-functionalized silica-based mesoporous materials: an update of syntheses and catalytic applications. RSC Advances 4(100) (2014): 57111-57124.

[48]   Samutsri, S., Panpranot, J., and Tungasmita, D.N. Propylsulfonic acid functionalized MCA cubic mesoporous and ZSM-5-MCA composite catalysts for anisole alkylation. Microporous and Mesoporous Materials 239 (2017): 253-262.

[49]   Gibson, L. Mesosilica materials and organic pollutant adsorption: part A removal from air. Chemical Society Reviews 43(15) (2014): 5163-5172.

[50]   Melero, J.A., van Grieken, R., and Morales, G. Advances in the synthesis and catalytic applications of organosulfonic-functionalized mesostructured materials. Chemical reviews 106(9) (2006): 3790-3812.

[51]   Kureshy, R.I., Ahmad, I., Pathak, K., Khan, N., Abdi, S.H., and Jasra, R.V. Sulfonic acid functionalized mesoporous SBA-15 as an efficient and recyclable catalyst for the synthesis of chromenes from chromanols. Catalysis Communications 10(5) (2009): 572-575.

[52]   Pal, R., Sarkar, T., and Khasnobis, S. Amberlyst-15 in organic synthesis. Arkivoc 1 (2012): 570-609.

[53]   Spivack, J.L. Amine modified catalysts for bisphenol production. 2002, Google Patents.

[54]   Leonid, V.A. Elements of X-ray crystallography. Mcgraw-hill (1997): 4-25.

[55]   Klug, H.P. and Alexander, L.E. X-ray diffraction procedures. (1954).

[56]   Lowell, S., Shields, J.E., Thomas, M.A., and Thommes, M. Characterization of porous solids and powders: surface area, pore size and density. Vol. 16: Springer Science & Business Media, 2012.

[57]   Fang, Q.-R., Makal, T.A., Young, M.D., and Zhou, H.-C. Recent advances in the study of mesoporous metal-organic frameworks. Comments on Inorganic Chemistry 31(5-6) (2010): 165-195.

[58]   Maimon, H. Scanning electron microscope. 2016.

[59]   https://en.wikipedia.org/wiki/Solketal. solketal. 2016.

[60]   AlOthman, Z.A. and Apblett, A.W. Synthesis and characterization of a hexagonal mesoporous silica with enhanced thermal and hydrothermal stabilities. Applied Surface Science 256(11) (2010): 3573-3580.

[61]   Reddy, S.S., Raju, B.D., Kumar, V.S., Padmasri, A., Narayanan, S., and Rao, K.R. Sulfonic acid functionalized mesoporous SBA-15 for selective synthesis of 4-phenyl-1, 3-dioxane. Catalysis Communications 8(3) (2007): 261-266.

[62]   Suzuki, T.M., Nakamura, T., Sudo, E., Akimoto, Y., and Yano, K. Synthesis and catalytic properties of sulfonic acid-functionalized monodispersed mesoporous silica spheres. Microporous and Mesoporous Materials 111(1) (2008): 350-358.

[63]   Konwar, L.J., et al. Shape selectivity and acidity effects in glycerol acetylation with acetic anhydride: Selective synthesis of triacetin over Y-zeolite and sulfonated mesoporous carbons. Journal of Catalysis 329 (2015): 237-247.

[64]   Nuntasri, D., Wu, P., and Tatsumi, T. High selectivity of MCM-22 for cyclopentanol formation in liquid-phase cyclopentene hydration. Journal of Catalysis 213(2) (2003): 272-280.

[65]   Shi, J., Wang, Y., Yang, W., Tang, Y., and Xie, Z. Recent advances of pore system construction in zeolite-catalyzed chemical industry processes. Chemical Society Reviews 44(24) (2015): 8877-8903.

[66]   Qing, W., Chen, J., Shi, X., Wu, J., Hu, J., and Zhang, W. Conversion enhancement for acetalization using a catalytically active membrane in a pervaporation membrane reactor. Chemical Engineering Journal 313 (2017): 1396-1405.

[67] Chen, L., Zhao, J., Yin, S.-F., and Au, C.-T. A mini-review on solid superbase catalysts developed in the past two decades. RSC Advances 3(12) (2013): 3799-3814.

[68] Ying-Ling, M., Shen, C.-H., and Chen, C.-C. Process for producing 2-(cyclohex-1'-enyl) cyclohexanone. 2013, Google Patents.

[69] Oger, N., Lin, Y.F., Le Grognec, E., Rataboul, F., and Felpin, F.-X. Graphene-promoted acetalisation of glycerol under acid-free conditions. Green Chemistry 18(6) (2016): 1531-1537.

[70] Ozorio, L.P., Pianzolli, R., Mota, M.B.S., and Mota, C.J. Reactivity of glycerol/acetone ketal (solketal) and glycerol/formaldehyde acetals toward acid-catalyzed hydrolysis. Journal of the Brazilian Chemical Society 23(5) (2012): 931-937.

[71] Bruckner, R. Advanced organic chemistry: reaction mechanisms. Academic press, 2001.

[72] da Silva, M., Julio, A., and Dorigetto, F. Solvent-free heteropolyacid-catalyzed glycerol ketalization at room temperature. RSC Advances 5(55) (2015): 44499-44506.

[73] Gonzalez-Arellano, C., De, S., and Luque, R. Selective glycerol transformations to high value-added products catalysed by aluminosilicate-supported iron oxide nanoparticles. Catalysis Science & Technology 4(12) (2014): 4242-4249.

[74] Pawar, R.R., Jadhav, S.V., and Bajaj, H.C. Microwave-assisted rapid valorization of glycerol towards acetals and ketals. Chemical Engineering Journal 235 (2014): 61-66.

[75] Deutsch, J., Martin, A., and Lieske, H. Investigations on heterogeneously catalysed condensations of glycerol to cyclic acetals. Journal of catalysis 245(2) (2007): 428-435.

[76] Adam, F., Batagarawa, M.S., Hello, K.M., and Al-Juaid, S.S. One-step synthesis of solid sulfonic acid catalyst and its application in the acetalization of glycerol: crystal structure of cis-5-hydroxy-2-phenyl-1, 3-dioxane trimer. Chemical Papers 66(11) (2012): 1048-1058.

[77] Umbarkar, S.B., et al. Acetalization of glycerol using mesoporous MoO 3/SiO 2 solid acid catalyst. <u>Journal of Molecular Catalysis A: Chemical</u> 310(1) (2009): 150-158.

APPENDIX

Calculate mole solketal in mixture solution

x = peak area of solketal / peak area of internal standard

y = mass of solketal (g)/mass internal standard (n-dodecane, g)

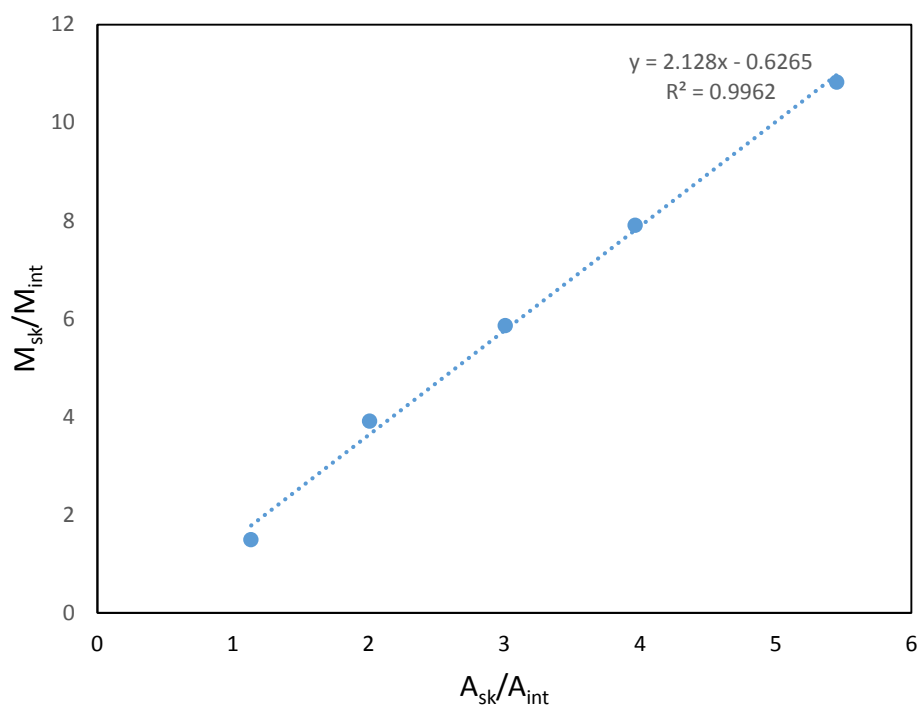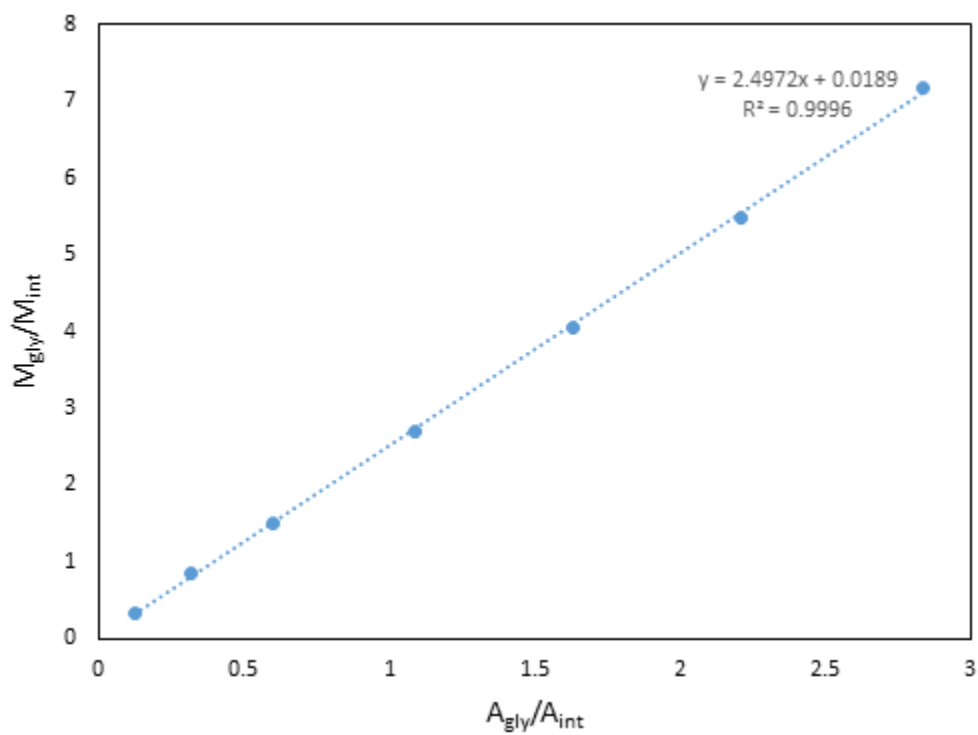Solketal   calibration cure   y = 2.128x-0.6265, R^2 = 0.9962

Figure A-1 calibration curve of solketal

Calculate mole glycerol in mixture solution

x = peak area of glycerol / peak area of internal standard

y = mass of glycerol (g)/mass internal standard (n-dodecane, g)

Glycerol   calibration cure   y = 2.4972x+0.0189, R^2 = 0.9996

Figure A-2 calibration curve of glycerol

Gas chromatograph

Acetalization of glycerol with acetone

Column oven programing

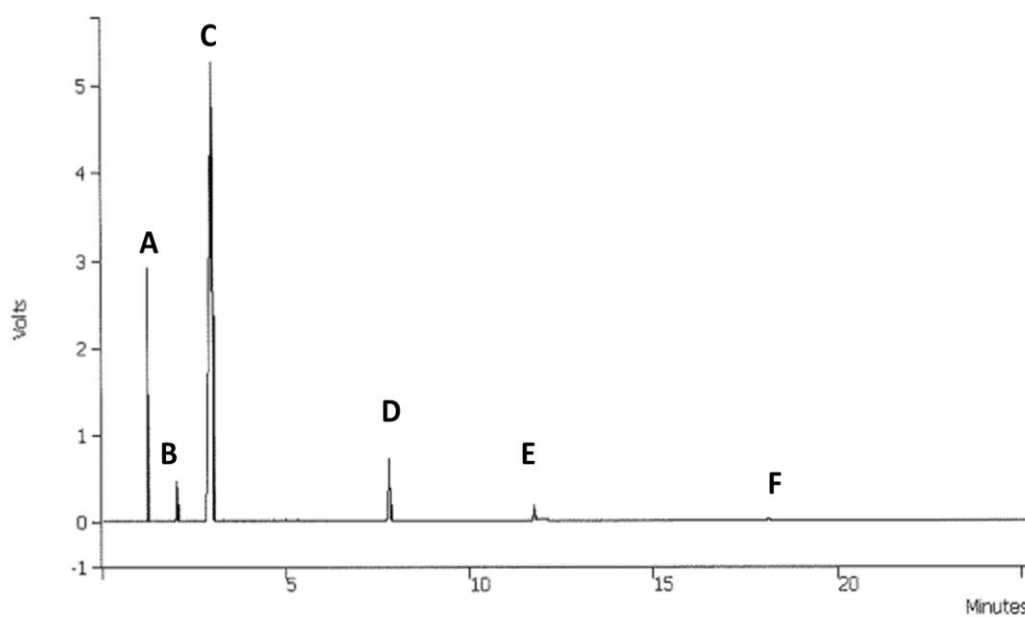| Temperature (°C)	Rate (°C/min)	Hold (min)
90	-	2
150	10	1
200	10	4
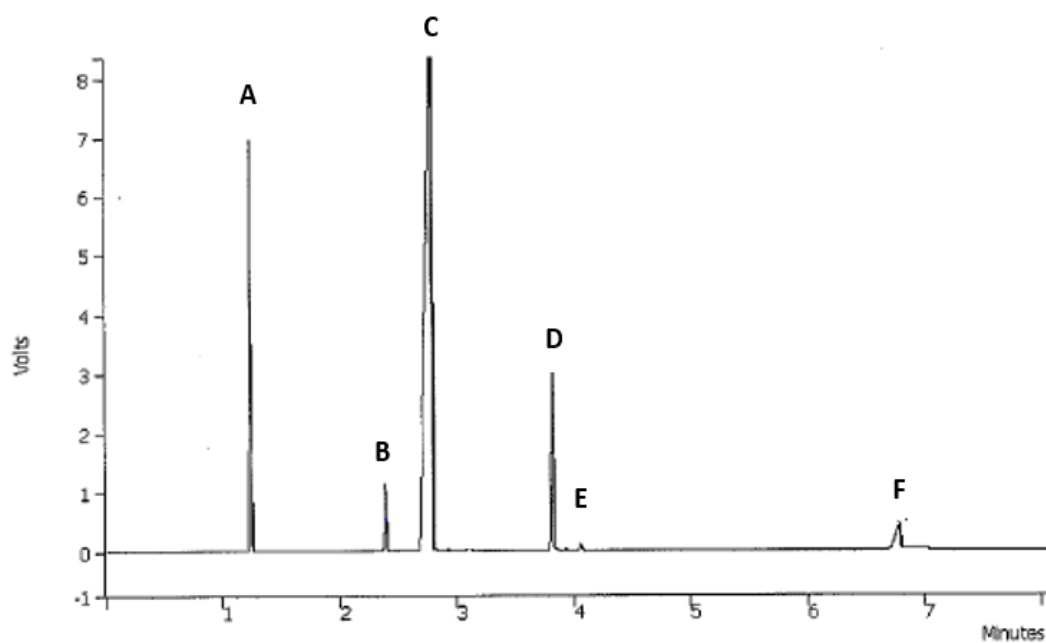
Figure A-3 Gas chromatogram of products from acetalization of glycerol with acetone

A = acetone   B = n-dodecane (internal standard)

C = dimetylforformamide (DMF)   D = five- membered ring

E = six- membered ring   F = glycerol

Acetalization of glycerol with cyclohexanone

Column oven programming

| Temperature ($^{\circ}$C)	Rate ($^{\circ}$C/min)	Hold (min)
90	-	2
110	10	2
150	10	2
170	10	4
200	10	4
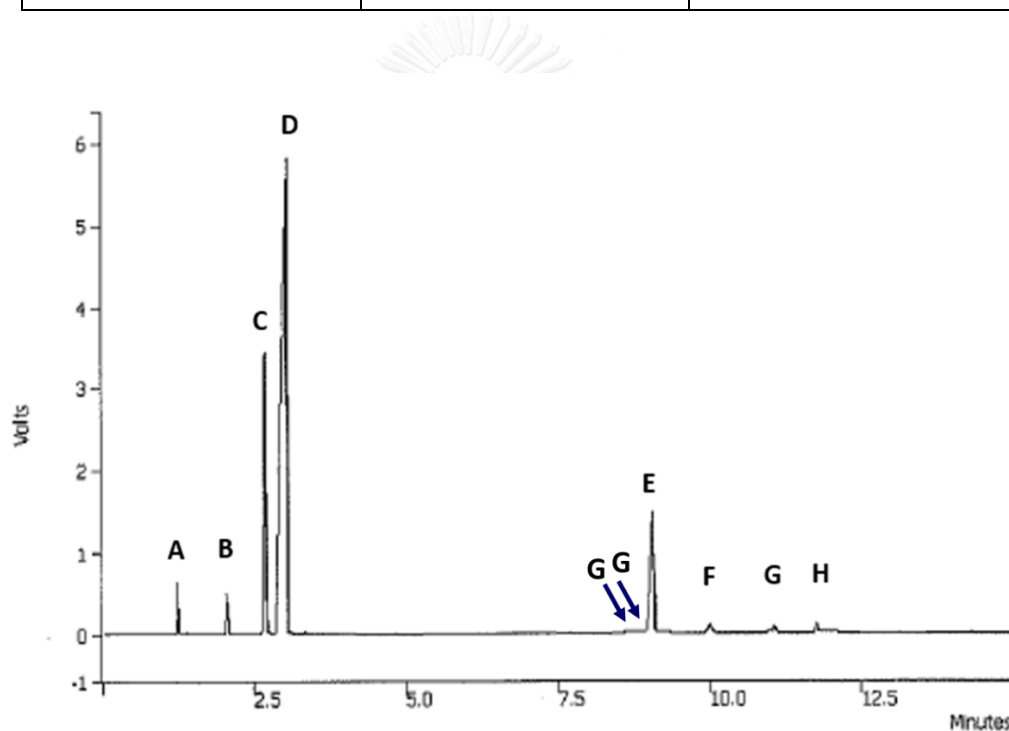
Figure A-4 Gas chromatogram of products from acetalization of glycerol with cyclohexanone.

A = acetone   B = n-dodecane (internal standard)

C = cyclohexanone   D = dimethylformamide (DMF)

E = five-membered ring   F = six- membered ring

G = other product   H = glycerol

Acetalization of glycerol with cyclooctanone

Column oven programming

Temperature ($^{\circ}$C)	Rate ($^{\circ}$C/min)	Hold (min)
90	-	2
110	10	2
150	10	2
170	10	4
200	10	4
230	10	5
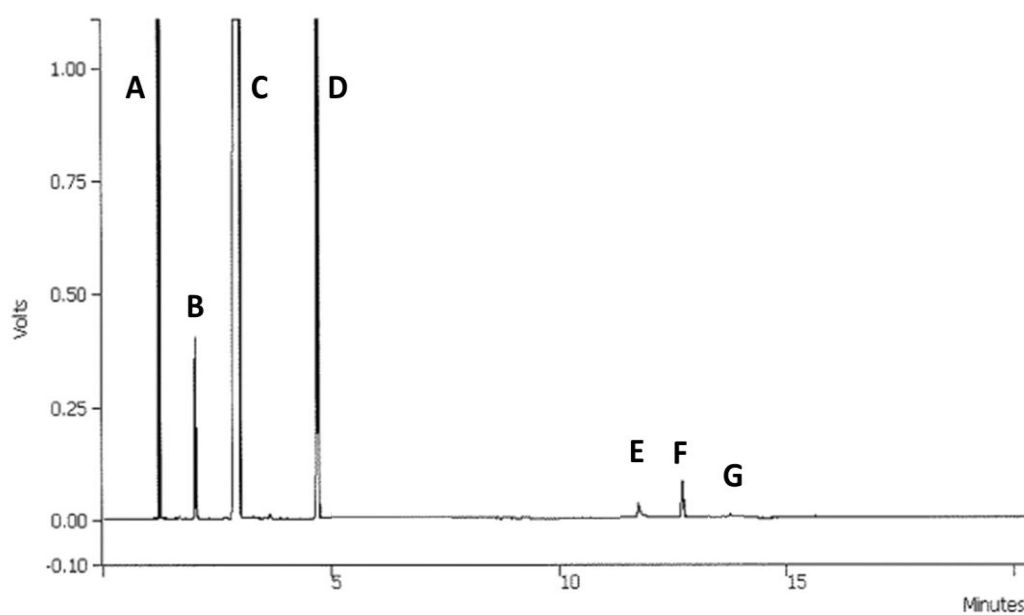
Figure A-5 Gas chromatogram of products from acetalization of glycerol with cyclooctanone

A = acetone

C = dimethylformamide (DMF)

E = glycerol

G = six - membered ring

B = n-dodecane (internal standard)

D = cyclooctanone

F = five- membered ring

Acetalization of glycerol with cyclododecanone

Column oven programming

Temperature ($^{\circ}$C)	Rate ($^{\circ}$C/min)	Hold (min)
90	-	2
110	10	2
150	10	2
170	10	4
200	10	4
230	10	10

Figure A-6 Gas chromatogram of products from acetalization of glycerol with cyclododecanone

A = acetone   B = n-dodecane (internal standard)

C = dimethylformamide (DMF)   D = cyclododecanone

E = glycerol   F = five membered ring

Acetalization of glycerol with benzaldehyde

Column oven programming

Temperature (^{o}C)	Rate (^{o}C/min)	Hold (min)
90	-	2
110	10	2
150	10	2
200	10	4
230	10	6
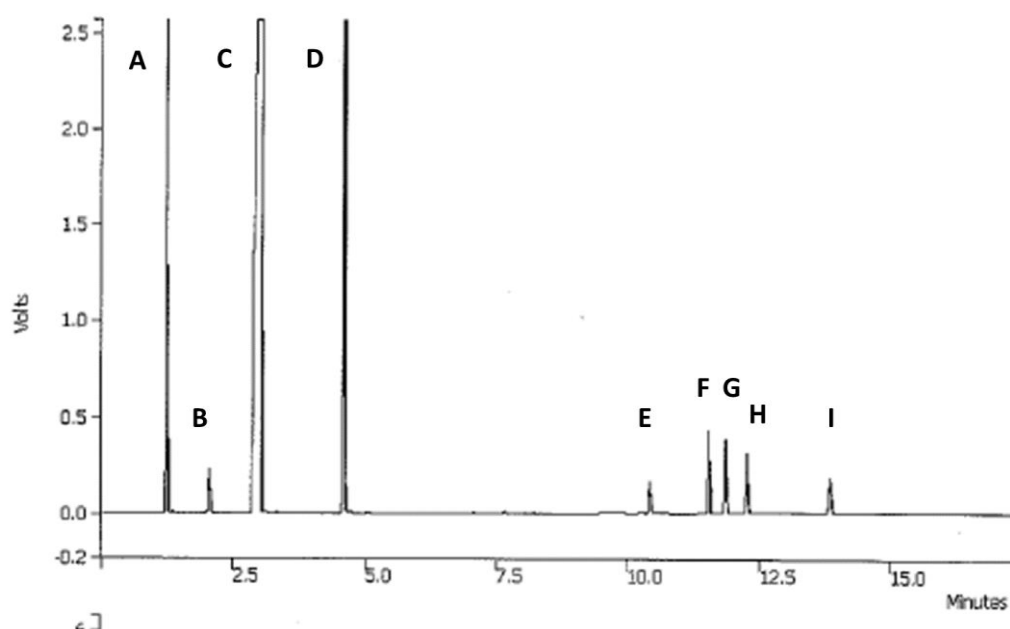
Figure A-7 Gas chromatogram of products from acetalization of glycerol with benzaldehyde.

A = acetone   B = n-dodecane (internal standard)

C = dimethylformamide (DMF)   D = benzaldehyde

E =glycerol   F = five-membered ring

G = five-membered ring   H = six-membered ring

I = six-membered ring

Gas chromatography–mass spectrometry (GC-MS)

Acetalization of glycerol with acetone
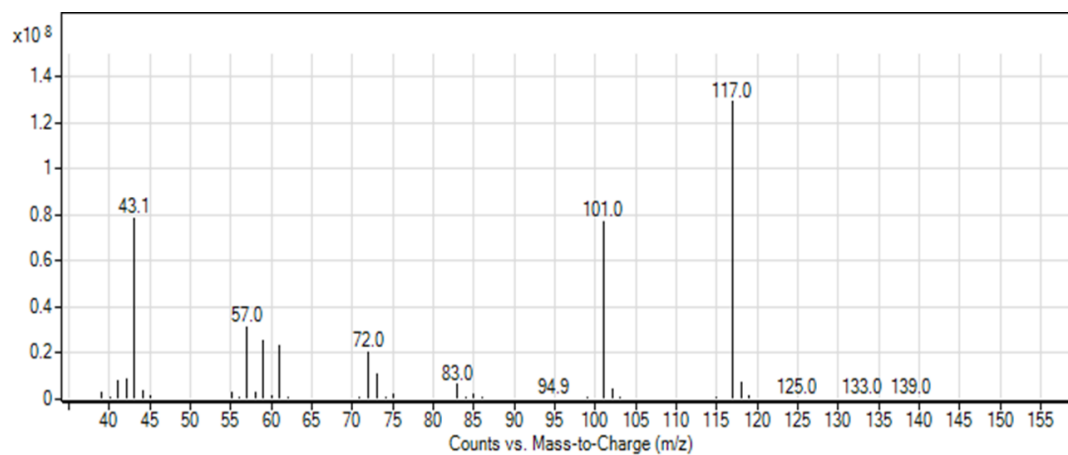
Solketal (five membered ring)

Figure A-8 Mass Spectrum of 2, 2 dimethyl-1, 3-dioxolane-4-methanol,

MW = 132 gmol^{-1}

m/z 132 gmol^{-1} m/z 117 gmol^{-1} m/z 101 gmol^{-1}
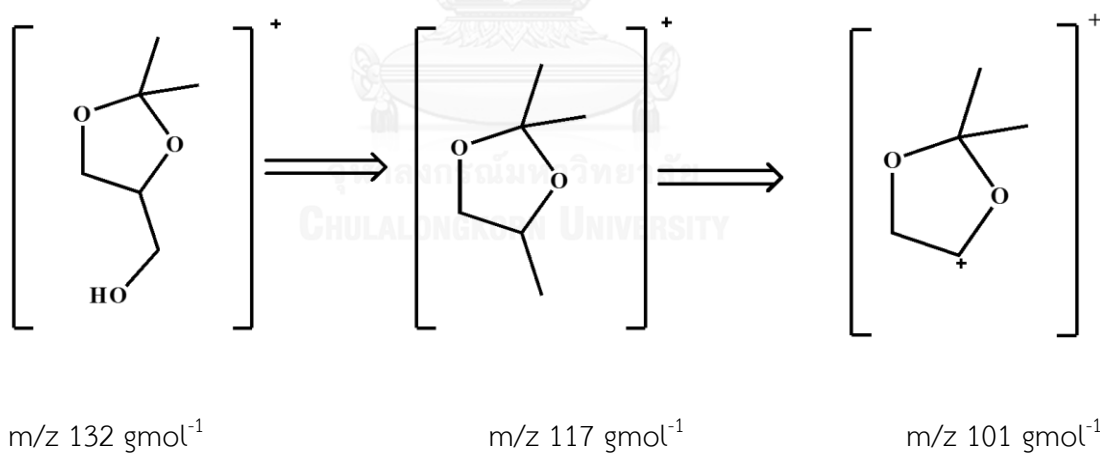
Acetalization of glycerol with acetone
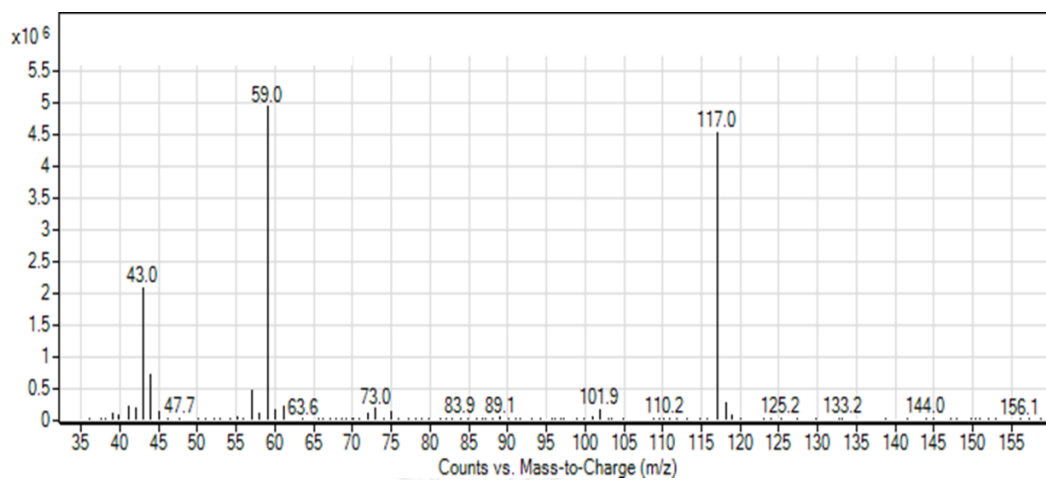
6 membered ring

Figure A-9 Mass Spectrum of 2, 2-dimethyl-1, 3- dioxolan-5-ol, MW = 117 gmol^{-1}

m/z 132 gmol^{-1} m/z 117 gmol^{-1} m/z 59 gmol^{-1}
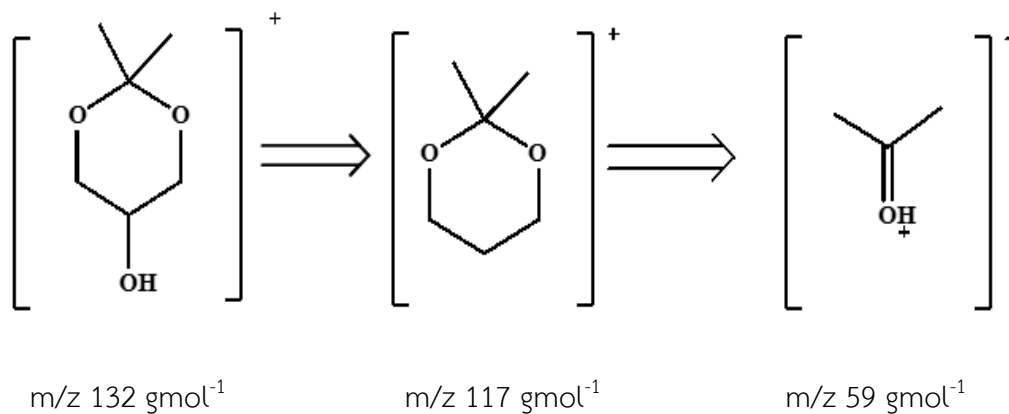
Acetalization of glycerol with cyclohexanone
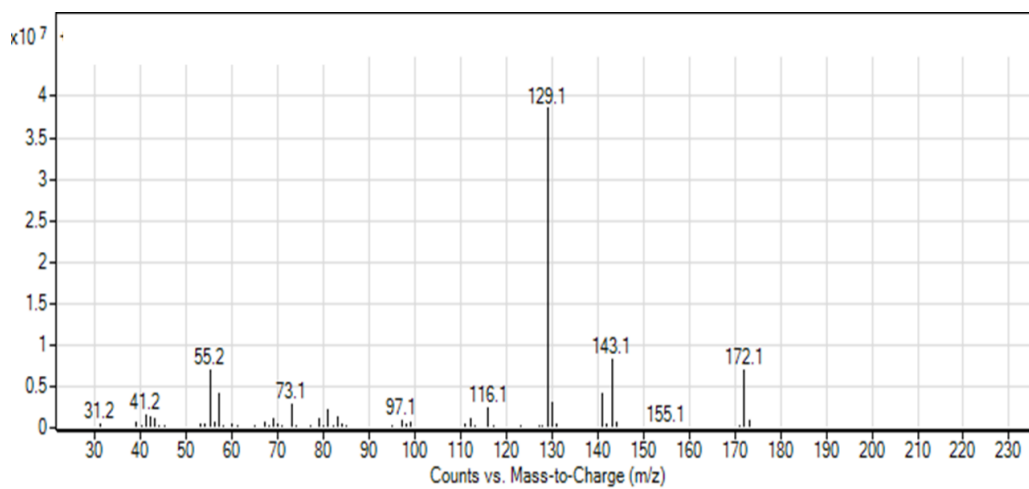
5 membered ring

Figure A-10 Mass Spectrum of (1,4-dioxaspiro [4,5] decan-2-ylmethnol) ,

MW = 172 gmol^{-1}

m/z 172 gmol^{-1} m/z 142 gmol^{-1} m/z 74 gmol^{-1}

Acetalization of glycerol with cyclohexanone

6 membered ring

Figure A-11 Mass Spectrum of 1,3dioxane (1,-dioxaspiro [5,5] undecan-3-ol),

MW = 172 gmol^{-1}

m/z 172 gmol^{-1} m/z 155 gmol^{-1} m/z 99 gmol^{-1}
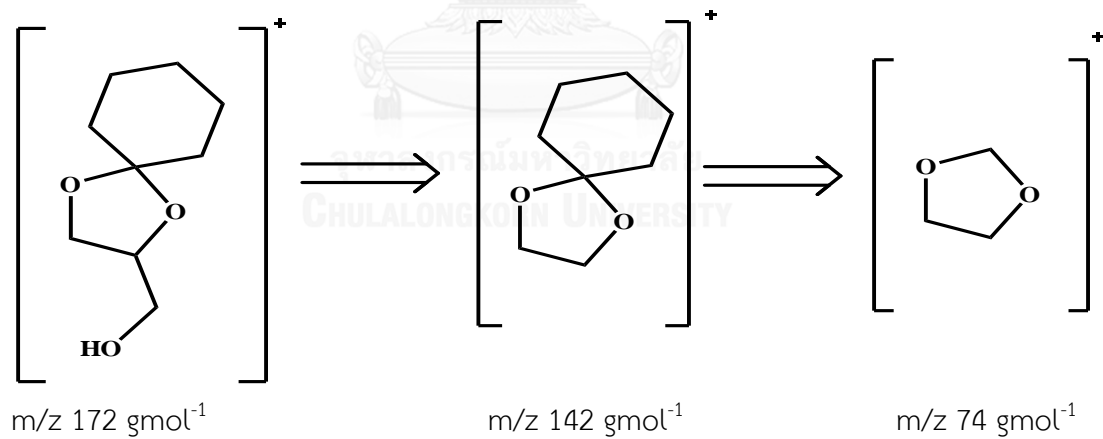
Acetalization of glycerol with cyclohexanone
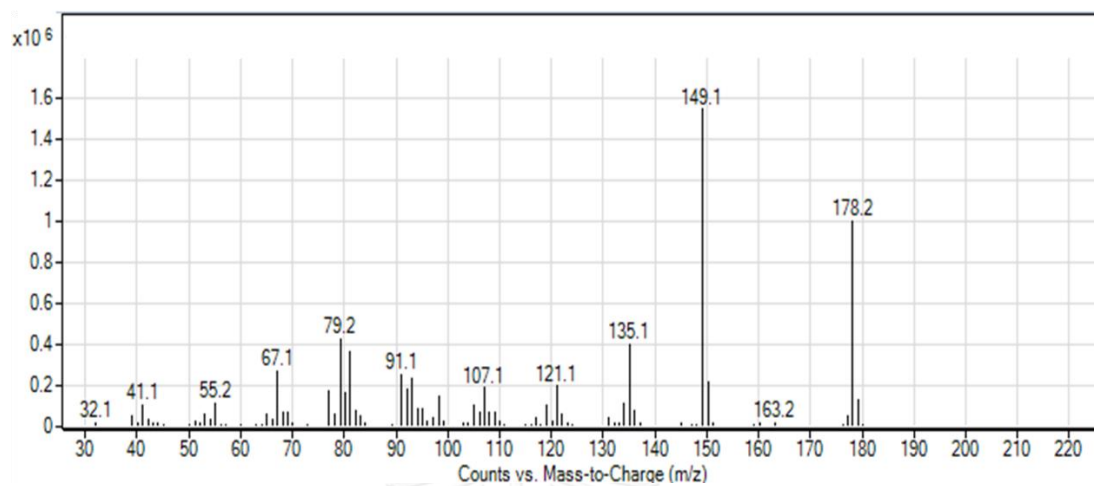
Other product

**Figure A-12** Mass Spectrum of 2-cyclohexenylcyclohexanone, MW = 178 gmol^{-1}

m/z 178 gmol^{-1} m/z 149 gmol^{-1}
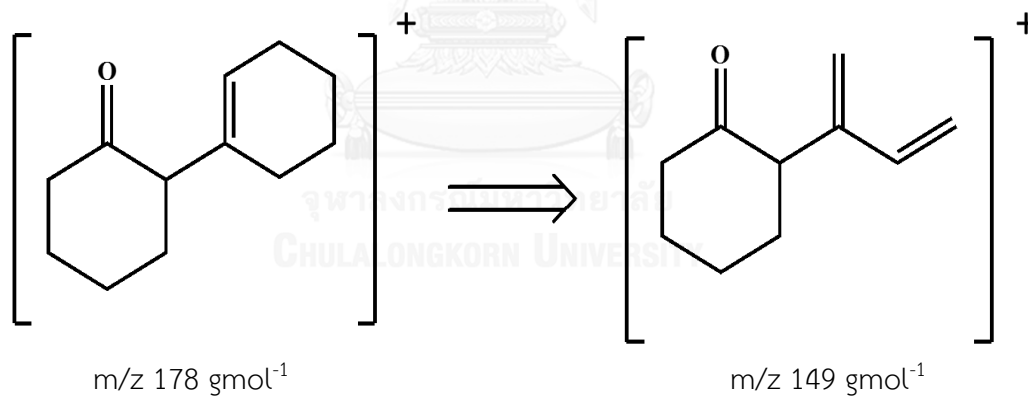
Acetalization of glycerol with cyclohexanone
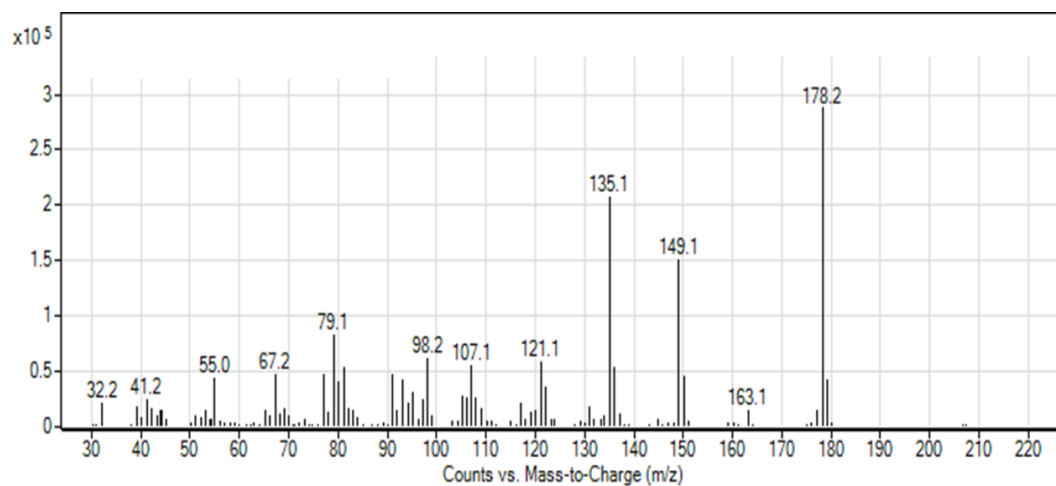
Other products

Figure A-13 Mass Spectrum of [1, 1'- bi (cylohexylidiene)]-2-one, MW = 178 gmol^{-1}

m/z 178 gmol^{-1} ⟹ m/z 135 gmol^{-1}
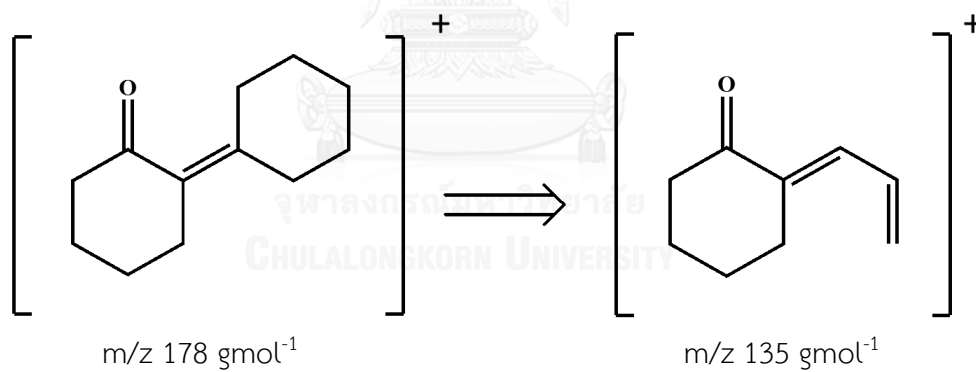
Acetalization of glycerol with cyclohexanone
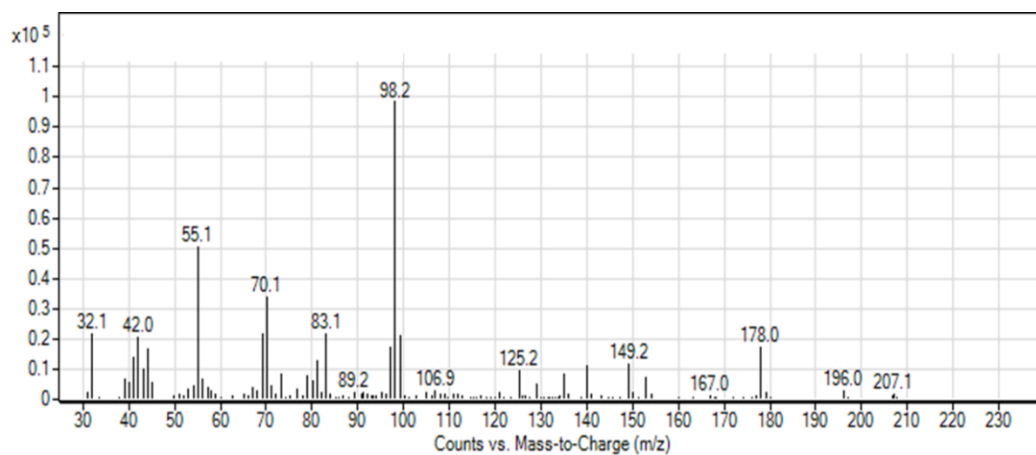
Other products

Figure A-14 Mass Spectrum of1'-hydroxybi (cyclohexan)-2-one, MW = 196 gmol^{-1}

m/z 196 gmol^{-1} m/z 178 gmol^{-1}
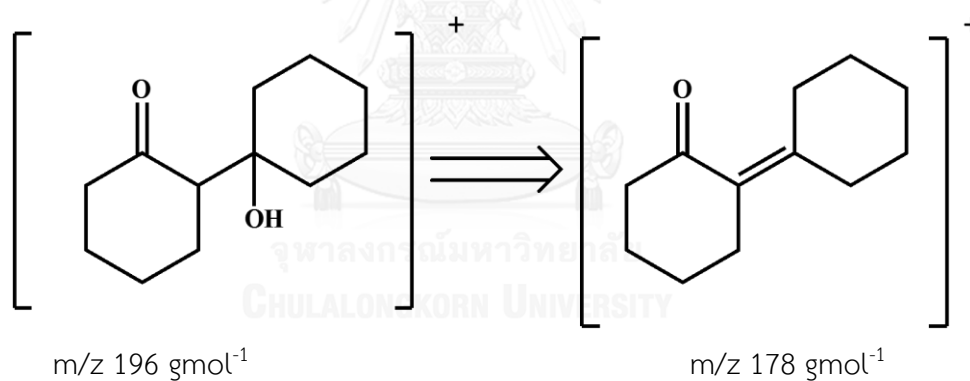
Acetalization of glycerol with benzaldehyde
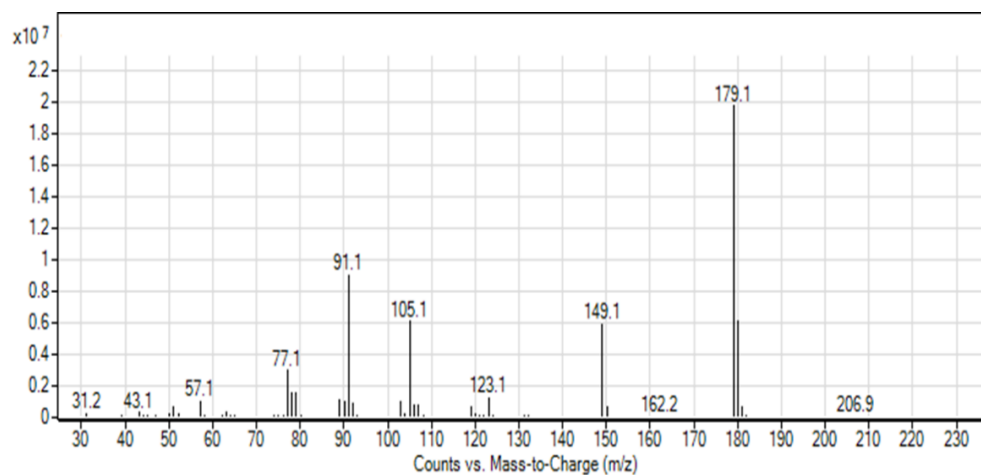
5 membered ring

Figure A-15 Mass Spectrum of [2-phenyl-1,3-dioxolane-4-yl) methanol] ,
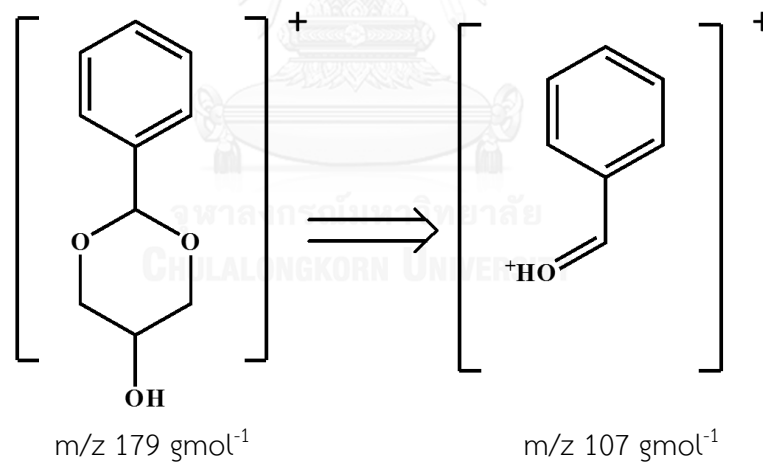
MW = 179 gmol^{-1}

m/z 179 gmol^{-1} m/z 162 gmol^{-1} m/z 150 gmol^{-1}
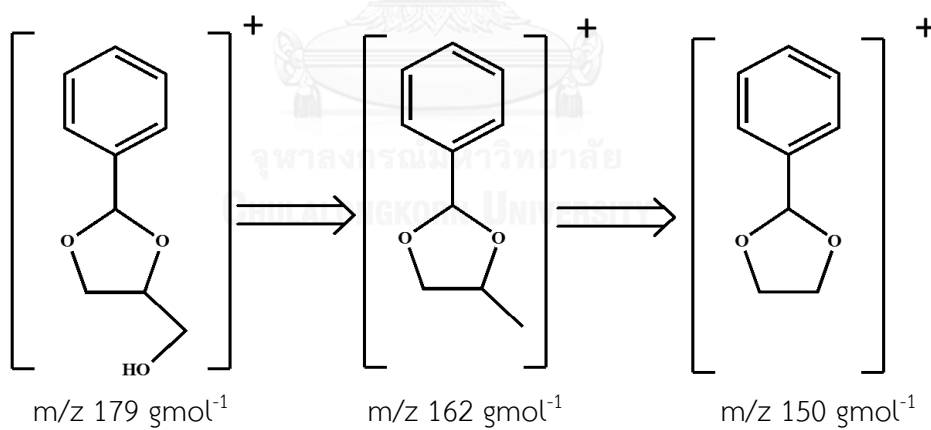
Acetalization of glycerol with benzaldehyde
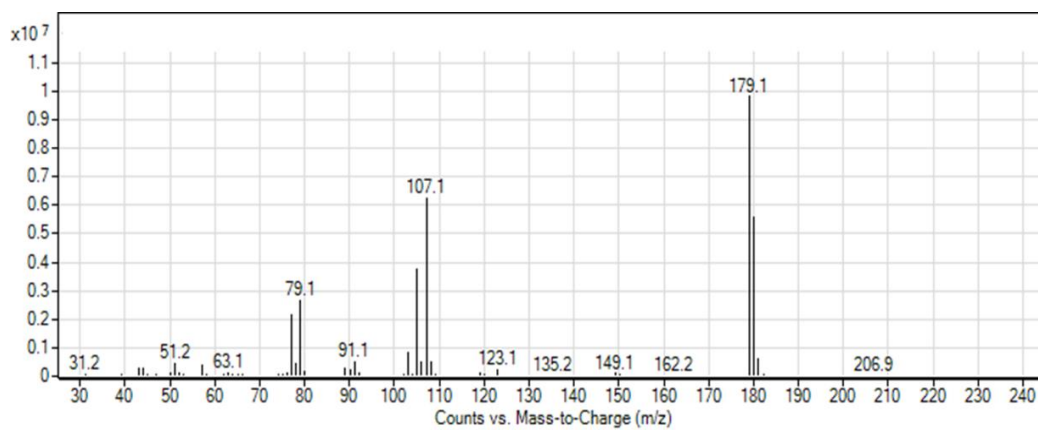
6 membered ring

Figure A-16 Mass Spectrum of 2-phynyl-1,3-dioxane-5-ol , MW = 179 gmol^{-1}

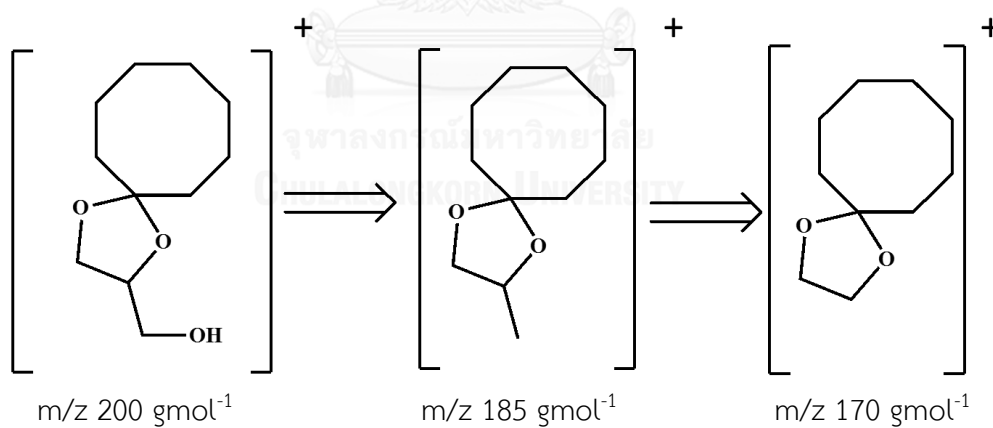m/z 179 gmol^{-1} m/z 107 gmol^{-1}

Acetalization of glycerol with cyclooctanone
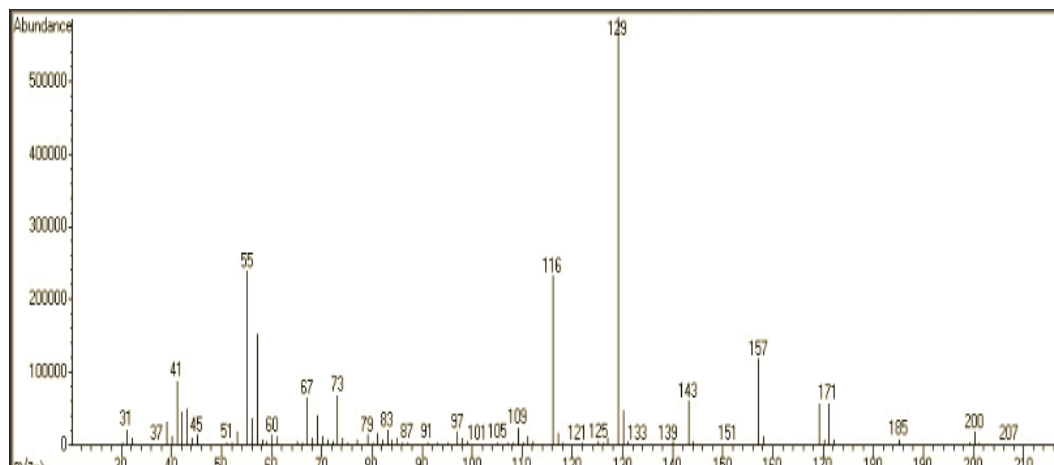
5 membered ring

Figure A-17 Mass Spectrum of (1,4dioxaspiro [4.7]dodecan-2-ylmethanol) ,
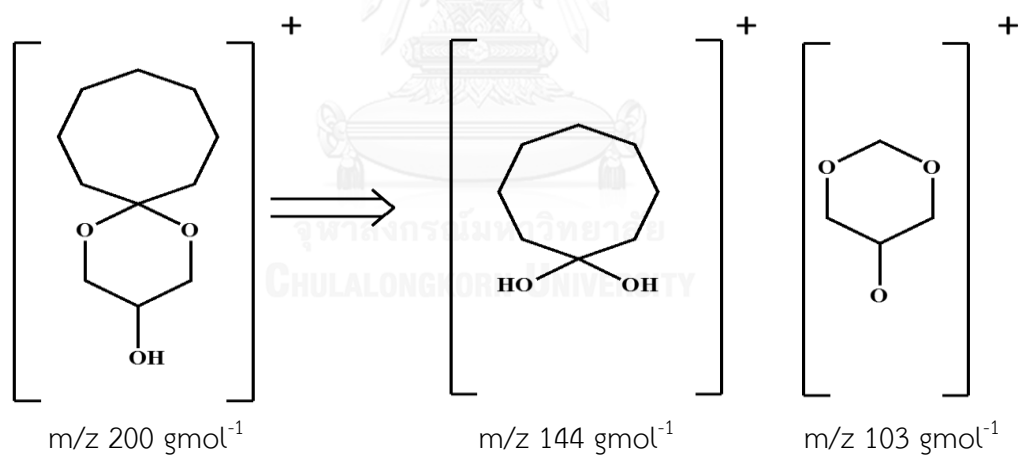
MW = 200 gmol^{-1}

m/z 200 gmol^{-1} m/z 185 gmol^{-1} m/z 170 gmol^{-1}

Acetalization of glycerol with cyclooctanone
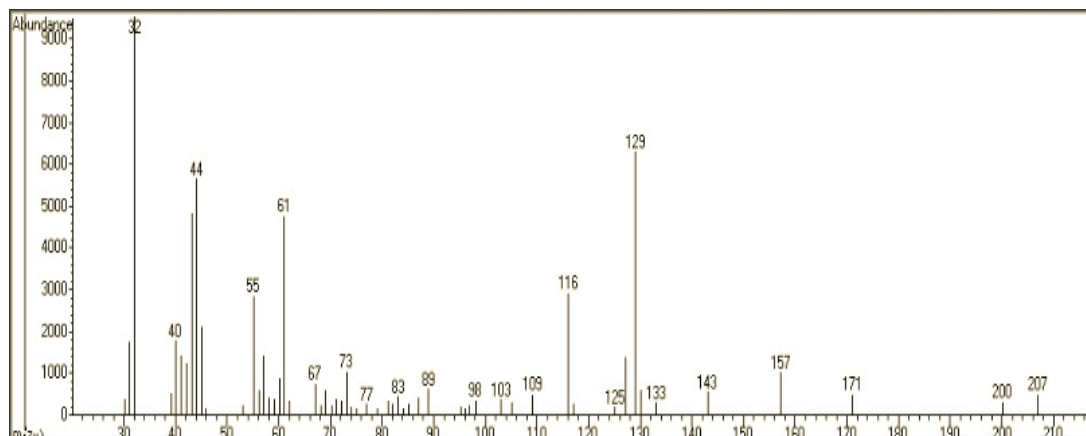
6 membered ring

Figure A-18 Mass Spectrum of (1,5dioxaspiro [5.7]tridecan-3-ol) , MW = 200 gmol^{-1}

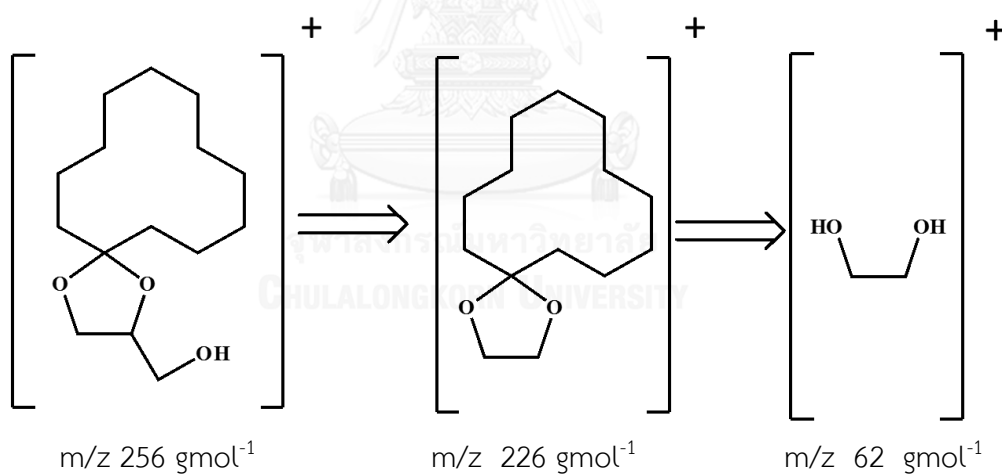m/z 200 gmol^{-1} m/z 144 gmol^{-1} m/z 103 gmol^{-1}

Acetalization of glycerol with cyclododecanone
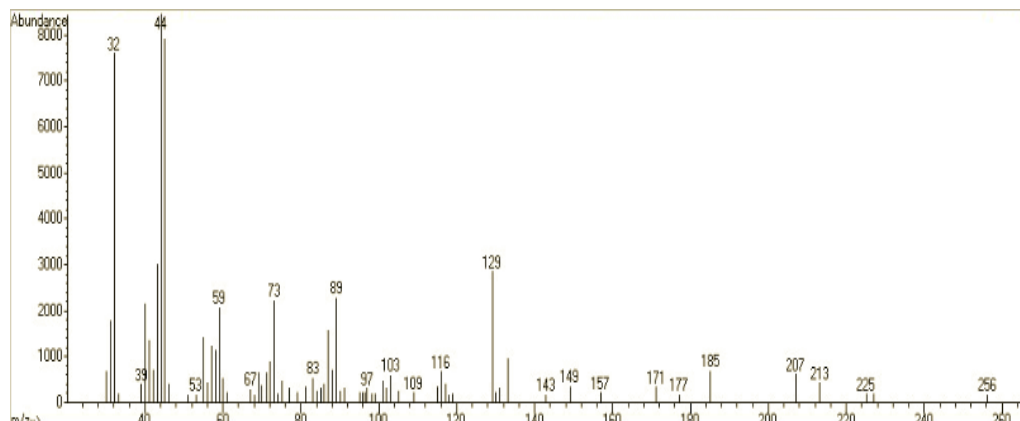
5 membered ring

Figure A-19 Mass Spectrum of 1,4 dioxaspiro [4,11]hexadecane-2-ylmethanol ,

MW = 256 gmol^{-1}

m/z 256 gmol^{-1} m/z 226 gmol^{-1} m/z 62 gmol^{-1}

VITA

Miss Rachatawan Yaisamlee was born on November 27, 1991 in Ayutthaya, Thailand. She graduated with Bachelor's Degree in Chemistry from Faculty of Science, Thammasart University in 2013. She continued her study in Petrochemistry and Polymer Science Program, Faculty of Science, Chulalongkron University in 2014 and completed in 2016. She received the Science Achievement Scholarship of Thailand from Office of the Higher Education Commission for both undergraduate and graduate studies. She also received a research grant from 90th anniversary of Chulalongkorn University (Ratchadaphiseksomphot Endowment Fund) during graduate study. She presented her research in Pure and Applied Chemistry International Conference (Paccon 2017) at Centara Government Complex Hotel & Convention Centre in the title of "Acetalization of glycerol with acetone over sulfonic beta catalyst"

Her present in 189/1 Moo.8, U-Thong Rd., Pratuchai, Ayutthaya, Thailand, 13000. Tel 09-5785-8599.